



2014

DEFORMATION AND SHEAR BEHAVIORS OF WEATHERED COMPACTED SHALE

Xu Zhang

University of Kentucky, xu.zhang907@gmail.com

Recommended Citation

Zhang, Xu, "DEFORMATION AND SHEAR BEHAVIORS OF WEATHERED COMPACTED SHALE" (2014). *Theses and Dissertations--Civil Engineering*. 23.
http://uknowledge.uky.edu/ce_etds/23

This Master's Thesis is brought to you for free and open access by the Civil Engineering at UKnowledge. It has been accepted for inclusion in Theses and Dissertations--Civil Engineering by an authorized administrator of UKnowledge. For more information, please contact UKnowledge@lsv.uky.edu.

STUDENT AGREEMENT:

I represent that my thesis or dissertation and abstract are my original work. Proper attribution has been given to all outside sources. I understand that I am solely responsible for obtaining any needed copyright permissions. I have obtained needed written permission statement(s) from the owner(s) of each third-party copyrighted matter to be included in my work, allowing electronic distribution (if such use is not permitted by the fair use doctrine) which will be submitted to UKnowledge as Additional File.

I hereby grant to The University of Kentucky and its agents the irrevocable, non-exclusive, and royalty-free license to archive and make accessible my work in whole or in part in all forms of media, now or hereafter known. I agree that the document mentioned above may be made available immediately for worldwide access unless an embargo applies.

I retain all other ownership rights to the copyright of my work. I also retain the right to use in future works (such as articles or books) all or part of my work. I understand that I am free to register the copyright to my work.

REVIEW, APPROVAL AND ACCEPTANCE

The document mentioned above has been reviewed and accepted by the student's advisor, on behalf of the advisory committee, and by the Director of Graduate Studies (DGS), on behalf of the program; we verify that this is the final, approved version of the student's thesis including all changes required by the advisory committee. The undersigned agree to abide by the statements above.

Xu Zhang, Student

Dr. L. Sebastian Bryson, Major Professor

Dr. Yi-Tin Wang, Director of Graduate Studies

DEFORMATION AND SHEAR BEHAVIORS OF WEATHERED COMPACTED SHALE

THESIS

A thesis submitted in partial fulfillment of the
requirements for the degree of Master of Science in Civil Engineering
in the College of Engineering
at the University of Kentucky

By

Xu Zhang

Lexington, Kentucky

Director: Dr. L. Sebastian Bryson, Associate Professor of Civil Engineering

Lexington, KY

2014

Copyright © Xu Zhang 2014

ABSTRACT OF THESIS

DEFORMATION AND SHEAR BEHAVIORS OF WEATHERED COMPACTED SHALE

As an abundant sedimentary rock, shale is widely used as construction material around the world. However, shale is a fissile and laminated material and is therefore subject to deterioration due to environmental and chemical forces (i.e., weathering), which is possible to cause high maintenance cost on associated structures and failures of earth slopes and embankments. However, currently, there is lack of efficient method to monitor the weathering process of shale. This thesis uses several shale samples collected from the commonwealth of Kentucky to study the deformation and shear behaviors of weathered compacted shale. A new electrical approach was developed to access the deformation behavior of shale. The long term deformation behaviors, such as collapse and swell can be predicted from specific electrical parameters. The critical state theory was used to describe the shear behavior of weathered compacted shale. Some findings observed by previous researchers were confirmed, and new empirical equations were provided to estimate the shear strength parameters of weathered compacted shale.

KEYWORDS: weathered compacted shale, weathering, durability, critical state, shear strength

Xu Zhang

November 10, 2014

DEFORMATION AND SHEAR BEHAVIORS OF WEATHERED COMPACTED SHALE

By

Xu Zhang

Dr. L. Sebastian Bryson
Director of Thesis

Dr. Yi-Tin Wang
Director of Graduate Studies

November 10, 2014

ACKNOWLEDGEMENTS

I would first like to acknowledge my families, Derui Zhang, Xiaomei Gao, Shize Chen, Shuangchun Zhang, Qinglin Zhang. Without their love and support, I would not have been able to accomplish so much. Six years ago, when I could not make a decision about which major I should chose in the university, my Mother encouraged me to choose civil engineering, and her advice at that time turned out to be a wise one. I have been interested in the courses that I took and I like the job that I am doing. I specially thank Qinglin for his constant support and encouragement, and for always pushing me to achieve my goals.

Secondly but very importantly, I would like to acknowledge my advisor Dr. L. Sebastian Bryson, who opened the door to the geotechnical world for me, guiding me and showing me all the interesting and fantastic things about geotechnical engineering. I will never forget taking the first course from him, where he was the most energetic professor I have ever seen, trying to use every parts of his body to share his knowledge to the students. I would also like to thank my colleagues, Dr. Isabel Gomez-Gutierrez, Corrie Walton-Macaulay, Josh Wells, Ryan Ortiz, Kobina Intsiful, and Melinda Jean-Louis who have made my time at University of Kentucky happy and memorable. I specially thank Isabel, for helping me get involved in shale research, teaching me hand by hand on laboratory operations and sharing knowledge about study and stories in lives.

I would also like to thank my undergraduate advisor Dr. Scott Yost, who guided me learning the culture of the country, the education system of the university and helped me plan my academic path. I also would like to thank Dr. Brad Davis, who was the professor of the first class that I took when I got in the US. Dr. Davis was always patient and willing to spend time after class to answer all my questions, which gave me great encouragement at that period of time as a new international student. I understand he was probably just doing a normal thing as a professor, but that was really a lot to me.

I also thank all my dear friends I made in the university, Yimo Cao, Caoli Zheng, Wenqi Li, Lei Han, Ying Li, Jie Pan, Wei Wan, and Zhi Zhang, who have been making me feel like been not far from my home country and making my four years of university life colorful and meaningful.

TABLE OF CONTENTS

ACKNOWLEDGEMENTS	iii
TABLE OF CONTENTS	v
LIST OF TABLES	viii
LIST OF FIGURES	ix
1 Introduction.....	1
1.1 Background.....	1
1.2 Research Tasks Description.....	3
1.3 Objectives of Research	4
1.4 Content of Thesis	5
2 A New Method to Assess the Durability of Shale	6
2.1 Introduction.....	6
2.2 Theoretical Basis of Shale-water Reaction	7
2.3 Test Shale and Testing Methodology.....	8
2.3.1 Test Shale.....	8
2.3.2 Testing Methodology	12
2.4 Discussion of Testing Results	15
2.4.1 pH Measurements	15
2.4.2 Shale-Water Electrical Conductivity Curve.....	17
2.4.3 Particle Size Effects on SWEC Curve	20
2.4.4 Sensitivity of A and B Parameters	22
2.4.5 Slaking Fluid Effects on SWEC Curve.....	23
2.4.6 Determination of SWEC Curve Parameters.....	24
2.5 The Methods to Assess Durability	29
2.5.1 Correlation between Curve Rates and Durability	29
2.5.2 Correlation between Curve Parameters and Durability	32
3 Accessing Mechanical Behaviors of Compacted Shale by Electrical Parameters	35

3.1	Introduction.....	35
3.2	Tested Materials.....	37
3.3	Deformation Behaviors of Compacted Shale.....	41
3.3.1	1-D Collapse Test on Compacted Shale.....	41
3.3.2	Discussion on Collapse Behavior of Compacted Shale	43
3.3.3	1-D Free Swell Test on Compacted Shale	46
3.3.4	Discussion on Swelling Behavior of Compacted Shale.....	47
3.4	Shear Behaviors of Compacted Shale.....	49
3.4.1	UU Test on Compacted Shale.....	49
3.4.2	Discussion on Shear Behavior of Compacted Shale	52
4	Shear Behavior of Weathered Compacted Shale	54
4.1	Introduction.....	54
4.2	Critical State Shear Strength Theory	56
4.3	Experiments and Results.....	58
4.3.1	Index Tests	59
4.3.2	Compaction Tests.....	60
4.3.3	CIU Tests	61
4.4	Analysis and Discussions.....	66
4.4.1	Effective Critical State Friction Angle.....	68
4.4.2	Normalized Undrained Shear Strength for Shale Compacted by Low Energy.....	71
5	Conclusions.....	73
5.1	Conclusion for Electrical Jar Test and SWEC Curve	73
5.2	Conclusion for Access Mechanical Behaviors of Compacted Shale by Electrical Parameters.....	74
5.3	Conclusion for Shear Behavior of Weathered Compacted Shale	75
	APPENDIX A.....	77
	APPENDIX B.....	106

APPENDIX C	112
APPENDIX D.....	114
REFERENCES	119
VITA.....	123

LIST OF TABLES

Table 2-1 Summarized information of tested shale	9
Table 2-2 Index properties, 1-D consolidation and durability data of test shale	10
Table 2-3 Mineralogy of test shale	11
Table 2-4 Shale particle size chart of electrical jar test	13
Table 2-5 Matrix of electrical jar tests performed	14
Table 2-6 Carbondale shale: size effects test data	22
Table 2-7 SWEC curve rates and parameters for test shales	24
Table 2-8 Chart of coefficient c to calculate EC_r	27
Table 2-9 Summary of residual electrical conductivity	28
Table 2-10 Equations of B parameters to estimate LSI and compression index.....	34
Table 3-1 Geological information of shale sample.....	38
Table 3-2 Index properties, 1-D consolidation and durability data of test shale	39
Table 3-3 Summary of electrical jar test.....	40
Table 3-4 Summary of collapse and swelling tests.....	42
Table 3-5 Equations to determine free swell by (a) PI, and (b) C_c	48
Table 3-6 Equations to determine free swell by (a) R_p and (b) B parameter	49
Table 4-1 Tested shale and index properties.....	59
Table 4-2 Optimum water content and maximum dry unit weight at three compaction energy....	60
Table 4-3 Critical state shear strength parameters for compacted shale.....	68

LIST OF FIGURES

Figure 2-1 Kentucky geologic map showing sample locations	9
Figure 2-2 Ternary sedimentary rock classification system	12
Figure 2-3 Normalized pH vs. log time with #0.25 particle size specimens: (a) tap water data and (b) distilled water data	16
Figure 2-4 Normalized pH vs. log time for different sizes of Carbondale shale weathered in tap water.....	17
Figure 2-5 Typical SWEC curves for the test shales weathered in (a) distilled water and (b) tap water.....	18
Figure 2-6 Typical SWEC curve indicating weathering rates and phases	19
Figure 2-7 Carbondale shale: four particle sizes electrical jar test results	21
Figure 2-8 Investigations of A and B Parameters on MMF Curve: (a) Case 1 & (b) Case 2	23
Figure 2-9 Standard SWEC curves plotted on an arithmetic time scale	25
Figure 2-10 Hyperbolic representation of standard SWEC curve	26
Figure 2-11 Correlations of mineralogy index with standard curve parameters: (a) A parameter and (b) B parameter	29
Figure 2-12 Correlation between primary weathering rate and loss slake index	30
Figure 2-13 Accuracy of two-point method for estimating R_p	31
Figure 2-14 Correlations between primary weathering rate and natural moisture content	32
Figure 2-15 Correlations of distilled water B parameter with (a) loss slake index and (b) compression index	33
Figure 3-1 Kentucky geological map showing sample locations.....	38
Figure 3-2 Carbondale sample compression curve of the collapse potential test	41
Figure 3-3 Variation of collapse potential as a function of dust fraction.....	43
Figure 3-4 Variation of collapse potential and index properties: (a) PI and (b) LL	44
Figure 3-5 Correlations of R_d with (a) collapse potential and (b) slake durability index	45

Figure 3-6 Swell-time curve of Carbondale shale	47
Figure 3-7 Variation of Free Swell with (a) Plasticity Index and (b) Compression Index	48
Figure 3-8 Variation of free swell with (a) R_p and (b) B Parameter	49
Figure 3-9 Stress-Strain Curves with Time Variables of Carbondale Shale.....	52
Figure 3-10 Undrained Shear Strength vs. Weathering Time for All Tested Samples	53
Figure 4-1 Critical state of compacted shale.....	57
Figure 4-2 Typical compaction curves of (a) Hance and (b) Newman shale samples.....	61
Figure 4-3 Typical stress paths of compacted shale consolidated at 400 kPa - (a) Hance and (b) Newman shale	63
Figure 4-4 Typical stress paths of compacted shale for each one of the compaction energy with all consolidation pressures	65
Figure 4-5 Critical states at maximum stress difference for (a) Hance and (b) Newman shale.....	67
Figure 4-6 Variation of critical state friction angle with liquid limit.....	69
Figure 4-7 Variation of critical state friction angle with clay friction	70
Figure 4-8 Variation of critical state friction angle with plasticity index	70
Figure 4-9 Variation of normalized undrained shear strength with plasticity index.....	71
Figure 4-10 Variation of normalized undrained shear strength with maximum dry unit weight...	72

1 Introduction

1.1 Background

Shale is a loosely used term applied to fine-grained clastic sedimentary rock (Blatt et al. 2006). This term often refers to other geological and engineering terms materials such as siltstone, mudstone and clayshale (Richardson and Wiles 1990). Shale is the most abundant sedimentary rock worldwide. Because of its abundance, it is often used as a construction material in many civil engineering applications. However, shale is a fissile and laminated material and is therefore subject to deterioration due to environmental and chemical forces. For example, in highway constructions, deterioration of shale may lead to bearing capacity failure of embankment and instability of the adjacent slopes. It has been pointed out by many researchers (Abeysekera et al., 1979; Manasseh and Olufemi, 2008; Bryson et al., 2012) that deterioration of shale is due to weathering effects by water. Currently, due to the lack of economical alternative materials, it is very important to study the deformation behaviors of shale as a result of water, including swelling and collapse of shale under wet condition, as well as the shear behavior of weathered shale. In addition, the durability of shale is an important parameter describing the material's susceptibility to breakdown upon exposure to water (Satttil and Higgins 1998). So the study of the deformation and shear behavior of weathered shale cannot be separate from the study of this material's durability.

Several researchers (Richardson and Wiles 1990; Koncagul and Santi 1999; Gemici 2001; Lashkaripour and Ghafoori 2003; Nandi and Whitelaw 2009; Bryson et al. 2011; Yagiz 2011) have reported that durability is correlated to various mechanical and index properties, such as shear strength, water content, quantity of clay minerals, clay fraction and dry/saturated unit weight. Two (2) most common durability tests reported in the literature are slake durability test

(Franklin and Chandra 1972) and jar slake test (Taylor and Spears 1981). The discussions on the limitations of the slake durability test are abundant in the literature, especially on the numbers of dry and wet cycles (Brown 1981; Taylor 1988; Gokceoglu et al. 2000; Czerewko and Cripps 2001). Based on different numbers of cycles and analysis methods, several new shale durability indexes and durability rating systems were introduced (Erguler and Ulusay 2009; Fuenkajorn 2011; Bryson et al. 2012).

Several researchers (Lawton et al., 1989; Lawton et al., 1991; Miller et al., 1997; Pappas and Vallejo, 1997) have been focusing on the study of collapse behavior happening on wetted compacted shale when adequate vertical overburden stress is applied. For example, It was found that variables having the most impact on collapse index were compaction moisture content, dry unit weight, plasticity index, and clay-size fraction (Miller et al., 2001; Lim and Miller, 2004). Other researchers (Low, 1961; O'Neill and Poormoayed, 1980; Hopkins and Gilpin, 1981; Hopkins, 1988; Orhan Erol and Dhowian, 1990; Wong, 1998) have investigated the swell behavior of shale. It was pointed out that the composition of minerals, the type of pore fluid and soil structures primarily determine the swell potential of soil, while the outside environmental conditions control the actual amount and rate of swell (Johnson and Snethen, 1978).

Several researchers (Wu et al. 1993; Yoshida and Hosokawa 2004; Aziz et al. 2010) have studied the water-induced granular decomposition of crushed shale. It was found that saturated crushed shale showed a greater loss of strength in comparison with dry compacted shale, and that saturated shale exhibited density-dependent behavior. Other researchers (Alonso et al. 1990; Pinyol et al. 2007; Alonso and Cardoso 2010) have investigated the effects of structure losing due to weathering on the mechanical behavior of shale.

1.2 Research Tasks Description

The current slake durability test has the limitation to assess the long-term durability of shale. Jar slake test is able to distinguish between durable and non-durable shale under a sufficient length of monitoring. Unfortunately, it is a qualitative method. The results of the test are subjective and the quality of the results is typically dependent on the skill set of the tester. It therefore can be expected that there is often significant variability in the jar slake test results reported in the literature. The research presented in this thesis is aimed to find a new durability test, which is able to eliminate the current limitations and to provide repeatable and reliable results.

Currently in the literature, there is lack of swell and collapse tests using compacted shale samples, which means the specimens are remodeled from crushed shale. There are also no clear standards on the specimen preparations and testing procedures for crushed shale. The previous researches on the weathering effects on the shear strength of compacted shale did not make a focus on the shear strength changes over the weathering time. This research is aimed to develop and perform swell and collapse tests on remodeled crushed shale, and perform unconsolidated-undrained triaxial tests with different lengths of weathering time.

Although the current shear behavior studies of shale were focused on short-term (i.e., immediately after construction), long-term behavior effected by weathering is more critical to shale-constructed structures. It is also found that not many studies have specifically focused on the various shear strength interpretations of weathered compacted shale. This paper re-interprets the test data by Hopkins and Deen (1984) and Hopkins (1988) on nine different types of shale from the commonwealth of Kentucky, and describes the shear behavior of weathered compacted shale and how the compaction energy affects the behavior. The shear behaviors are described using fundamental soil mechanics theory. Shear strength parameters are calculated and used to compare to various material properties obtained from laboratory experiments.

1.3 Objectives of Research

The objectives of this research are as follows:

1) Develop a new durability test method on shale, which is able to access the durability in long-term with repeatable and reliable results

- Propose new testing procedures based on the theory of reactions between and water
- Conduct the proposed new test on several shale samples obtained from Kentucky
- Analyze the test results and develop test result indexes to describe the long-term durability of shale

2) Study the deformation behavior of shale (i.e., collapse and swell)

- Develop test procedures on remodeled crushed shale for swelling and collapsing measurements
- Analyze the test results and investigate the correlations between the deformation behavior of shale and other shale properties.

3) Study the shear behavior of shale

- Develop test procedures on remodeled crushed shale for shear strength measurements over different weathering time.
- Analyzed the shear strength changes over the length of weathering time
- Re-interpret the test data by Hopkins and Deen (1984) and Hopkins (1988), and describe the shear behavior of shale using soil mechanics theory.
- Investigate the correlations between the shear behavior of shale and other shale properties

1.4 Content of Thesis

This thesis consists of five (5) chapters with attached appendix. The contents of each specific part are as follows:

Chapter 2 presents the attempt and process to develop a new electrical method to quantitatively measure the long-term durability of shale.

Chapter 3 presents the testing methods for measurement of 1-D collapse potential and 1-D free swell and the testing methods for measurement of undrained shear strength with weathering effect on compacted shale. The correlations between deformation and shear behaviors of shale and other shale properties are also presented.

Chapter 4 presents the re-interpretation of test data by Hopkins and Deen (1984) and Hopkins (1988). In this chapter, critical state theory was used to describe the shear behavior of weathered compacted shale. The correlations between the shear parameters and other shale properties are also presented.

Chapter 5 presents the conclusions for each of the previous chapters. The recommendations for future research are also included.

Appendix A presents the test data of electrical jar test. Appendix B presents the test data of collapse test. Appendix C presents the test data of swell test. Appendix D presents the test data of undrained-unconsolidated triaxial test.

2 A New Method to Assess the Durability of Shale

2.1 Introduction

Shale is a loosely used term applied to fine-grained clastic sedimentary rock (Blatt et al. 2006). This term often refers to other geological and engineering materials such as siltstone, mudstone and clayshale (Richardson and Wiles 1990). Shale is the most abundant sedimentary rock worldwide. Because of its abundance, it is often used as a construction material in many civil engineering applications. However, shale is a fissile and laminated material and is therefore subject to deterioration due to environmental and chemical forces. For highway construction applications, deterioration of shale may lead to bearing capacity failure of highway embankment and instability of the adjacent slopes. The susceptibility of shale to deterioration is typically quantified by durability. The durability of shale is an important parameter describing the material's susceptibility to breakdown upon exposure to water (Sattil and Higgins 1998). Several researchers (Richardson and Wiles 1990; Koncagul and Santi 1999; Gemici 2001; Lashkaripour and Ghafoori 2003; Nandi and Whitelaw 2009; Bryson et al. 2011; Yagiz 2011) have reported that durability is correlated to various mechanical and index properties, such as shear strength, water content, quantity of clay minerals, clay fraction and dry/saturated unit weight.

Two most common durability tests reported in the literature are slake durability test (Franklin and Chandra 1972) and jar slake test (Taylor and Spears 1981). The discussions on the limitations of the slake durability test are abundant in the literature, especially on the numbers of dry and wet cycles (Brown 1981; Taylor 1988; Gokceoglu et al. 2000; Czerewko and Cripps 2001). Based on different numbers of cycles and analysis methods, several new shale durability indexes and durability rating systems were introduced (Erguler and Ulusay 2009; Fuenkajorn 2011; Bryson et al. 2012). The Jar slake test is able to distinguish between durable and non-durable shale under a sufficient length of monitoring. Unfortunately, it is a qualitative method. The results of the test

are subjective and the quality of the results is typically dependent on the skill set of the tester. It therefore can be expected that there is often significant variability in the jar slake test results reported in the literature.

The proposed new quantitative method presented in this paper utilizes the immersion aspect of the jar slake test, which simulates the deterioration of shale under saturated conditions. The proposed method also captures the long-term behavior of shale from the aspect of water induced deterioration or weathering for up to 14 days. However, the proposed method eliminates the subjectivity associated with the jar slake test, which provides repeatable and reliable results. The proposed method uses electrical conductivity (EC) measurements of a shale-water solution to quantify the durability of shale. The proposed method also includes additional considerations for preparation of specimen, the effects of slaking fluid and the influence of the shale mineralogy. The proposed method was developed through original laboratory experimentation and reanalysis of data presented by Kirkendoll (2012) and Gomez-Gutierrez (2013).

2.2 Theoretical Basis of Shale-water Reaction

The durability of shale is related to the quantity and type of clay minerals present in shale matrix (Taylor and Spears 1981). This relation is the basis of the proposed method to assess long-term durability of shale. Clay minerals are negatively charged due to isomorphous substitution, which is the process that substitutes one atom for another in the structure of clay minerals at the time the clay minerals form (Weaver 1989; Velde 1992). The negative charge must be balanced by positive charged ions. Therefore, positive charged cations such as Na^+ , K^+ and Ca^{2+} attach to the surface of clay minerals to create balanced charge. When pieces of shale are immersed in water, as in the jar slake test, a process of ion exchange between shale and water will start. The hydronium ion (H_3O^+) from water will replace the electrically conductive cations (i.e., Na^+ , K^+ and Ca^{2+}) attached to shale. As a result, the ion exchange will cause an increase in pH due to the separation of hydroxyl ion (OH^-). Meanwhile, the concentration of different cations in the shale-

water solution will increase. Electrical conductivity, as a measurement of charge mobility correlated with the ionic concentration (Klein 1999), will also increase due to the presence of cations in the aqueous solution. This process is time-dependent and will occur until all the cations on the clay surface are exchanged by H_3O^+ or when the aqueous solution becomes saturated with the cations. For a jar test, the exchange of H_3O^+ is assumed to be proportional to the amount of slaking.

Several researchers (Noble 1977; Pye and Miller 1990; Klein 1999; Klein and Santamarina 2003) have investigated the ion exchange process. Pye and Miller (1990) placed 50 g 0.6 to 2.36 mm size shale fragments into beakers containing 1250 mL distilled water and measured the elemental concentration (including Mg, Ca, K, Fe, Na and Mn) over time using atomic absorption spectrophotometry and atomic emission spectrophotometry. These researchers showed that the greater disintegration of shale pieces (i.e., the greater amount of slaking), the stronger the ion exchange. The EC and pH of a shale-water solution will change in accordance with some function with respect to time. It is assumed that this function will be unique to the specific shale mineralogical characteristics and lithology, and the initial pH and EC of the slaking fluid. Thus the amount of slaking (i.e., durability) of a given shale specimen will be strongly related to the rate of change of EC and pH of a shale-water solution. This research evaluated this assumption by comparing traditional slake durability behavior of shale samples with time-dependent EC and pH changes in a shale-water solution.

2.3 Test Shale and Testing Methodology

2.3.1 Test Shale

In this study, seven shale samples with various durability, geological ages and formations were collected from seven different locations in Kentucky, United States. The geological and location information of the shale samples are summarized in Table 2-1.

Table 2-1 Summarized information of tested shale

Geologic Name	Geologic Period	Location in Kentucky	Sample Code
Bull Fork	Ordovician	Boone County	BC
Tradewater	Pennsylvanian	Philpot	BS
Fort Payne	Mississippian	Campbellsville	CB
Grundy	Pennsylvanian	Clay County	CC
Carbondale	Pennsylvanian	Webster County	CD
Great Lake	Ordovician	Maysville	MV
Upper Pottsville	Pennsylvanian	Martin County	UP

As presented in Table 2-1, two of the samples are from the Ordovician Period (510 to 440 million years ago), which are mainly composed of limestone and located in north central Kentucky. Four of the samples are from the Pennsylvanian (325 to 290 million years ago). These shales are from the eastern and western coal fields of Kentucky, and are composed mostly of sandstone, conglomerates and coals. There is only one sample from Mississippian-age strata (360 to 325 million years ago), which is located in central Kentucky. This formation is dominated by limestone and sandstone. A Kentucky Geologic Map with the locations of test shale is shown in Figure 2-1.

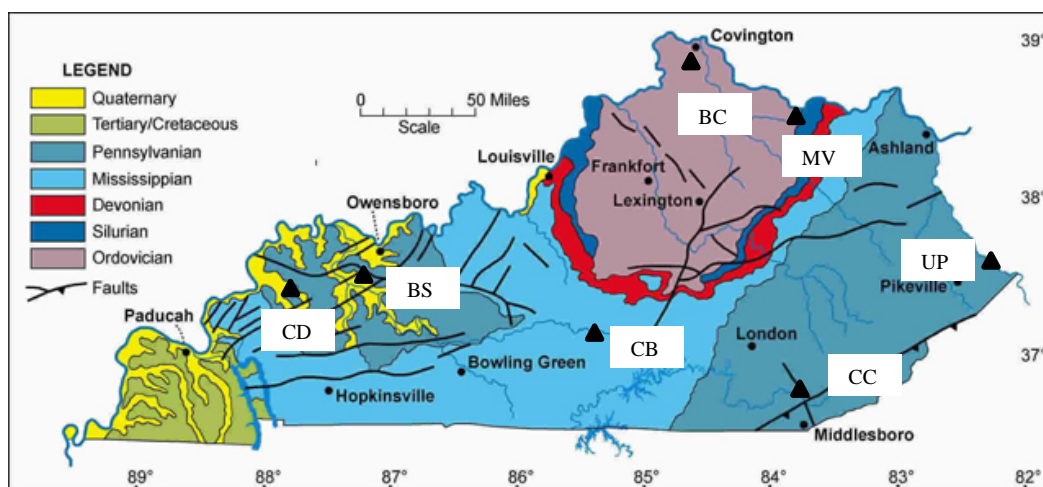


Figure 2-1 Kentucky geologic map showing sample locations

Samples were collected from excavations on ongoing construction sites. The shale samples were carefully bagged or wrapped after collection to preserve the natural moisture contents. The preliminary shale size reduction was done using a jaw crusher with predetermined maximum and minimum dimensions of 15.88 mm (5/8 in.) and 9.53 mm (3/8 in.). Basic laboratory testing was performed on all shale samples. The testing included water content tests (ASTM D2216), Atterberg limits tests (ASTM D4318), one-dimensional consolidation tests (ASTM D2435), slake durability tests (ASTM D4644) and loss slake index tests (Bryson et al., 2012). Additional testing and analysis was performed on five of the seven shale samples (i.e., Bull Fork, Tradewater, Fort Payne, Grundy and Carbondale), that included further particle size reduction, particle size analysis (ASTM D422) and x-ray diffraction (XRD) tests on the fraction of the material passing No. 200 sieve. The index test results and the geotechnical test results are summarized in Table 2-2, and the mineralogy test data are summarized in Table 2-3.

Table 2-2 Index properties, 1-D consolidation and durability data of test shale

Geologic Name	ω_n (%)	LL (%)	PL (%)	PI (%)	C_c	C_s	$I_d(2)$ (%)	LSI (%)
Bull Fork	3.29	26	19	7	0.050	0.013	77.17	0.22
Tradewater	5.24	29	21	8	0.063	0.014	80.81	0.50
Fort Payne	4.40	25	23	2	0.017	0.009	92.62	0.11
Grundy	1.30	23	19	4	0.025	0.009	96.51	0.07
Carbondale	2.89	24	19	5	0.048	0.009	94.74	0.15
Great Lake	2.09	21	15	6	0.042	0.011	71.64	0.21
Upper Pottsville	1.40	20	18	2	0.020	0.012	94.86	0.03

ω_n = natural moisture content; LL = liquid limit; PL = plasticity limit; PI = plasticity index;
 C_c = compression index; C_s = swell index; $I_d(2)$ = slake durability index; LSI = loss slake index.

In Table 2-2, the data shows that the natural moisture contents for the shale were between 1.3 and 5.3 percent. Tradewater shale had the highest moisture content of 5.42 percent. The test shale samples had plasticity indexes from 2 to 8 percent. The range of liquid limit from 20 to 29 percent and plasticity limit from 15 to 23 percent are also shown. Tradewater shale also had the highest compression and swell indexes of 0.063 and 0.014 respectively. Both ASTM slake

durability index ($I_d(2)$) and loss slake index, LSI (Bryson et al. 2012) are shown. Bull Fork shale had the lowest $I_d(2)$ of 77.17 percent, while Grundy shale had the highest of 96.51 percent. LSI are compared to $I_d(2)$ showing that LSI values are likely to be larger for less durable shale, which implies greater rate of deterioration. Both Grundy and Upper Pottsville shale have LSI less than 0.1 percent, which are ranked as the lowest among test shale. Bull Fork shale has the highest LSI of 0.22 percent.

Table 2-3 Mineralogy of test shale

Geological Name	Chlorite (%)	Illite (%)	Kaolinite (%)	Quartz (%)	Calcite (%)	Dolomite (%)	Siderite (%)	Carbonate (%)	Shale Classification
Bull Fork	5	11	9	12	45	15	0	60	Marlstone
Tradewater	4	30	22	24	4	0	12	16	Mudstone
Fort Payne	2	9	3	29	3	43	0	46	Marlstone
Grundy	7	35	22	16	4	5	6	15	Mudstone
Carbondale	8	37	23	19	7	0	0	7	Mudstone
Carbonate = Calcite + Dolomite + Siderite									

Table 2-3 shows the results of mineralogical analysis and the classification of shale samples. The test shales were composed mainly of illite, kaolinite, quartz and carbonates. The quantities of other common minerals such as Feldspar, Pyrite and Gypsum are also obtained, but due to percentages less than 5, they are not shown in the table. It is noticed that Fort Payne shale had the lowest content of kaolinite of 30 percent and highest content of illite and Quartz of 50 and 13 percent respectively. Bull Fork shale had the highest content of chlorite at 12 percent, while the other shale samples had less than 8 percent. Gomez-Gutierrez (2013) found that the summation of chlorite and illite contents correlated linearly with the content of kaolinite. Therefore the ratio of $(Ch+I)/K$ was developed as a mineralogy index. The shale samples were classified according to the mineralogy data and the ternary sedimentary rock classification system (Tucholke et al. 2004) shown in Figure 2-2. This system defines rock types primarily based on the portions of carbonate. With more than 30 percent of carbonates, Bull fork and Fort Payne shales

were classified as Marlstone. With less than 30 percent of carbonates, Tradewter, Grundy, Carbondale shales were classified as Mudstone.

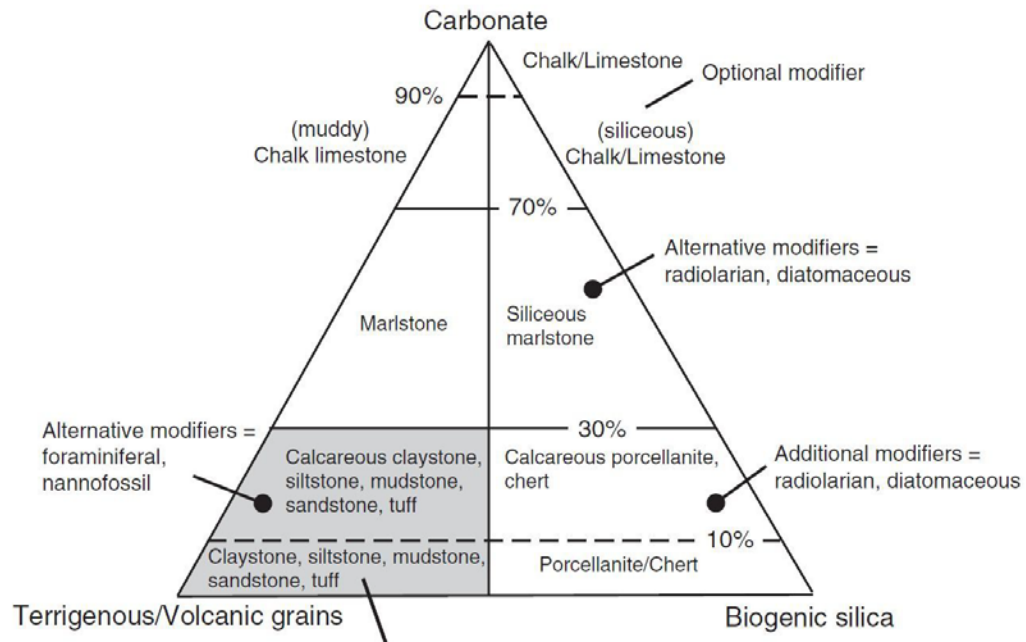


Figure 2-2 Ternary sedimentary rock classification system

2.3.2 Testing Methodology

The proposed new method to assess the durability of shale is referred to as Electrical Jar Test. This test uses a handheld pH/conductivity meter to measure pH and EC. Specifically, an Oakton PC300 meter was used for this research. The PC300 meter was equipped with a pH electrode and a conductivity probe. The conductivity probe had a build-in temperature sensor, which was able to automatically compensate both pH and EC readings to a default temperature (25 °C in this study). An aqueous solution is created by mixing shale specimen and slaking fluid, which is referred herein as the shale-water solution. When taking measurement of pH and EC, the pH electrode and conductivity probe are submerged into the solution at the same time. It is previously stated, the pH and EC values are direct measurements of the concentrations of electrically active ions, which was assumed to reflect the slaking of shale.

2.3.2.1 Specimen Preparation

With the same amount of mass, it was expected that the specimen with smaller particle size will deteriorate faster, as it would have larger reaction surface between shale and water. In other words, the deterioration might be a function of the surface area of shale. Thus, four specimen size ranges were elected to assess the influence of the particle size on electrical readings of shale-water solution. The ranges of the materials tested are shown in Table 2-4. All tested samples were oven-dried for at least 10 hours at 110 °C, in order to have all test samples with the same initial moisture condition. The drying temperature and period were in accordance with ASTM D2216.

Table 2-4 Shale particle size chart of electrical jar test

Sieve Pass	Sieve Retained	Size Code
1 inch (25.4 mm)	3/4 inch (19.0 mm)	0.75
3/4 inch (19.0 mm)	1/2 inch (12.7 mm)	0.5
1/2 inch (12.7 mm)	1/4 inch (6.35 mm)	0.25
1/4 inch (6.35 mm)	No. 4 (4.76 mm)	4

2.3.2.2 Test Procedure

Approximately 500 mL of slaking fluid was poured into a test beaker. The pH and EC of the slaking fluid were measured before it was combined with the shale specimen. The sample were allowed to cool for approximately 30 minutes after being taken from the oven, after which time, roughly 100 gram of oven-dried sample was poured into the slaking fluid and the timer started. An aquarium pump (5W 115V 60Hz) connected with a 3.18 mm tube was applied as the agitation tool. The bubbling action produced by the pump was used to agitate aqueous solution in order to uniformly disperse the particles into solution. The pump was used to agitate the shale-water solution for 30 to 45 seconds before each measurement. Care was taken during the agitation that the tube did not touch the specimen so that the weathering rate was not disturbed. The pH electrode and conductivity probe were inserted into the solution at the same time immediately

after agitation, and the pH and EC measurements were recorded when readings became stable. The time intervals were selected as 1, 2, 4, 8, 15, 30, 60, 100, 200, etc. minutes to fit log time plot. The agitation tube and probes were washed with distilled water between measurements. The beakers containing the shale-water solution were covered with plastic wrap when the measurements were not taken, to minimize containment from airborne dust and evaporation. However, drops of water surface level were observed at approximately 18 days after the beginning of the tests. In order to reduce the variability in the electrical measurements, the readings obtained after 14 days were not included in the data analysis.

For this study, tap water and distilled water were used as slaking fluid. The tap water used in this study had an initial pH value from 7.45 to 7.65, and an initial EC from 449 to 486 μS . The distilled water used had an initial pH from 5.7 to 6.2 and an initial EC from 0.68 to 4.62 μS . Three shales were tested on four sizes with tap water. All shales of #0.25 size were tested using both tap and distilled water. A matrix of tests performed is shown in Table 2-5.

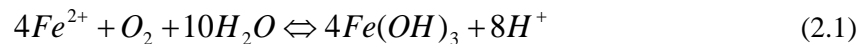
Table 2-5 Matrix of electrical jar tests performed

Geologic Name	Size Code				
	0.75	0.5	0.25	4	10
Bull Fork			●		
Tradewater			●		
Fort Payne			●		
Grundy	○	○	●	○	
Carbondale	○	○	●	○	
Great Lake	○	○	●	○	
Upper Pottsville			●		
○: tests performed using tap water only					
●: tests performed using both tap and distilled water					

2.4 Discussion of Testing Results

2.4.1 pH Measurements

The pH data were normalized by dividing the measured readings by the initial pH of slaking fluid. The purpose of the normalization is to have a better understanding of pH changes associated with the deterioration of shale. Theoretically, when time is equal to zero, the normalized pH is equal to one and if the pH becomes greater than one with time, it means the shale-water solution is becoming more alkaline. It was previously mentioned that the concentration of OH⁻ ion will increase with time due to the losing of H₃O⁺ ions in the solution. Figure 2-3 shows the pH trends for all seven shale samples with the #0.25 particle size weathered in tap water and four shale samples with the #0.25 size weathered in distilled water. It can be seen that most of the shale-water solutions tended to be more alkaline with time and only one solution (i.e., Tradewater shale) shows a more acidic change. According to the mineralogy data, Tradewater shale has highest percentage of siderite (FeCO₃). The oxidation of ferrous iron (Fe²⁺) is a possible cause of the acidic solution, which is illustrated in the oxidation-hydrolysis reaction given as:



It was also noticed that the pH sensor was likely to be more sensitive in distilled water, which had an initial condition of neutral pH and very low EC. However, a clear and unified trend for all samples was not observed. Another finding concerning the pH change is that the variation of pH trends between different samples sizes was not significant, which can be seen in Figure 2-4. The figure presents the results of Carbondale shale as an example, while the other two samples (i.e., Grundy and Great Lake shales) used to consider the size effects show the similar results.

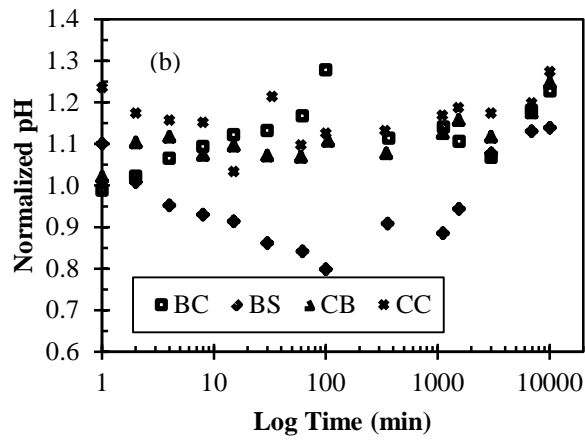
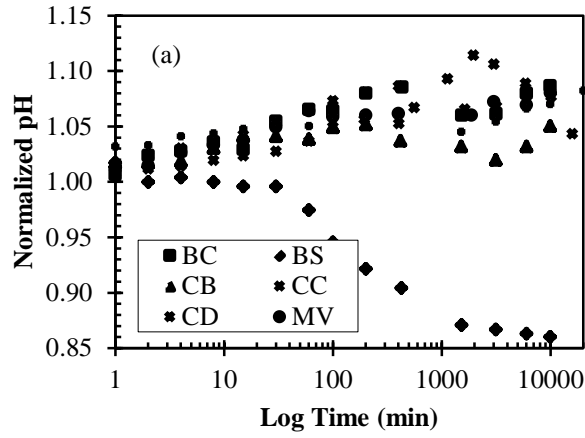


Figure 2-3 Normalized pH vs. log time with #0.25 particle size specimens: (a) tap water data and (b) distilled water data

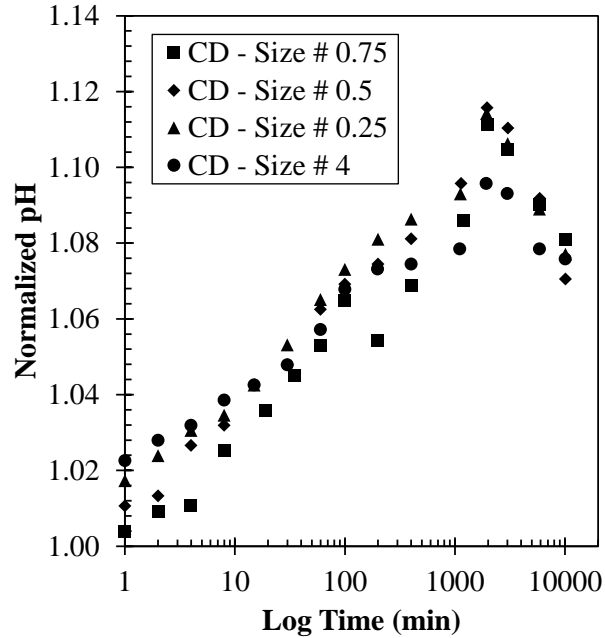


Figure 2-4 Normalized pH vs. log time for different sizes of Carbondale shale weathered in tap water

2.4.2 Shale-Water Electrical Conductivity Curve

It was observed in all tests performed that the EC of the shale-water solutions increased with time. Herein, the curve describing the increasing trend is referred to as Shale-Water Electrical Conductivity (SWEC) curve. Figure 2-5 shows the EC data with time for both tap and distilled water. For these tests, #0.25 particle size was used. As presented previously in Table 2-2, Carbondale is medium durable shale ($I_d(2)$ between 90 percent and 95 percent) among all seven shale samples, while Grundy is very durable shale ($I_d(2)$ is greater than 95 percent) and Tradewater is non-durable shale ($I_d(2)$ is lower than 90 percent). It is observed in Figure 2-5 that the less durable is the shale, the higher the rate of increase for EC over time. It is also observed that the SWEC curve is in sigmoidal shape when plotted on a log time scale. The sigmoidal shape appears to capture behavior common to all the test samples.

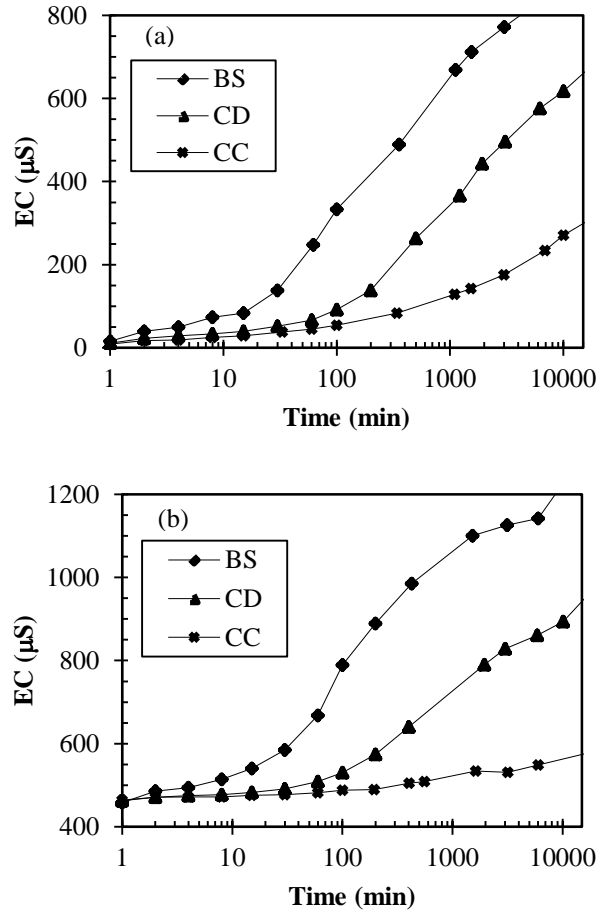


Figure 2-5 Typical SWEC curves for the test shales weathered in (a) distilled water and (b) tap water

Figure 2-6 shows a typical sigmoidal curve divided into regions that correspond to general behaviors associated with the deterioration of shale. In general, there are three regions of the EC increase with time. At the beginning when shale-water solution is just mixed, the EC increases at a relatively gentle slope, and then it is followed up by a steep slope. The first region is the Dissolution Phase, which describes the dissolution of surface clay minerals of shale specimen. This phase is not a direct indication of the shale durability; instead it is controlled by the initial surface conditions of the specimen, such as the area and roughness of the shale surface. The slope of the curve in the dissolution phase is referred to as Dissolution Rate and notated as R_d . The

second region is the Primary Weathering Phase, which describes the slaking of shale particles. Therefore, this phase will be directly related to the shale durability. The slope of the curve in the primary weathering phase is referred to as Primary Electrical Weathering Rate and notated as R_p . At the end of the primary weathering phase, the increase rate tends to yield toward some steady-state condition. This is called the Residual Phases. In this phase, the concentration of different ions in shale-water solution is reaching its ultimate level. As a result the EC will not have further significant change. It is noticed that the more durable the shale, the longer time it takes to proceed through the three phases. Referring back to Figure 2-5, at the end of the test period (i.e., 14 days), the Tradewater shale (i.e., the non-durable shale) was in the residual phase, while Carbondale (i.e., the medium durable shale) had just finished the primary phase, and Grundy (i.e., the very durable shale) was still in its primary phase.

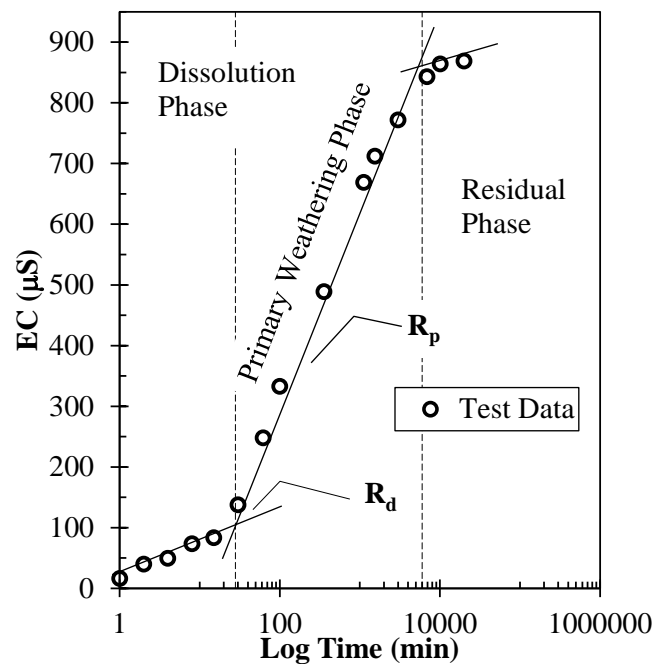


Figure 2-6 Typical SWEC curve indicating weathering rates and phases

As has thus been presented, the SWEC curve can be defined by a sigmoidal model. For this study, the Morgan-Mercer-Flodin (MMF) four-parameter mathematical growth model was

found to best fit the experimental data. The basic form of the MMF model applied to the experimental data is given in Equation (2.2).

$$EC = \frac{C \cdot A + D \cdot t^B}{A + t^B} \quad (2.2)$$

In the equation, EC is in unit of μS and time, t is in minutes. The four parameters A, B, C and D have physical meanings, and were also found to be correlated to material properties of the test shale and the physical/chemical conditions in which the specimens were weathered. The C parameter is the EC when t is equal to zero. In another words, the C parameter is the initial EC of the slaking fluid (EC_o), which is measured at the beginning of the testing. The D parameter is the EC when t approaches infinite (∞), which can be called as the residual EC and notated as EC_r . The A and B parameters are assumed to be material parameters that control the rate of slaking (i.e., deterioration) during the dissolution and primary weathering phases. Equation (2.2) can be rewritten as Equation (2.3).

$$EC = \frac{EC_o \cdot A + EC_r \cdot t^B}{A + t^B} \quad (2.3)$$

2.4.3 Particle Size Effects on SWEC Curve

Three shale samples were tested using all four particle sizes with tap water to study the particle size effects. The purpose of this study was to determine which size can provide the best testing performance. Figure 2-7 shows Carbondale shale results as an example. It was shown that the smaller size specimen had a higher value of EC at the same point of time. The smaller was the size, the less time it took to proceed through different phases.

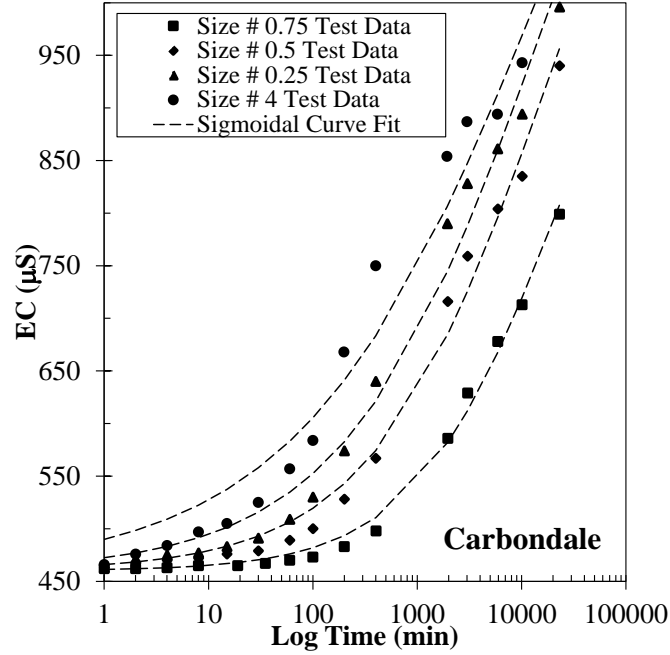


Figure 2-7 Carbondale shale: four particle sizes electrical jar test results

The different particle sizes were quantified by using specific surface area (SSA), which can be calculated by the following equation given by Carrier (2003).

$$SSA = \frac{SF}{\sqrt{d_{\max} \cdot d_{\min}}} \quad (2.4)$$

where SSA is in unit of m^2/g ; SF is the volume-surface shape factor; $\sqrt{d_{\max} \cdot d_{\min}}$ is the geometric mean particle size between two sieve sizes in units of cm. For a particular size in this study, d_{\max} is the sieve opening of which it passes and d_{\min} is the sieve opening of which it is retained. Also it was assumed that the shale particle is spherical, so that $SF = 6$ (Fair et al. 1933; Carrier 2003). Table 2-6 shows the sigmoidal curve parameters and the SSA values for Carbondale shale on four different particle sizes. The results for the other two shales are similar to Carbondale shale.

Table 2-6 Carbondale shale: size effects test data

Specimen Size	EC _o (μS)	EC _r (μS)	A	B	R ²	SSA (m ² /g)
0.75	460	1199	554.1	0.632	0.995	2.731
0.5	460	1410	158.6	0.518	0.989	3.863
0.25	460	1494	84.1	0.453	0.984	6.681
4	460	1530	37.9	0.367	0.969	10.913
R ² = the coefficient of determination of sigmoidal curve fit						

It can be seen in Table 2-6 that the larger specimen size, the smoother the curve trend can be achieved (i.e., a higher value of R²). As discussed previously, the primary weathering phase is the key phase to study the shale-water reactions and also the direct presentation of shale durability. Therefore, the most proper particle size should be able to present a complete primary weathering phase as much as possible within the designed monitoring window (i.e., 14 days). It was stated earlier that the smaller the particle size, the less time it takes to proceed to the primary weathering phase. Generally speaking, it is necessary to choose a particle size that can provides ideal performance on the shape of the curve, as well as enough time to show a clear growing trend of EC in the primary weathering phase. The #0.25 particle size meets both criteria and was selected as the “standard” size of electrical jar test.

2.4.4 Sensitivity of A and B Parameters

In order to evaluate how A and B parameters control the shape of the curve, the EC_o and EC_r are set to be fixed and equal to 450 μS and 1000 μS respectively. Figure 2-8 show the cases used for the evaluation. In the first case [Figure 2-8(a)], the A parameter is fixed and equal to 50, while the curves with four different B parameters are plotted. In the second case [Figure 2-8(b)], the B parameter is fixed and equal to 0.5, while the curves with four different A parameters are plotted. It can be seen that with the increase of B, R_d increases and R_p also increases. It is also noticed that with a fixed B, R_p is constant and the R_d decreases with the increasing of A.

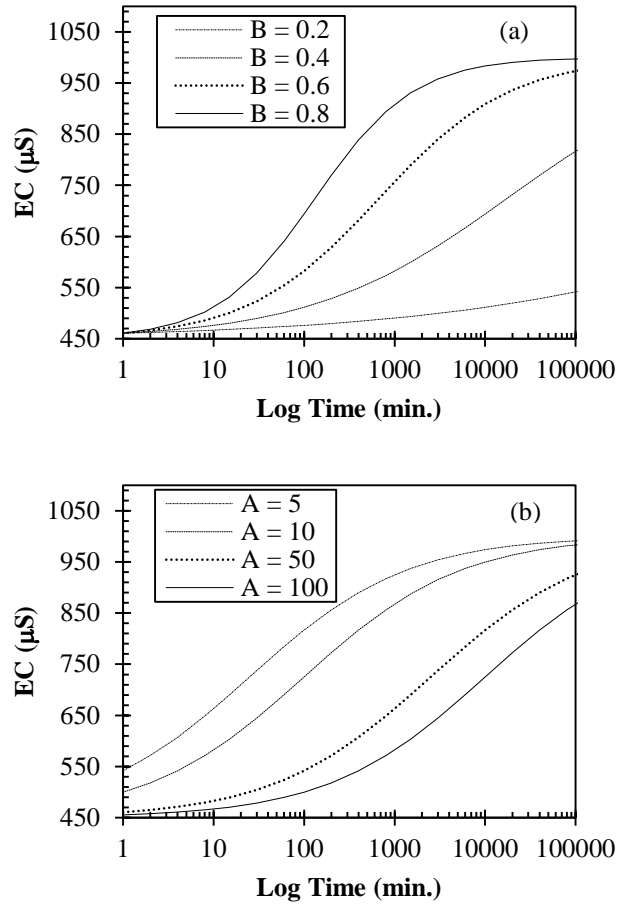


Figure 2-8 Investigations of A and B Parameters on MMF Curve: (a) Case 1 & (b) Case 2

2.4.5 Slaking Fluid Effects on SWEC Curve

It was mentioned that the electrical jar tests were performed using both tap and distilled water. The intent was to evaluate the influence of the slaking fluid on the SWEC curve and to select a “standard” slaking fluid for electrical jar test. Referring back to Figure 2-5, regardless of the slaking fluid, the SWEC curve always shows sigmoidal shape. However, EC_o and EC_r were significantly different due to the initial differences of EC between tap and distilled water. The A and B parameters and dissolution and primary weathering rates are listed in Table 2-7. In the table, both tap and distilled water data are shown. For this analysis, all specimens were in the #0.25 particle size. The curve parameters and slopes are significantly different. It was found that

the differences of curve parameters between tap and distilled water cannot be normalized by simply dividing the initial EC of the slaking fluid. It is most likely because SWEC curve is a time-dependent curve. The change of the slaking fluid does not only change the range in which the EC of the solution can increase, it also changes the rate of which the EC of the solution increases. The EC of tap water usually varies by time and location. In order to obtain repeatable electrical measurements, distilled water is recommended as the “standard” slaking fluid for electrical jar test. Therefore, the standard SWEC curve was obtained under the condition, in which distilled water was used as the slaking fluid, while the #0.25 size was used as the specimen size.

Table 2-7 SWEC curve rates and parameters for test shales

Geologic Name	Particle Size 0.25 / Tap Water				Particle Size 0.25 / Distilled Water			
	R _d (μS/min.)	R _p (μS/min.)	A	B	R _d (μS/min.)	R _p (μS/min.)	A	B
Bull Fork	46.9	86.8	9.4	0.319	72.7	169.7	13.4	0.455
Tradewater	61.7	225.1	24.5	0.492	49.7	297.1	36.2	0.574
Fort Payne	259.4	254.0	9.6	0.258	79.3	203.4	16.1	0.360
Grundy	5.7	28.6	163.4	0.303	13.3	82.4	91.8	0.473
Carbondale	13.7	201.4	84.1	0.453	19.5	271.6	94.1	0.541
Great Lake	44.6	135.4	10.1	0.326	67.7	183.1	15.0	0.458
Upper Pottsville	12.6	13.4	39.0	0.187	10.1	31.0	22.8	0.390

2.4.6 Determination of SWEC Curve Parameters

2.4.6.1 The Residual Electrical Conductivity (EC_r)

The SWEC curve presents sigmoidal shape when it is plotted against log time. However, when the EC data are plotted on an arithmetic time scale, it will present a hyperbolic shape, where the EC yields towards an ultimate value over time (Figure 2-9).

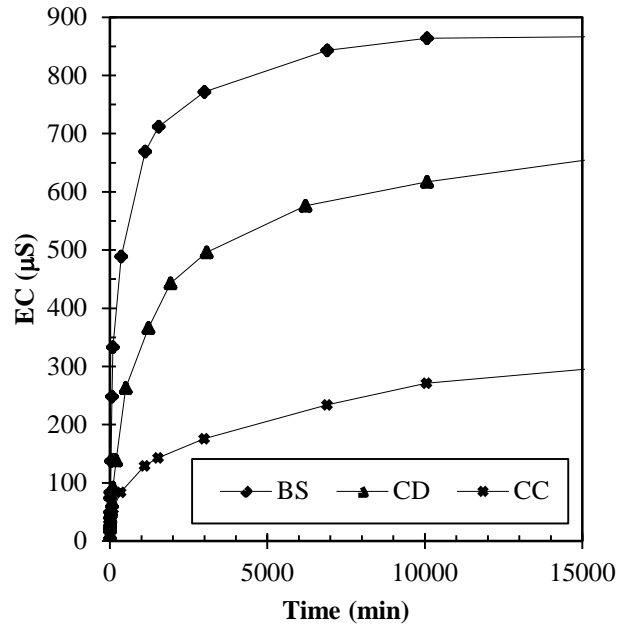


Figure 2-9 Standard SWEC curves plotted on an arithmetic time scale

The use of hyperbolic model was often proposed to represent the stress-strain behavior of different type of soil (Kondner 1963; Al-Shayea et al. 2003). Similar to the hyperbolic representation of a stress-strain curve, it was hypothesized that the plotting of (time/EC) against time will present a straight line in form of Equation (2.5). Then the ultimate EC value (i.e., EC_r) can then be calculated by Equation (2.6). The analysis is shown in Figure 2-10, which uses Carbondale shale as an example. It can be read from the figure that $a = 0.85629$ and $b = 0.00145$.

$$\frac{t}{EC} = a + b \cdot t \quad (2.5)$$

$$EC_r = \frac{1}{b} \quad (2.6)$$

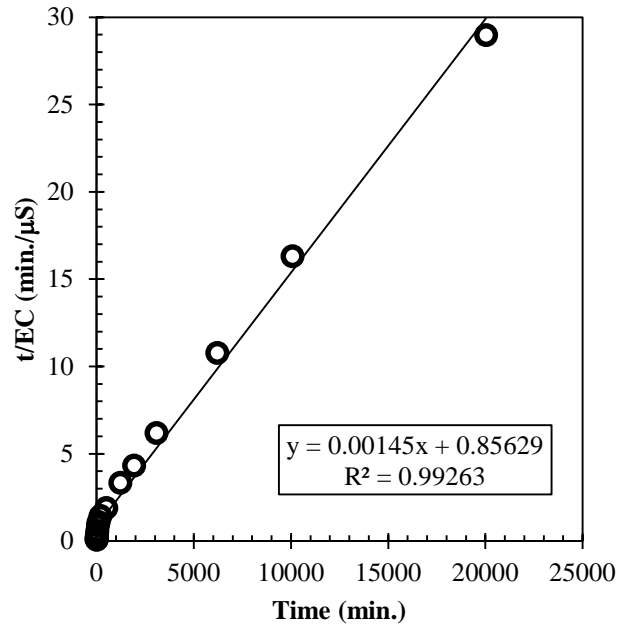


Figure 2-10 Hyperbolic representation of standard SWEC curve

Because the hyperbolic representation of the data yielded a straight line, a simplified criterion was developed to estimate EC_r that required minimal data to execute. The criterion requires two points and a coefficient, instead of using the whole data. The two points were chosen at approximately two hours and two days, respectively. The coefficient is based on the durability nature of shale, which is notated as c . Referring back to Figure 2-5, when the measured EC data are plotted in the semi-log time scale, there are usually three kinds of trends at the end of the monitoring window (i.e., 14 days) and they are described in the following three cases.

- Case 1: Clear trend is noticed that the weathering process is at the end of the primary weathering phase and the residual phase has started or is about to begin. The example is Tradewater shale.
- Case 2: The primary weathering phase has been well developed and is approaching the end, while the residual phase has not started yet. A good example is Carbondale shale.

- Case 3: The end of the monitoring window cuts the SWEC curve at certain middle point within the primary weathering phase (see Grundy shale in Figure 2-5).
- The coefficient values, c corresponding to each case are listed in Table 2-8.

Table 2-8 Chart of coefficient c to calculate EC_r

Case #	$I_d(2)$	c
1	< 90 percent	1.2
2	90 percent < $I_d(2)$ < 95 percent	1.8
3	> 95 percent	3.0

Considering the three cases described above, the EC_r can be calculated by Equations (2.7) and (2.8).

$$b' = \frac{\frac{2880 \cdot \text{min}}{EC_{2880}} - \frac{120 \cdot \text{min}}{EC_{120}}}{(2880 - 120) \cdot \text{min}} = \frac{\frac{2880 \cdot \text{min}}{EC_{2880}} - \frac{120 \cdot \text{min}}{EC_{120}}}{2760 \cdot \text{min}} \quad (2.7)$$

$$EC_r = \left(\frac{1}{b'} \right) \cdot c = \frac{2760 \cdot c}{\frac{2880}{EC_{2880}} - \frac{120}{EC_{120}}} \quad (2.8)$$

Since b is the “true” hyperbolic slope obtained by using the whole test data, b’ is referred as the modified hyperbolic slope, EC_{2880} and EC_{120} are the EC at 2 days (2880 min.) and 2 hours (120 min.), respectively. The EC_r calculated using this criterion is shown in Table 2-9.

Table 2-9 Summary of residual electrical conductivity

Geologic Name	Particle Size 0.25 / Distilled Water		
	1/b' (μS)	c	EC _r (μS)
Bull Fork	570	1.3	741
Tradewater	809	1.3	1051
Fort Payne	624	1.8	1123
Grundy	191	3.0	572
Carbondale	582	1.8	1048
Great Lake	557	1.3	724
Upper Pottsville	83	1.8	150

2.4.6.2 The A and B Parameters

It is found that the values of A and B parameters were somewhat correlated with the mineralogy data. Referring back to Table 2-3, percentage of carbonate and the mineralogy parameter, (Ch+I)/K were used to perform the correlation on the A and B parameters obtained under standard condition (i.e., distilled water and particle size 0.25), and the results are shown in Figure 2-11. The correlations can be expressed by Equation (2.9) and (2.10), both of which are power relations.

$$A = 742 \cdot (\text{Carbonate})^{-0.978} \quad (2.9)$$

$$B = 0.673 \cdot \left(\frac{Ch+I}{K} \right)^{-0.482} \quad (2.10)$$

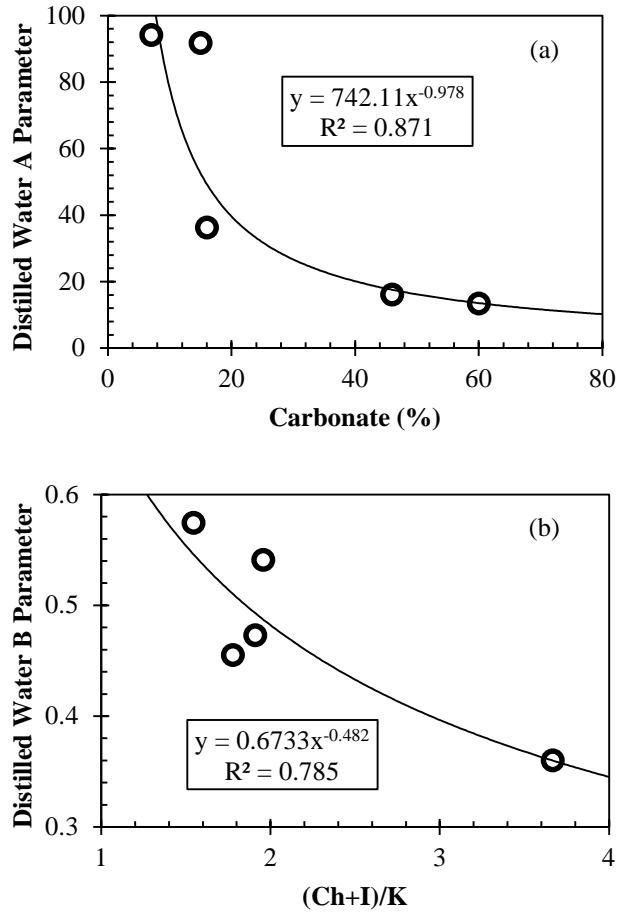


Figure 2-11 Correlations of mineralogy index with standard curve parameters: (a) A parameter and (b) B parameter

2.5 The Methods to Assess Durability

2.5.1 Correlation between Curve Rates and Durability

It was verified by this study that R_p exponentially related with LSI, which further proved that R_p presents the long-term durability of shale (Figure 2-12). It is seen that a shale with high R_p has a high LSI (i.e., low durability). Equation (2.11) can be used to estimate LSI from R_p . It was also found that the $I_d(2)$ as an index for short-term durability did not correlate well with R_p .

$$LSI = 0.0319 \cdot e^{0.0081 \cdot R_p} \quad (2.11)$$

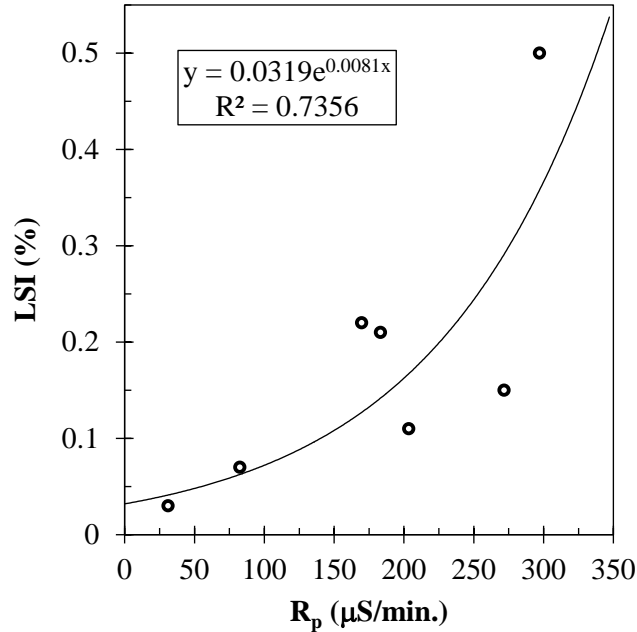


Figure 2-12 Correlation between primary weathering rate and loss slake index

A two-point method was proposed to obtain R_p with a two-day electrical jar test. The most important assumption for two-point method is that the EC of the shale-water solution will increase linearly over a certain period of time in a semi-log plot. It is known that the dissolution and primary weathering phases display different linear trends. Therefore, the two points taken have to be within the primary weathering phase to obtain an accurate estimation of the R_p . As previously stated, the process of the weathering phases can be effected by several factors, including the type of slaking fluid, the size of the specimen and also the durability natures of the test shale. When distilled water is applied as the slaking fluid, it will not be considered as an influence factor. Referring back to Figure 2-5, it was reasonable to state that most of the shale started or had proceeded into the primary weathering phase at time equal to 120 minutes. For special cases, such as when the test shale is very durable, it will take much longer time to reach the primary weathering phase, which is shown in Figure 2-5, considering Grundy shale as an example. It can be seen that the primary phase didn't happen until approximately 1000 minutes. As previously mentioned, the normalization by dividing the measured data by the initial

conductivity of the weathering fluid cannot eliminate the slaking fluid difference and it is possible to introduce uncertain errors while comparing different sets of data. The slaking fluid effects on SWEC curve needs further investigations.

Regardless of the limitations stated above, the two-point method is still recommended when limited time is allowed to perform a complete electrical jar test. The two points are recommended to be taken at 120 minutes (2 hours) and 2880 minutes (2 days) for size #0.25 specimen of this study. The equation to predict R_p by two-point method can be written as Equation (2.12).

$$R_p = \frac{EC_{2880} - EC_{120}}{\lg(2880) - \lg(120)} \quad (2.12)$$

Using the aforementioned two-point method, R_p were calculated from measurements taken at 2 hours and 2 days. To illustrate the accuracy of the two-point method, actual R_p values measured from the full SWEC curve were plotted versus the R_p obtained from two-point method in Figure 2-13.

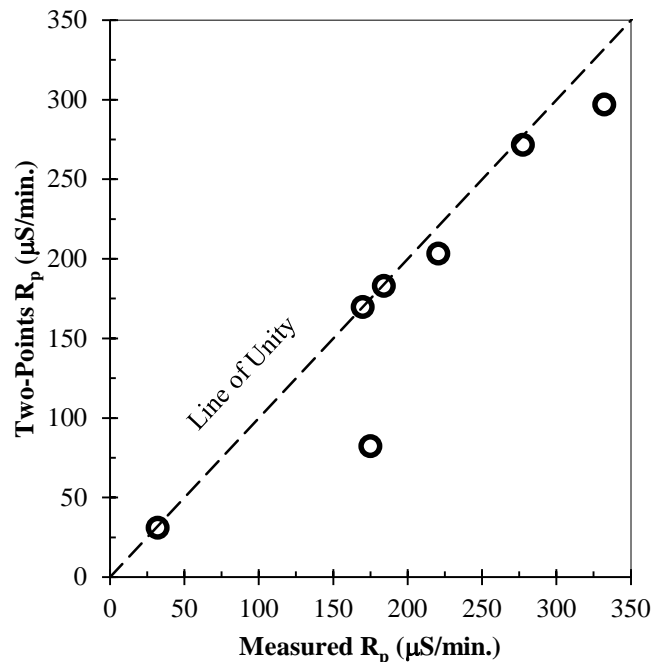


Figure 2-13 Accuracy of two-point method for estimating R_p

Figure 2-14 shows the variation of ω_n with R_p . In general, it is seen that a shale sample with a high R_p has a high ω_n , and shale with low R_p has a low ω_n , which establish ω_n as a valid property index to estimate shale durability and allow using simple index property to determine R_p . The equation of the trend line that fit through the data is given as

$$R_p = 149 + \ln(\omega_n) + 33.2 \quad (2.13)$$

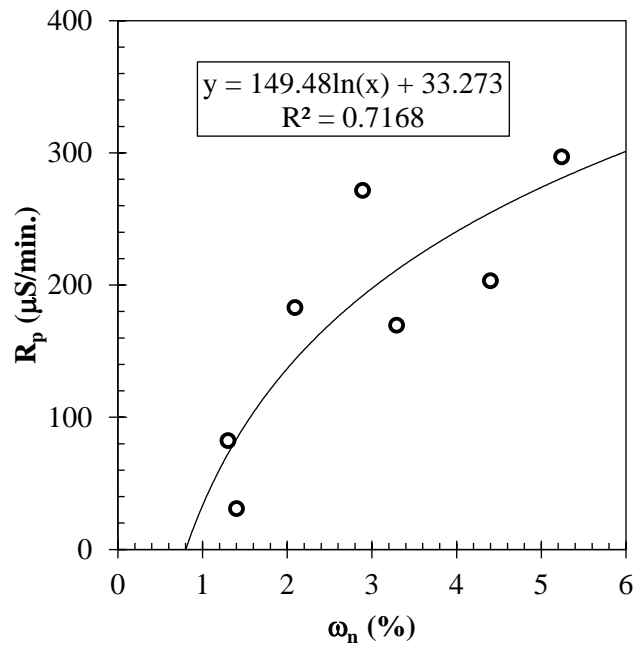


Figure 2-14 Correlations between primary weathering rate and natural moisture content

2.5.2 Correlation between Curve Parameters and Durability

Considering the limitation of two-point method because of the diversity of shale type, performing a complete electrical jar test up to 20,000 minutes (approximately 2 weeks) is beneficial, so that a full SWEC curve can be delineated. It is not only because a more accurate R_p value can be obtained, but it was also found in this study that the B parameter can be used to present the durability of shale as well. It is earlier stated in Section 2.4.6.2 that the B parameter controls the slope of the primary weathering phase, so that similar to R_p , the B parameter

correlates several shale properties, which are shown in Figure 2-15. A shale with higher B value has higher LSI (i.e., less durable) and higher compression index, C_c (i.e., easier to be compressed). As previously discussed, parameter B can be determined by mineralogy. The B parameter also tended to varying on the basis of the lithology of the shale. This behavior is shown in Figure 2-15. Bull Fork and Fort Payne are known as Marlstone, while Tradewater, Grundy and Carbondale are known as Mudstone. Based on the observed trends, Great Lake is a possible Marlstone, while Upper Pottsville is a possible Mudstone. The correlation analysis is conducted based on shale types.

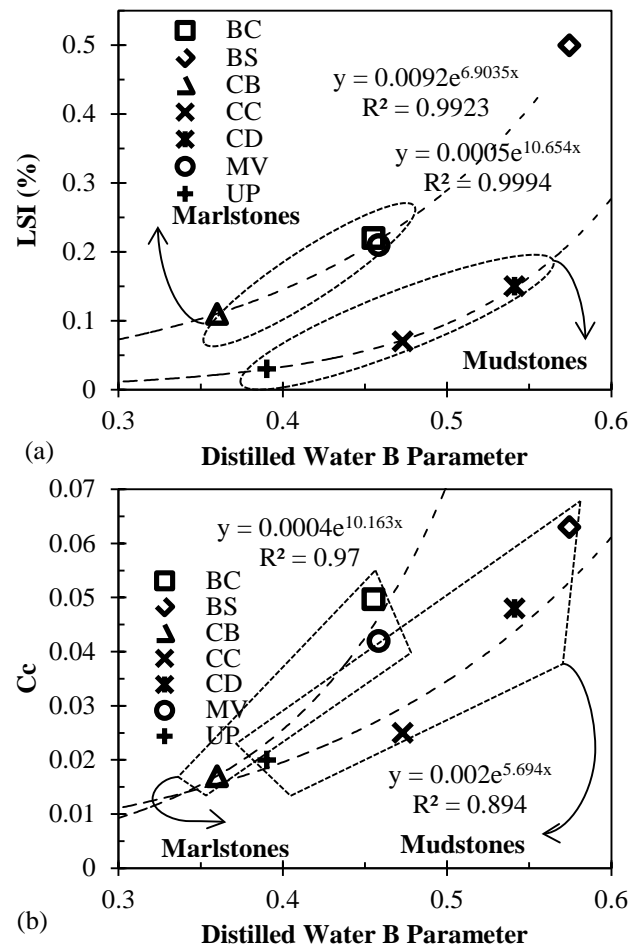


Figure 2-15 Correlations of distilled water B parameter with (a) loss slake index and (b) compression index

The equations of the trend lines in Figure 2-15 are given in Table 2-10.

Table 2-10 Equations of B parameters to estimate LSI and compression index

Marlstone	$LSI = 0.0092 \cdot e^{6.9 \cdot B}$	(2.14)
	$C_c = 0.0004 \cdot e^{10.2 \cdot B}$	(2.15)
Mudstone	$LSI = 0.0005 \cdot e^{10.7 \cdot B}$	(2.16)
	$C_c = 0.002 \cdot e^{5.7 \cdot B}$	(2.17)

3 Accessing Mechanical Behaviors of Compacted Shale by Electrical Parameters

3.1 Introduction

The term shale broadly describes indurated, non-metamorphosed sediments composed mainly of clay or silt and formed by diagenesis, which is the sum of the physical, chemical, and biological changes that take place in sediments as they become consolidated into rocks. Shale is generally categorized as mudrock and is distinguished from other mudrocks, such as siltstones, clayshales, and marlstones in that it is fissile and laminated (Richardson and Wiles 1990). Shale is often encountered in roadway cuts throughout the United States. Consequently, shale is widely used as a construction material for highway embankments. Although shale usually gives acceptable engineering behavior immediately after construction, the strength, durability, and compressibility of shale tends to deteriorate over time when exposed to wet conditions. Specifically, shale is subjected to collapse or swelling during rainy season, causing significant deformations. The shear strength of shale may also decrease as a result of annual cycles of dry and rainy seasons, which may lead to failure of road embankments and instability of slopes. Several researchers (Abeysekera et al. 1979; Manasseh and Olufemi 2008; Bryson et al. 2012) have pointed out that the deterioration of shale is primarily due to weathering effects of cyclic wetting and drying. Therefore, it is very important to quantify changes in mechanical behavior of shale caused by weathering.

Collapse of wetted compacted shale occurs when adequate vertical overburden stress is applied. The effects of water-induced collapse on compacted soil are well documented in the literature. Lawton et al. (1989) and Lawton et al. (1991) performed both double-oedometer test and double-triaxial test to study the one dimensional collapse of compacted clayey sand, which used a “soaked” sample and a “as-compacted” sample going through the same overburden pressures stages. Then the differences of strains at the same overburden pressure were measured

to be collapse or swelling. While other researchers, such as Miller et al. (1997), used single-oedometer tests to evaluate the collapse susceptibility of compact soil, which were performed in accordance with ASTM D 5333. It was found that variables having the most impact on collapse index were compaction moisture content, dry unit weight, plasticity index, and clay-size fraction (Miller et al. 2001; Lim and Miller 2004). Pappas and Vallejo (1997) developed a static-compression-creep test to study the water-induced settlement (i.e., collapse) of nondurable shale associated with coal mine waste embankments, where they found the nondurable shale absorbed 15 percent of its volume in water.

The water adsorption and swelling of shale is caused by the hydration of positive ions on the clay surface, which reduces the free energy of water and provides a driving force for swelling (Low 1961; O'Neill and Poormoayed 1980). The composition of minerals, the type of pore fluid and soil structures primarily determine the swell potential of soil, while the outside environmental conditions control the actual amount and rate of swelling (Johnson and Snethen 1978). Hopkins and Gilpin (1981) and Hopkins (1988) performed swell-deflection and swell-pressure tests on air-dried, on shale samples obtained in Kentucky using consolidometer. They found that the vertical swelling strain was a function of the percentage of clay fraction obtained from the hydrometer test. Orhan Erol and Dhowian (1990) performed oedometer tests on undisturbed shale samples from Saudi Arabia to determine free swell and swell pressure. It was suggested that the swell parameters can be predicted by geotechnical indices including liquid limit, plasticity index, in situ water content and clay content. Wong (1998) also adopted oedometer swell test on shale cores obtained from drilled hole located at Alberta, Canada. It is noticed that this research included the types and concentrations of pore fluid as an influence to study the swell behavior. Wong (1998) found that the swelling of shale was dependent on the type and concentration, stress and swelling history.

Several researchers (Spears and Taylor 1972; Taylor 1988) performed triaxial and direct shear-box tests on shale core specimens, which ranged from fresh to completely weathered. The

results showed that the effective cohesion parameter was most susceptible to the physical disintegration processes (i.e., weathering), while the effective phi angle also showed a 42 percent decrease from the fully weathered shale. Richardson and Wiles (1990) conducted consolidated undrained triaxial shear strength test on compacted shale samples, using water and silicon oil as pore fluids and based on the differences of the testing results. A shale durability rating system was developed.

Currently in the literature, there is lack of swelling and collapse tests using compacted crushed shale samples. There are also no clear standards on the specimen preparations and testing procedures for crushed shale. Lastly, the previous research efforts investigating the effects of weathering on the shear strength of compacted shale did not focus on the shear strength changes over the weathering time. The intent of this research is to develop and perform swell and collapse tests on remodeled crushed shale, and perform unconsolidated-undrained triaxial tests with different lengths of weathering time. Finally, correlations between deformation behaviors (i.e., collapse and swelling) and electrical parameters of compacted shale are found. The electrical parameters are generated from electrical jar test and shale-water electrical conductivity (SWEC) curve.

3.2 Tested Materials

In this study, seven shale samples with various durability, geological ages and formations were collected from seven different locations in Kentucky, United States. The geological and location information of the shale samples are summarized in Table 3-1.

Table 3-1 Geological information of shale sample

Geologic Name	Geologic Period	Location in Kentucky	Sample Code
Bull Fork	Ordovician	Boone County	BC
Tradewater	Pennsylvanian	Philpot	BS
Fort Payne	Mississippian	Campbellsville	CB
Grundy	Pennsylvanian	Clay County	CC
Carbondale	Pennsylvanian	Webster County	CD
Great Lake	Ordovician	Maysville	MV
Upper Pottsville	Pennsylvanian	Martin County	UP

As presented in Table 3-1, two of the samples are from the Ordovician Period (510 to 440 million years ago), which are mainly composed of limestone and located in north central Kentucky. Four of the samples are from the Pennsylvanian (325 to 290 million years ago). These shales are from the eastern and western coal fields of Kentucky, and are composed mostly of sandstone, conglomerates and coals. There is only one sample from Mississippian-age strata (360 to 325 million years ago), which is located in central Kentucky. This formation is dominated by limestone and sandstone. A Kentucky Geologic Map with the locations of test shale is shown in Figure 3-1.

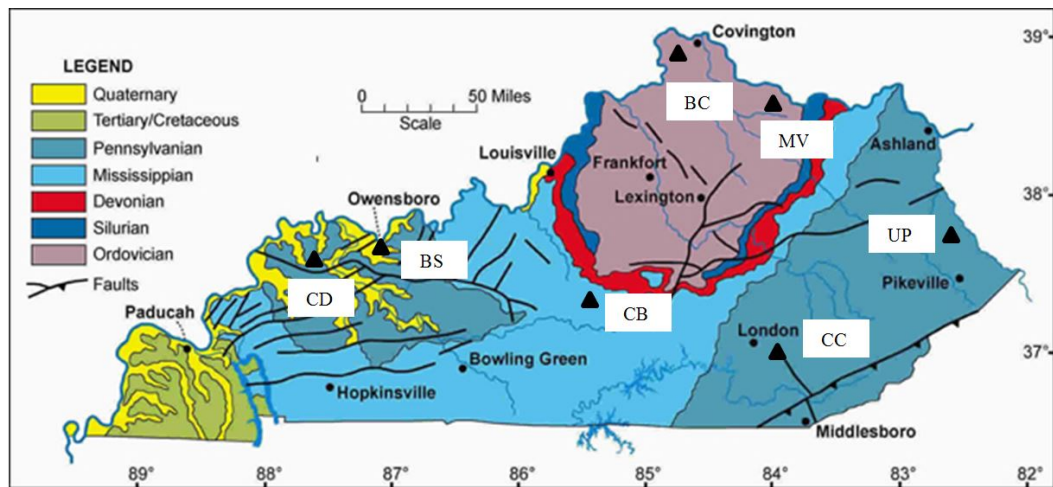


Figure 3-1 Kentucky geological map showing sample locations

Samples were collected from excavations on ongoing construction sites. The shale samples were carefully bagged or wrapped after collection to preserve the natural moisture contents. The preliminary shale size reduction was done using a jaw crusher with predetermined maximum and minimum dimensions of 15.88 mm (5/8 in.) and 9.53 mm (3/8 in.). Basic laboratory testing was performed on all shale samples. The testing included water content tests (ASTM D2216), Atterberg limits tests (ASTM D4318), one-dimensional consolidation tests (ASTM D2435), slake durability tests (ASTM D4644) and loss slake index tests (Bryson et al., 2012). The index test results and the geotechnical test results are summarized in Table 3-2.

Table 3-2 Index properties, 1-D consolidation and durability data of test shale

Geologic Name	ω_n (%)	LL (%)	PL (%)	PI (%)	C_c	C_s	$I_d(2)$ (%)	LSI (%)
Bull Fork	3.29	26	19	7	0.050	0.013	77.17	0.22
Tradewater	5.24	29	21	8	0.063	0.014	80.81	0.50
Fort Payne	4.40	25	23	2	0.017	0.009	92.62	0.11
Grundy	1.30	23	19	4	0.025	0.009	96.51	0.07
Carbondale	2.89	24	19	5	0.048	0.009	94.74	0.15
Great Lake	2.09	21	15	6	0.042	0.011	71.64	0.21
Upper Pottsville	1.40	20	18	2	0.020	0.012	94.86	0.03

ω_n = natural moisture content; LL = liquid limit; PL = plasticity limit; PI = plasticity index;
 C_c = compression index; C_s = swell index; $I_d(2)$ = slake durability index; LSI = loss slake index.

In Table 3-2, the data shows that the natural moisture contents for the shale were between 1.3 and 5.3 percent. Tradewater shale had the highest moisture content of 5.42 percent. The test shale samples had plasticity indexes from 2 to 8 percent. The range of liquid limit from 20 to 29 percent and plasticity limit from 15 to 23 percent are also shown. Tradewater shale also had the highest compression and swell indexes of 0.063 and 0.014 respectively. Both ASTM slake durability index ($I_d(2)$) and loss slake index, LSI (Bryson et al. 2012) are shown. Bull Fork shale had the lowest $I_d(2)$ of 77.17 percent, while Grundy shale had the highest of 96.51 percent. LSI are compared to $I_d(2)$ showing that LSI values are likely to be larger for less durable shale, which implies greater rate of deterioration. Both Grundy and Upper Pottsville shale have LSI less than

0.1 percent, which are ranked as the lowest among test shale. Bull Fork shale has the highest LSI of 0.22 percent.

The electrical jar test and the SWEC model were used to perform electrical and mineralogical analysis in this study. It was found that the electrical conductivity (EC) of shale-water solution as a function of time increases following a sigmoidal shape curve (i.e., SWEC curve) in the electrical jar test. The SWEC equation was written to quantitatively describe the curve.

$$EC = \frac{EC_o \cdot A + EC_r \cdot t^B}{A + t^B} \quad (3.1)$$

In Equation (3.1), EC_o is the initial EC of the slaking fluid and EC_r is the EC when time approaches infinite. The A and B parameters control the shape of the SWEC curve (i.e., the rate of slaking). The R_d and R_p parameters are the slopes of the SWEC curve at dissolution and primary weathering phases, respectively. A summary of test data obtained from electrical jar tests performed with 6.35 mm to 12.7 mm shale pieces in distilled water are presented in Table 3-3.

Table 3-3 Summary of electrical jar test

Geologic Name	Particle Size 6.35 mm - 12.7 mm / Distilled Water			
	R_d ($\mu\text{S}/\text{min.}$)	R_p ($\mu\text{S}/\text{min.}$)	A	B
Bull Fork	72.681	169.726	13.449	0.455
Tradewater	49.711	297.083	36.226	0.574
Fort Payne	79.309	203.387	16.102	0.360
Grundy	13.279	82.428	91.795	0.473
Carbondale	19.541	271.611	94.143	0.541
Great Lake	67.652	183.094	14.970	0.458
Upper Pottsville	10.102	30.997	22.809	0.390

In order to obtain additional deformation and strength properties of the shale samples, three experimental methods were used in this study, which were one-dimensional (1-D) collapse test, 1-D free swell test and unconsolidated-undrained triaxial compression (UU) test. Collapse tests

were performed on five samples (Bull Fork, Tradewater, Fort Payne, Grundy and Carbondale). Swell tests were performed on all seven samples, and the UU tests were conducted with four samples (Bull Fork, Tradewater, Grundy and Carbondale).

3.3 Deformation Behaviors of Compacted Shale

3.3.1 1-D Collapse Test on Compacted Shale

The test method for measurement of collapse potential of compacted shale in this study followed ASTM D5333 with some modifications on the specimen preparation. The collapse tests were performed using automatic consolidation apparatus. The specimens were prepared to fit into a standard consolidation ring with a 6.35 cm (2.5 inches) diameter by 2.54 cm (1 inch) height. The target dry unit weight for all test specimens was 16.28 kN/m³.

The specimen was inundated with tap water at a loading pressure of 45 kPa. A plot showing the axial strain of the specimen versus the applied loading pressure for a complete test using Carbondale as an example is shown in Figure 3-2.

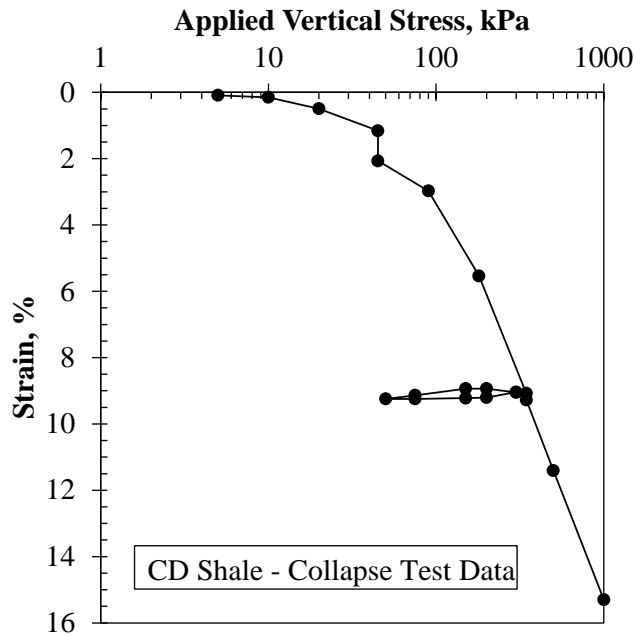


Figure 3-2 Carbondale sample compression curve of the collapse potential test

Figure 3-2 shows that there is a collapse (i.e. sudden change of axial strain) after the inundation. As described in ASTM D5333, collapse is the decrease of soil height after wetting under a constant applied vertical stress, which can be in quantity by an index called collapse potential (I_c). The I_c value can be determined at any stress level, which was determined at 45 kPa in this study. According to ASTM, I_c can be calculated as follows:

$$I_c = \frac{d_f - d_i}{h_o} \times 100 \quad (3.2)$$

where d_f is the dial reading at the appropriate stress level after wetting; d_i is the dial reading at the appropriate stress level before wetting; h_o is the initial specimen height.

A summary of the collapse potential for all tested samples are shown in Table 3-4. The free swell test results are also shown in the table. The method of free swell test will be discussed in the subsequent section. As shown in Table 3-4. Bull Fork shale has the highest I_c value, while Grundy shale has the lowest. Referring back to Table 3-2, among the five shale samples used for collapse tests, Bull Fork shale had the lowest $I_d(2)$ and Grundy shale had the highest $I_d(2)$.

Table 3-4 Summary of collapse and swelling tests

Sample Code	I_c (%)	e_{fs} (%)	t_{fs} (min.)	R_{fs} (%/min.)
BC	2.04	1.90	6	0.316
BS	1.38	6.60	60	0.110
CB	1.22	1.03	5	0.207
CC	0.38	0.73	13	0.056
CD	0.91	2.30	40	0.057
MV	-	1.64	6	0.273
UP	-	1.25	55	0.023

I_c = collapse potential; e_{fs} = free swell;
 t_{sf} = time at the end of primary swell; R_{fs} = rate of primary swell.

3.3.2 Discussion on Collapse Behavior of Compacted Shale

The collapse potential (I_c) obtained from this research increases with increasing clay-size fraction (CF, percentage of mass of particles less than $2 \mu m$), liquid limit (LL), plasticity index (PI). Similar relationships have been reported by previous researchers (Lawton et al. 1992; Rao and Revanasiddappa 2000; Lim and Miller 2004). It is important to note that the CF used in this study is not a “natural” index. The “natural” or “true” CF is determined by fractionation procedures suggested by Pansu and Gautheyrou (2007). In this study, the CF was produced by the compaction method developed by (Gomez-Gutierrez 2013), in which the compaction technique ensured that all shale samples were crushed by the same amount of energy through the same procedure. The clay size particles produced is dependent on the relative hardness of the shale. To prevent any confusion, Bryson et al. (2012) suggested the crushed material smaller than $2 \mu m$ be referred to as the dust friction (DF). A plot of I_c versus DF along with the logarithmic trendline is shown in Figure 3-3.

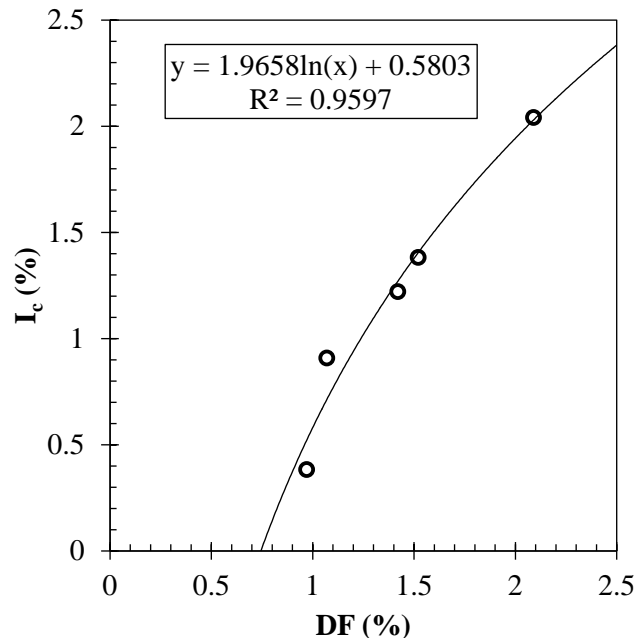


Figure 3-3 Variation of collapse potential as a function of dust fraction

As it can be seen in Figure 3-3, the collapse potential is highly correlated with the dust friction, as evident by a coefficient of determination (R^2) of 0.96. This high degree of correlation allows an empirical expression to be developed as given by Equation (3.3).

$$I_c = 1.966 \cdot \ln(DF) + 0.5803 \quad (3.3)$$

Figure 3-4 presents plots of I_c versus LL and PI. Although specific correlations are not evident from the data, it is observed that the general trend shows that the I_c increased with increasing LL and PI. It is noted that the data tended to group together according to different geological periods.

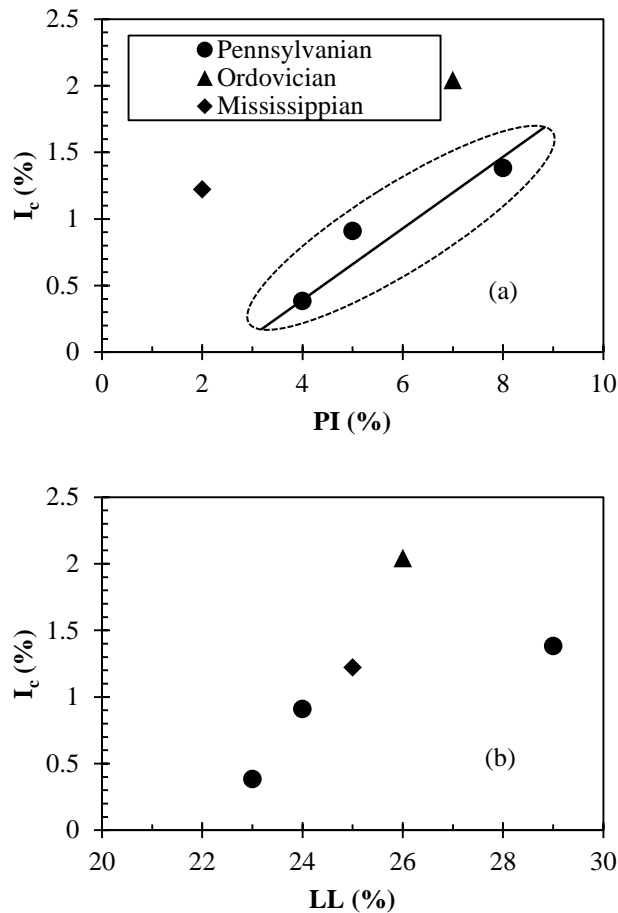


Figure 3-4 Variation of collapse potential and index properties: (a) PI and (b) LL

The collapse potential typically fully developed within 100 minutes after the inundation of the tested samples. The electrical jar test and SWEC curve introduced a definition of the dissolution phase, which usually happened in 200 minutes after the mixture of water and shale. The relationship between the instant collapse deformation induced by water and the electrical parameters from SWEC curve was evaluated. It is found that the dissolution rate, R_d was strongly related to I_c [Figure 3-5(a)]. The shale has a higher value of R_d showed a higher potential of collapse. An equation to estimate collapse potential from R_d is given.

$$I_c = 0.086 \cdot R_d^{0.686} \quad (3.4)$$

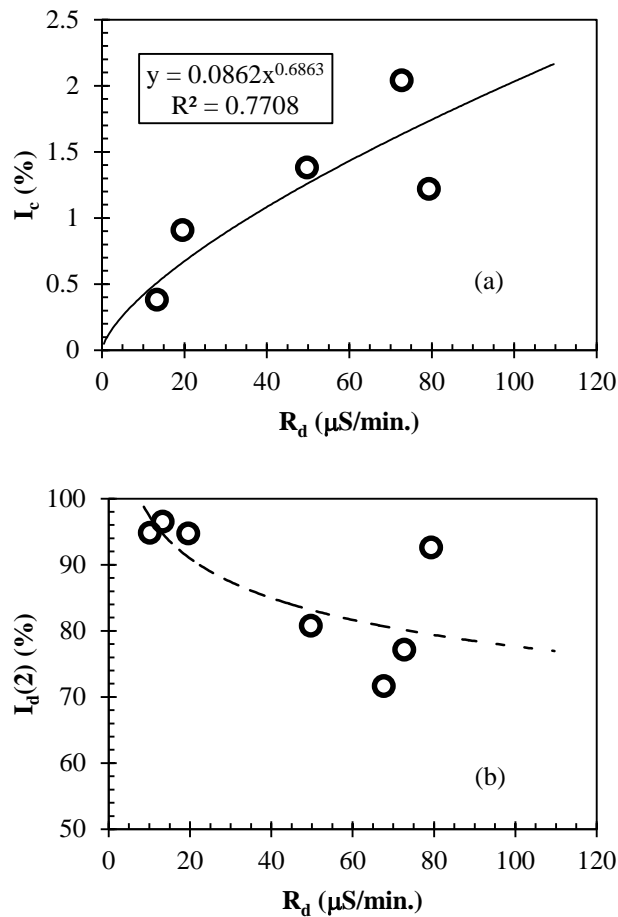


Figure 3-5 Correlations of R_d with (a) collapse potential and (b) slake durability index

R_d is very easy to be obtained from laboratory testing. Simple testing procedures include taking electrical conductivity measurement at 2 minutes and 15 minutes. The slope of the conductivity change between the 2 measurements is equal to R_d . Similar to the slake durability index [$I_d(2)$], R_d presents an instant (i.e., within 60 min.) change of shale properties after weathering. These two variables are possibly related. The correlation between $I_d(2)$ and R_d are shown in Figure 3-5(b), which presents that a shale with lower R_d has a less durable performance in the slake durability test. It is reasonable that those durability indexes focusing on the rate of deterioration or long-term weathering effects, such as LSI and R_p , don't correlate well with the water-induced collapse of shale.

3.3.3 1-D Free Swell Test on Compacted Shale

The method to measure 1-D free swell of compacted shale follows ASTM D4546, Method A. The test sample used for the free swell tests was 63.5 mm (2.5 in.) in diameter and 25.4 mm (1 in.) in height. As with the collapse tests, the targeted dry unit weight was 16.28 kN/m³.

The weight of the loading plate on top of the specimen plus the top porous stone and the loading ball is 222.4 g, which applied an original loading pressure of 0.689 kPa. An additional 0.5 kPa was applied as a seating pressure for 1 hr before inundating the specimen, which resulted in a total seating pressure of 1.189 kPa. According to the definition provided by ASTM D4546, the magnitude of free swell is the swell strain following the absorption of water at a near zero seating pressure of 1 kPa. The actual seating pressure of 1.189 kPa was small enough to be considered as a free-swell condition. Tap water was used to inundate the shale in this study.

The specimen completely submerged under water at all times and the seating pressure remained constant as the changes in the specimen height were measured throughout the testing. The test periods were at least 24 hours to have adequate time for the primary swell to be finished. A typical swell-time curve is shown in Figure 3-6 using Sample Carbondale as an example, which started with relatively faster swelling (i.e., primary) and followed by slower swelling (i.e.,

secondary). All specimens finished the primary swell within one hour. Tradewater shale had the highest free swell, 6.6 percent, while Grundy shale had the lowest free swell, 0.73 percent. A summary of the free swell for all tested samples are shown in Table 3-4, where the time at the end of primary swell and rate of the primary swell versus time are also listed.

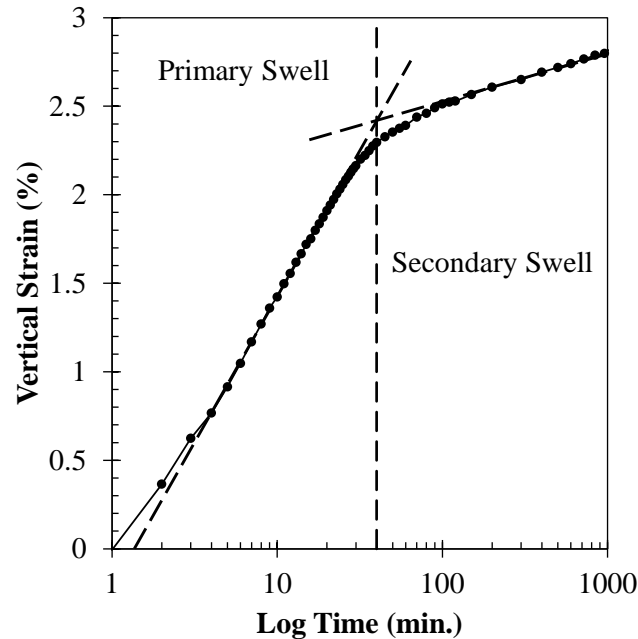


Figure 3-6 Swell-time curve of Carbondale shale

3.3.4 Discussion on Swelling Behavior of Compacted Shale

The free swell data obtained from this study showed that shale with higher plasticity index, compression index and natural moisture content tends to have a higher value of free swell. These relations are shown in Figure 3-7 and Table 3-5. It can be seen that the values of R^2 are very high, which implies that PI and C_c can be used to estimate the free swell of compacted shale. Similar relationships were documented by pervious researchers (Abdullah et al. 1997; Gomez-Gutierrez et al. 2011).

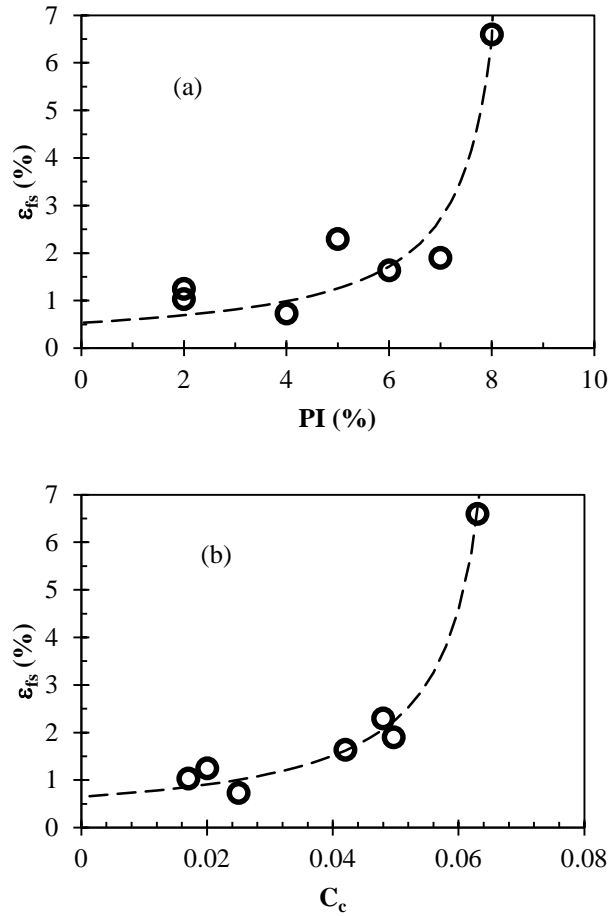


Figure 3-7 Variation of Free Swell with (a) Plasticity Index and (b) Compression Index

Table 3-5 Equations to determine free swell by (a) PI, and (b) C_c

(a)	$\varepsilon_{fs} = (1.867 - 0.214 \cdot PI)^{-1}$	$R^2 = 0.907$	(3.5)
(b)	$\varepsilon_{fs} = (1.545 - 22.112 \cdot C_c)^{-1}$	$R^2 = 0.984$	(3.6)

It is also found that the free swell correlates very strong with R_p and B parameter from SWEC curve (Figure 3-8 and Table 3-6). With R^2 values over 0.9, the empirical equations to calculate free swell is expressed as equation (3.7) and (3.8). Higher values of R_p and B both indicate less durability of shale, which means a higher swelling capability.

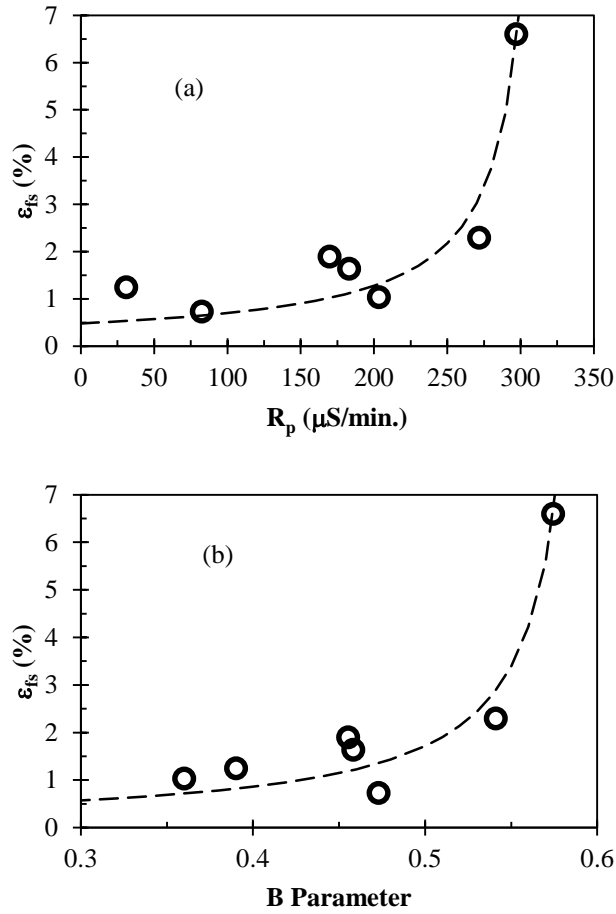


Figure 3-8 Variation of free swell with (a) R_p and (b) B Parameter

Table 3-6 Equations to determine free swell by (a) R_p and (b) B parameter

(a)	$\varepsilon_{fs} = (2.072 - 0.006 \cdot R_p)^{-1}$	$R^2 = 0.903$	(3.7)
(b)	$\varepsilon_{fs} = (3.471 - 5.775 \cdot B)^{-1}$	$R^2 = 0.929$	(3.8)

3.4 Shear Behaviors of Compacted Shale

3.4.1 UU Test on Compacted Shale

In this research, the UU tests on compacted shale were performed following ASTM D2850 with modifications on preparation of specimen and pressure control methods suggested by

Gomez-Gutierrez (2013). All tests were conducted with different time variables of weathering, which means different lengths of soaking time before shearing the specimens.

The targeted diameter for the cylindrical test specimen was 70 mm with a height of 150 mm. The grain size distribution of the test specimen and the targeted dry unit weight were the same as used for the collapse tests. A detailed procedure on preparing the cylinder specimen can be found in Gomez-Gutierrez (2013). The test had three phases; the flooding phase, the soaking phase and the shear phase.

In the flooding phase, 20.7 kPa (3 psi) cell pressure and 13.8 kPa (2 psi) sample pressure were applied to the specimen, which resulted in an effective pressure 6.895 kPa (1 psi). This was created to flood the specimen while minimizing the disturbance of the specimen. The sample pressure difference made the water flow into the specimen from bottom and out from top, and air will not be trapped in the specimen. The water used to flood the specimen was tap water. The flooding phase was designed to saturate the specimen as much as possible. In most tests, about 750 mL water was pumped into the specimen and about 450 mL water flowed out of the specimen, and there was no air bubbles observed to flow out of the specimen at the end of flooding phase.

All sample valves were closed at the end of the flooding phase and during the soaking phase, to avoid any volume change of the specimen. The time variables were selected as “no weathering”, 1 hour, 2 hours, 2 days and 14 days. These times were selected based on the SWEC curve of electrical jar test. The “No weathering” meant that the specimen was placed into the shear phase immediately after the flooding. However, since the applied sample pressure needed time to be stabilized, the actual “no weathering” time was about 5 to 15 minutes before the beginning of the shear phase, which is approximately within the dissolution phase on the SWEC curve. 1 to 2 hours, 2 days and 14 days are approximately the switch point between dissolution and primary weathering phases, during the primary weathering phase and the end point of the electrical jar test monitoring period, respectively.

At the beginning of shear phase, all sample pressure and cell pressure inlet valves were reopening. Cell pressure 20.7 kPa (3 psi) and sample pressure 13.79 kPa (2 psi) were applied to the specimen. It usually took 5 to 15 minutes to reach target pressures. After the stabilization of pressures, the samples pressure valves were closed and the piston holding the top of the specimen and transferring the normal stress was unlocked, which was clocked at all times before the shear phase to avoid any volume change of specimen. The specimen was then sheared with a rate of 0.3 percent/minute, until the target axial strain of 30 percent was achieved.

The same procedure was repeated for four samples with four of five time variables of each. Typical stress-strain curves with four time variables for the UU test is shown in Figure 3-9 with Carbondale as an example. As seen in Figure 3-9, the maximum principal stress difference (i.e., deviator stress) continued to increase throughout testing. The term “failure” defined by ASTM D2850 is that failure is often taken to correspond to the maximum deviator stress attained or the deviator stress at 15 percent axial strain, whichever is obtained first during the performance of a test. No maximum deviator stress was reached before 15 percent of axial strain, so the failure shear stresses in this research were determined at 15 percent axial strain. The Tresca failure criterion is used to interpret the undrained shear strength (s_u), which says that s_u is one-half the principal stress difference at failure.

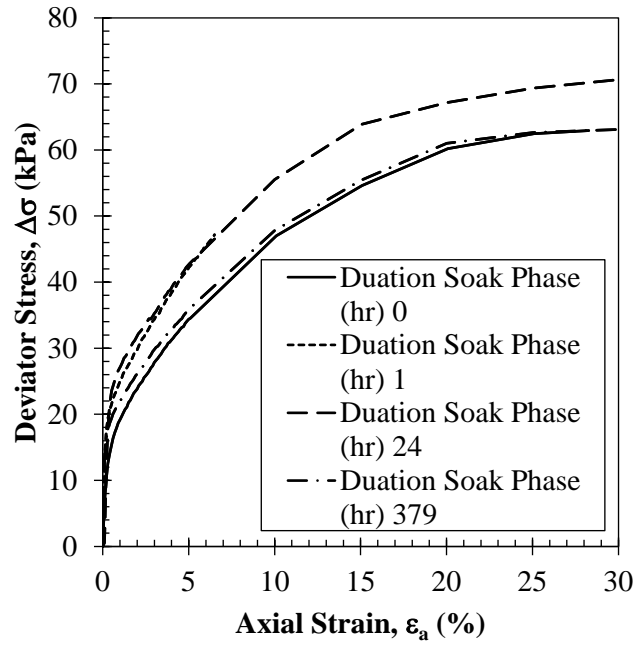


Figure 3-9 Stress-Strain Curves with Time Variables of Carbondale Shale

3.4.2 Discussion on Shear Behavior of Compacted Shale

As seen in Figure 3-10, all shale samples showed similar trend of s_u with respect to time. Specifically, Bull Fork shale presented a different behavior. Bull Fork shale has the highest fine content among all tested shale, which was about 5.8 percent, while the fine contents of the other shale were less than 4.3 percent. The difference in fine content introduces significant variations in flooding phase. It usually took about one hour to finish the flooding phase for most samples. However the same volume of water took as long as three hours to flood the Bull Fork shale. The actual flooding time also depended on how uniformly the shale sizes were mixed. Due to the abnormal lengths of flooding time, the UU tests results of Bull Fork shale were not regarded as a true representation of the changes in shear strength over weathering time.

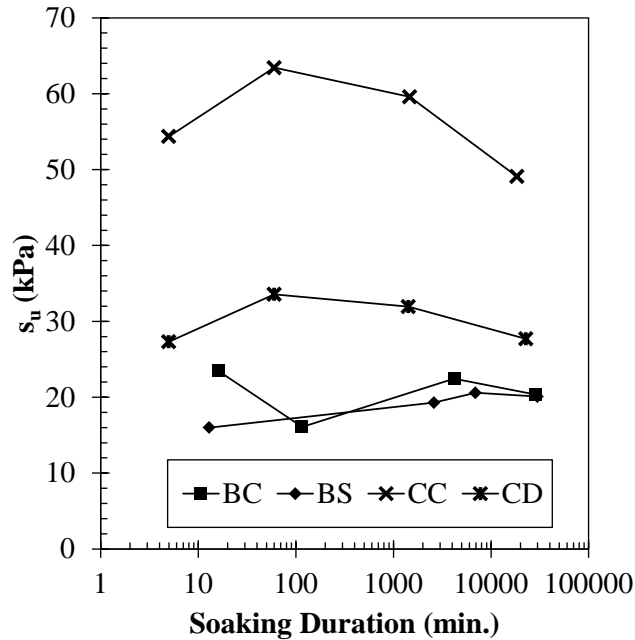


Figure 3-10 Undrained Shear Strength vs. Weathering Time for All Tested Samples

Comparing to the initial condition (i.e., “no weathering”), the shear strength of compacted shale experienced an increase and then decrease over time. It is illustrated that additional bonding between shale particles was created during the primary weathering phase and such bonding was then damaged over time in the primary weathering phase. The fine content of compacted shale might fill the spaces between larger shale particle and form cementing bonds. The weathering techniques adopted in this study simulates slaking. During the primary weathering process, physical disintegration is considered to be the control over chemical effects (Taylor 1988) on shear strength. Taylor pointed out that under saturation conditions entrapped air is pressurized as water is drawn into the shale by capillarity. The slaking process will thus cause the skeletal structure to be stressed. Van Eeckhout (1976) concluded that because internal discontinuities of shale progressively lengthened following wetting and drying, increasing water content would be permitted in the shale mass. As a result, less fracture energy would be required to fail the shale.

4 Shear Behavior of Weathered Compacted Shale

4.1 Introduction

In the United States and around the world, shale is widely used as a construction material for road embankments due to the lack of other more appropriate materials. The embankments constructed with compacted shale are often associated with high repair and maintenance cost, because shale tends to degrade with time due to weathering. The degradation causes that the shale changes from a hard rock-like material with high strength into a soft fine-grained soil mass with low strength and high deformability. This process usually occurs over a long period of time, resulting in excessive settlement, and local and global instability. The more serious problem typically occurs in those areas where the shale is subjected to repeated cycles of wetting and drying (Strohm Jr et al. 1978).

The common procedures applied in the construction of embankment is firstly breaking or crushing the shale mass into smaller pieces, and then compacting to specified water content and dry unit weight. Therefore, the behavior of the compacted shale is strongly influenced by the grain size distribution (GSD) of the broken shale, the compaction energy employed as well as the material properties of the shale.

Previous researchers (Abeyesekera et al. 1979; Witsman and Lovell 1979; Lovell and Johnson 1980; Oakland and Lovell 1982; Nwabuokey and Lovell 1986) have carried out studies of durability classification of shale and mechanical behavior of compacted shale embankments. Specifically, Abeyesekera et al. (1979) performed isotropic consolidated undrained triaxial (CIU) tests on “fresh” unweathered compacted New Providence shale collected from the state of Indiana. During the tests, the GSD of the crushed shale, water content, dry unit weight, compaction energy and the dimension of the specimen were controlled. These researchers found

that the compaction process imparted an as-compacted pressure to the shale. When the effective triaxial consolidation pressure was smaller than the as-compacted pressure, the compacted shale behaved as highly overconsolidated (OC) clay. When the consolidation pressure was equal or nearly equal to the as-compacted pressure, the behavior was similar to normally consolidated (NC) clay. The significance of this finding is that NC soils typically experience more deformation and exhibit lower shear strength than OC soils. This suggests that shear behavior of compacted shale is heavily dependent on the compaction energy. Liang and Lovell (1983) studied the behavior of samples taken from shale embankments and the relationships between shear strength, water content, dry unit weight, roller type and number of roller passes. It was found that the water content had a major influence on shear behavior. Samples with lower water content tended to be stiffer and were more likely to dilate at small strains.

Although the aforementioned studies were focused on short-term (i.e., immediately after construction) shear behavior, long-term behavior effected by weathering is more critical to shale-constructed structures. Several researchers (Wu et al. 1993; Yoshida and Hosokawa 2004; Aziz et al. 2010) have studied the water-induced granular decomposition of crushed shale. It was found that saturated crushed shale showed a greater loss of strength in comparison with dry compacted shale, and that saturated shale exhibited density-dependent behavior. Other researchers (Alonso et al. 1990; Pinyol et al. 2007; Alonso and Cardoso 2010) have investigated the effects of structure losing due to weathering on the mechanical behavior of shale. However, not many studies have specifically focused on the various shear strength interpretations of weathered compacted shale.

This paper re-interprets the data from index and mechanical tests conducted by Hopkins and Deen (1984) and Hopkins (1988) on nine different types of shale from the commonwealth of Kentucky. The shale samples were chosen to represent diverse hardness, geological ages and formations. The shale samples were taken from talus piles that had accumulated near the bottom of the highway cut sections, which are able to simulate the conditions of these materials after

several years in an embankment. This paper describes the shear behavior of weathered compacted shale and how the compaction energy affects the behavior. The shear behaviors are described using fundamental soil mechanics theory. Shear strength parameters are calculated and used to compare to various material properties obtained from laboratory experiments.

4.2 Critical State Shear Strength Theory

As was stated previously, the shear behavior of weathered compacted shale will be described using soil mechanics theory. It is therefore noted that when a soil is loaded, it goes through different stress states that are functions of the properties of the material and its stress history. These stress states result in different mechanical behavior. Specifically, when shear stresses are applied, the material can reach various post-yield states which can be called failure. The most appropriate definition of failure in soil mechanics depends on the type of construction and the stress conditions during service life of the geotechnical system. In this paper, critical state theory will be used to describe the failure of weathered compacted shale.

When soil is sheared under drained or undrained conditions to large strains, it will reach an ultimate state (i.e., critical state) of perfect plasticity, which is characterized by continuous shear deformation at constant volume or constant effective stress. Critical state is a failure state independent of stress history and drainage conditions and is a material property of soil. The critical state failure criterion is described in Figure 4-1. In the figure, failure is represented by the critical state line (CSL), which has an intercept through the origin and slope given by the effective critical state friction angle, ϕ'_c . The CSL is given by equation (4.1).

$$\tau_{ff} = \sigma'_{ff} \cdot \tan(\phi'_c) \quad (4.1)$$

Where τ_{ff} is the shear stress on the failure plane at failure (i.e., the shear strength) and σ'_{ff} is the normal stress on the failure plane at failure.

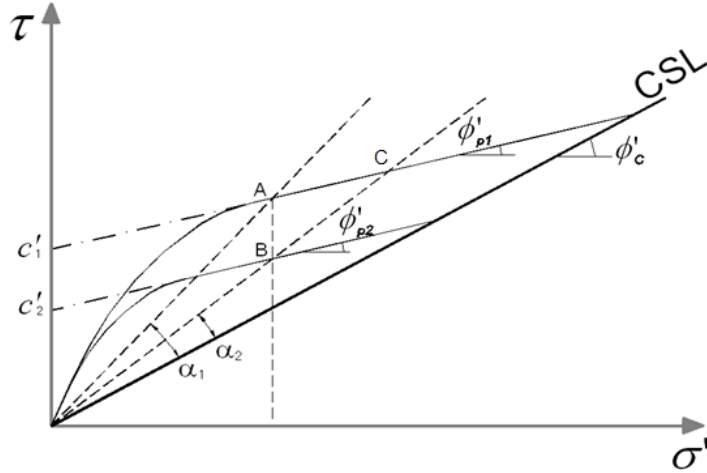


Figure 4-1 Critical state of compacted shale

One special condition of critical state occurs when saturated soil is loaded under undrained condition and reaches a state of constant effective stress during continued shear. This failure condition is described by Tresca failure criterion, which states failure is accomplished when the stresses reach a point of one half of the maximum principal stress difference, $(\sigma'_1 - \sigma'_3)_{\max}$, where σ'_1 is major principal stress and σ'_3 is minor principal stress. The failure shear stress is referred to as the undrained shear strength, s_u . Tresca failure criterion is given in equation (4.2).

$$s_u = \frac{(\sigma'_1 - \sigma'_3)_{\max}}{2} \quad (4.2)$$

It has been found that for NC soil, s_u is proportional to the effective overburden pressure, σ'_{ov} (Grace et al. 1957; Mesri 1989). Therefore, the ratio of s_u over σ'_{ov} for NC soil, $(s_u / \sigma'_{ov})_{NC}$, is a stress-dependent property that describes s_u for any stress condition at constant void ratio, e . For OC soil, Ladd and Foott (1974) found that s_u / σ'_{ov} was not constant but is related to $(s_u / \sigma'_{ov})_{NC}$ through the overconsolidation ratio, OCR by equation (4.3).

$$\left(\frac{s_u}{\sigma'_{ov}} \right)_{OC} = \left(\frac{s_u}{\sigma'_{ov}} \right)_{NC} \cdot OCR^m \quad (4.3)$$

Where $OCR = \sigma'_c / \sigma'_{ov}$, σ'_c is the preconsolidation pressure and m is a material constant (Ladd and Foott 1974; Jamiolkowski 1985; Ladd 1991).

When the initial condition of soil is such that there is an increase in the pore pressure under undrained shearing or the specimen is compressed under drained shearing, the material reaches the critical state on the right side of CSL, which is also referred to as wet side. This occurs on soil that is NC, slightly OC or has high water content. Otherwise, when the pore pressure decreases under undrained shearing or the sample dilates under drained shearing, soil reaches the critical state on the left side of CSL, i.e., the dry side. This kind of soil is heavily OC or has low water content. Dry-side soil reaches the point of maximum stress obliquity before reaching the critical state. In this case, the soil comes to the peak state located above the CSL. With additional shearing the soil will reach the critical state.

4.3 Experiments and Results

This study utilized data from laboratory tests conducted by Hopkins and Deen (1984) and Hopkins (1988) on nine shale samples from Kentucky. These shale samples were taken from talus piles which had accumulated near the bottom of highway cut sections. These materials were assumed to represent the natural conditions of the compacted shale after several years in the embankments. The geologic information of the tested shale samples are summarized in Table 4-1. Index, compaction and triaxial tests were performed on all shale samples. The index testes were done according to ASTM procedures. Three kinds of compaction tests were used, standard effort (ASTM D698, method A), modified effort (ASTM D1557, method A) and a low-energy method,

which is equivalent to 20 percent of the energy used by standard effort. The low-energy method was developed by Hopkins (1984), using an 8.2 N aluminum hammer, a 305 mm drop height, three layers, and 15 blows per layer. The isotropic consolidated undrained compression (CIU) tests were performed following ASTM D4767. The complete procedures of sampling and testing are described by Hopkins (1988) and Bryson et al. (2011). The results of tests are re-interpreted in Section 4.3.1 to 4.3.3.

Table 4-1 Tested shale and index properties

Geologic Name	Geologic Period	Descriptions	LL (%)	PI (%)	G _s	Fine (%)	CF ¹ (%)	USCS ²
New Albany	Devonian	Hard black shale	NP ³	NP	2.5	88	14	ML
Hance	Pennsylvanian	Hard medium gray shale	NP	NP	2.7	87	8	ML
Upper Drakes	Ordovician	Hard gray shale	24	15	2.9	85	21	CL
Nancy	Mississippian	Medium hard gray shale	31	11	2.7	98	25	CL
Osgood	Middle Silurian	Hard gray shale	26	7	2.7	96	26	CL
Crab Orchard	Silurian	Soft olive-gray shale	38	14	3.7	98	33	CL
Kope	Ordovician	Soft gray clay shale	30	8	2.8	96	34	CL
Newman	Mississippian	Soft gray shale	35	12	2.7	93	32	CL
New Providence	Mississippian	Soft greenish-gray shale	40	15	2.6	97	31	CL

1: CF = percentage smaller than 0.002 mm; 2: USCS = Unified Soil Classification System;
3: NP = non-plastic

4.3.1 Index Tests

The results of the index tests are summarized in Table 4-1. The descriptions of shale hardness listed in the table were based on the qualitative classification method by Brown (1981). The New Albany and Hance shales had 88 and 87 percent of fines (percentage pass #200 sieve) and they were non-plastic (NP). They are classified as low plasticity silt, ML. Also, these two shale samples have the lowest clay fraction among all the shale (14 percent and 8 percent respectively). These facts indicate that New Albany and Hance did not have high content of clay minerals and probably had high colloidal quartz content. The other shales have 85 percent to 98

percent of fines, the liquid limit (LL) ranged from 24 percent to 40 percent and the plasticity index (PI) ranged from 7 percent to 15 percent. Therefore, these shales classify as low plasticity clays, CL. The specific gravity ranged between 2.5 and 2.9.

4.3.2 Compaction Tests

The results of compaction tests are shown in Table 4-2. The table shows the values of optimum water content, ω_{opt} and the maximum dry unit weight, $\gamma_{d(max)}$.

Table 4-2 Optimum water content and maximum dry unit weight at three compaction energy

Geologic	Modified		Standard		Low	
Name	ω_{opt} (%)	$\gamma_{d(max)}$ (kN/m ³)	ω_{opt} (%)	$\gamma_{d(max)}$ (kN/m ³)	ω_{opt} (%)	$\gamma_{d(max)}$ (kN/m ³)
New Albany	12.6	17.7	19.8	15.2	22.0	15.1
Hance	8.7	21.0	11.8	19.6	15.5	18.5
Upper Drakes	6.6	22.5	10.3	20.5	13.4	19.6
Nancy	7.2	21.1	12.2	18.8	16.2	17.5
Osgood	6.8	21.7	10.5	19.5	15.5	18.6
Crab Orchard	7.5	20.8	11.4	18.6	18.1	17.4
Kope	7.6	20.7	13.0	18.3	14.2	17.1
Newman	10.3	19.8	15.0	17.9	19.7	16.5
New Providence	8.0	20.0	11.4	17.7	17.8	16.5

In order to illustrate the compaction behavior, two examples of typical test results are presented in Figure 4-2, which shows the typical different compaction behavior between hard shale (Hance) and soft shale (Newman). The figure shows that Hance shale reached a $\gamma_{d(max)}$ at a lower ω_{opt} than Newman shale, and Hance shale had a higher $\gamma_{d(max)}$ than Newman shale. As expected, Figure 4-2 shows the dependences of dry unit weight and water content on the compaction energy, where the highest energy carries the highest $\gamma_{d(max)}$ and the lowest ω_{opt} .

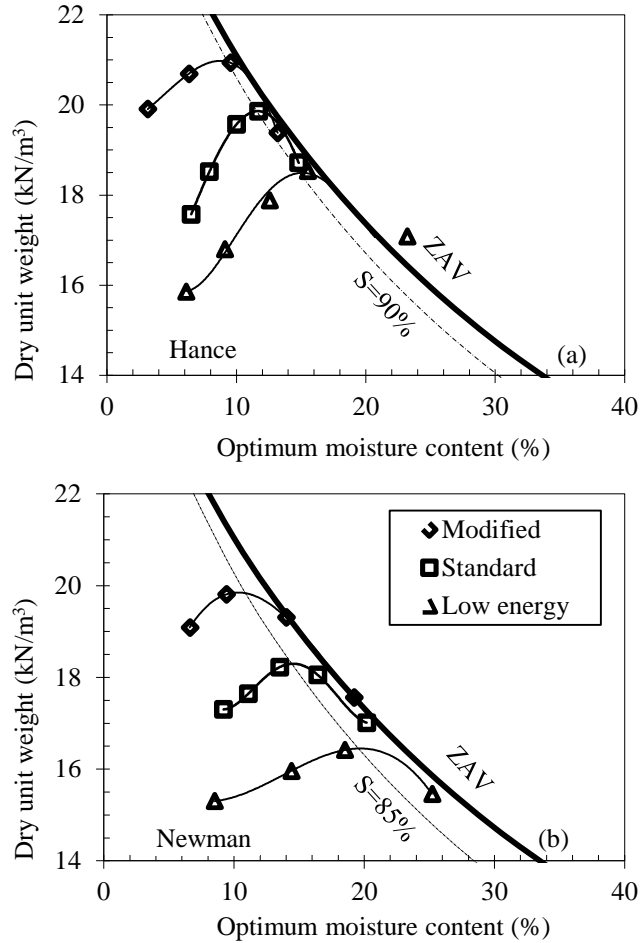


Figure 4-2 Typical compaction curves of (a) Hance and (b) Newman shale samples

4.3.3 CIU Tests

For each compaction energy, at least three (3) CIU tests were performed at different isotropic consolidation pressure (i.e., cell pressure during the isotropic consolidation phase, which is also the initial mean effective stress for the shear phase), which implies that for each weathered compacted shale at least nine (9) CIU tests were performed. The isotropic consolidation pressure ranged from 206.84 kPa to 482.63 kPa. The stress path graphs were used to present the shear behaviors of compacted shale, which describe the stress and pore-water pressure response of a soil under different stress regimes. The nomenclature used here to describe the stress path is derived from the stress invariant concept, which can be applied to any stress condition. The stress

condition for each point is given in q-p' space, where p' is effective mean stress that is the average effective stress on the sample, and q is the deviatoric stress that is distortional stress or stress difference on the sample (Budhu 2011). For axisymmetric conditions of a triaxial test, the mean effective stress is given by $p' = (\sigma'_1 + 2 \cdot \sigma'_3) / 3$, the deviatoric stress is given by $q = \sigma'_1 - \sigma'_3$. Figure 4-3 shows the stress paths of the CIU tests performed on the specimens of Hance and Newman shale compacted to modified, standard and low energies with the isotropic consolidation pressure of approximately 400 kPa. Figure 4-3 shows that for both samples and three energies of compaction, the stresses followed different paths that were functions of the change in the increment of the pore water pressures due to the increment in the deviatoric stresses.

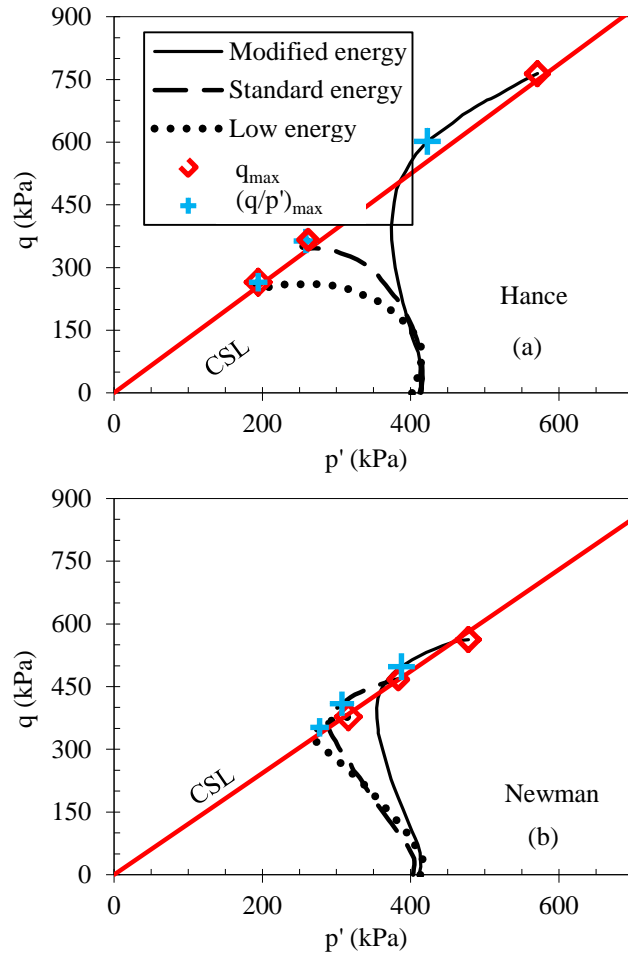


Figure 4-3 Typical stress paths of compacted shale consolidated at 400 kPa - (a) Hance and (b) Newman shale

According to Figure 4-3, the Hance samples compacted to standard and low energies presented positive increments in the pore water pressure. These increments caused the stress paths to veer left towards the points of maximum deviatoric stresses, q_{max} . In the condition that the Hance samples were compacted to modified energy, negative increments in the pore water pressure occurred, which caused the stress paths to veer right. These samples reached the point of maximum stress obliquity, $(q/p')_{max}$, before they reached the point of q_{max} . It is shown in Figure 4-3 that the q_{max} points create a line with intercept of the origin and a slope given by M , where M

= q_{max}/p' . The samples reached a condition of stress that was independent of compaction energy, which means that the samples reached the critical state when they reached the point of q_{max} .

In a similar fashion, Figure 4-4 shows the same stress paths of all CIU tests performed on Hance and Newman shales, which were plotted for each one of the compaction energy with all consolidation pressures. The stress paths of Hance shale show heavily overconsolidated (OC) response for all samples compacted to modified energy. For samples compacted to standard energy and consolidated at low pressure (between 200 kPa and 400 kPa), the responses were heavily OC, while samples consolidated at higher pressure (greater than 400 kPa) responded as slightly OC soil. Hance shale compacted to low energy displayed normally consolidated (NC) behavior. Similar behaviors were observed for Newman shale. Heavily OC behaviors were observed for the modified energy stress paths consolidated at low pressures; while tests compacted to standard and low energy and consolidated at high pressures has slightly OC behaviors.

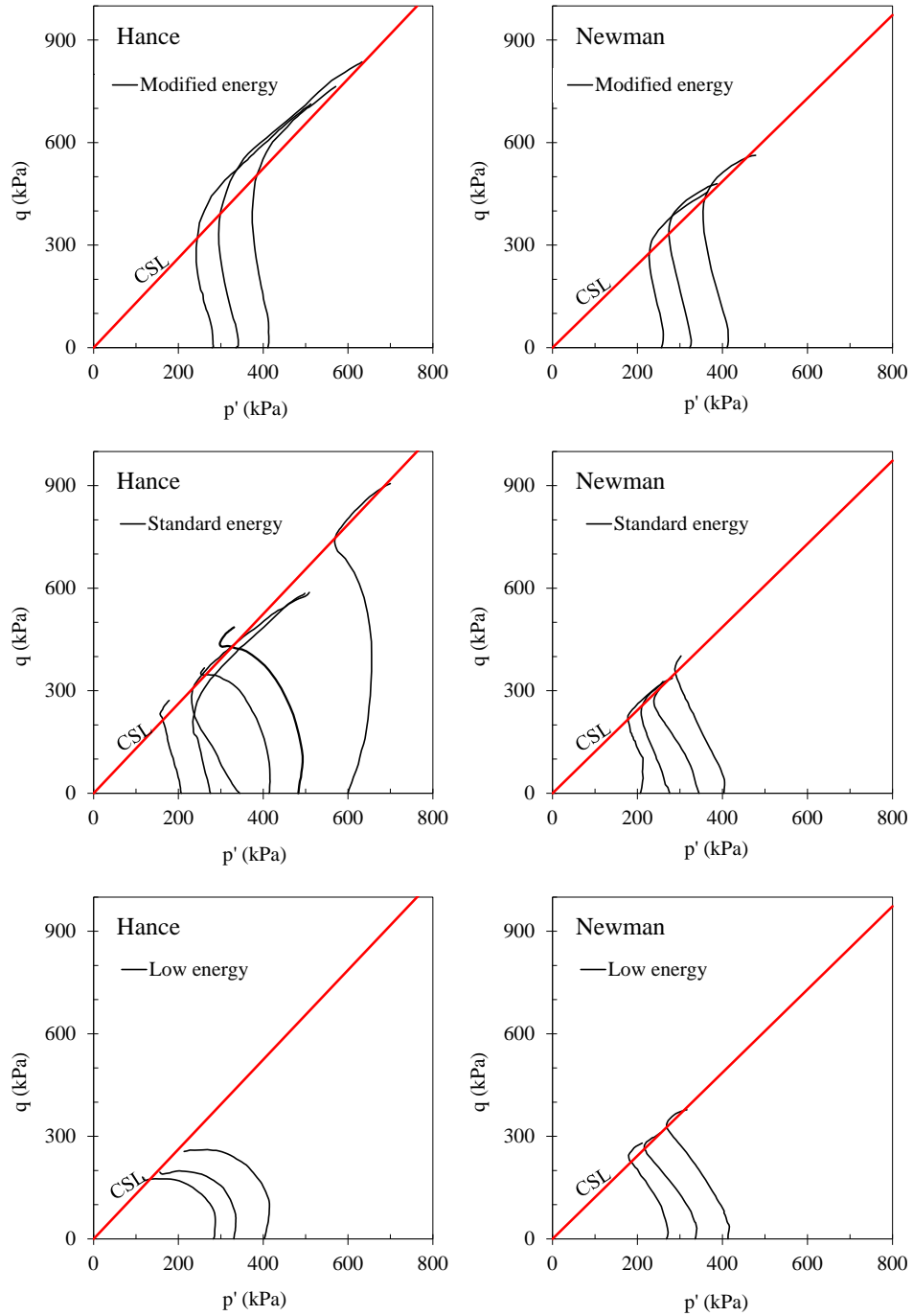


Figure 4-4 Typical stress paths of compacted shale for each one of the compaction energy with all consolidation pressures

4.4 Analysis and Discussions

From the CIU tests results, it was observed that the critical states were reached at the points of maximum deviatoric stresses as shown in Figure 4-3 and Figure 4-4. Figure 4-5 shows the points of q_{\max} vs. p'_c (i.e. the mean effective stress at critical state) for all compaction energy conditions in plots of $q-p'$ normalized to the isotropic consolidation pressure (p'_o). This figure shows that for the same shale, the specimens reached q_{\max}/p'_o values on a single line (i.e. the critical state line, CSL) regardless of the compaction energy or the consolidation pressure. As Figure 4-5 shows, for modified and standard energy compacted shale, the p'_c/p'_o values were more spread apart over the CSL and were, in general, higher than one. Also, their q_{\max}/p'_o was higher than one. This is a typical heavily OC behavior. It can be established that the greater the p'_c/p'_o values, the higher the overconsolidation ratio will be and thus the greater strength the shale will gain due to compaction. This figure also shows that at low compaction energy conditions, q_{\max}/p'_o values were roughly constant or clustering in a small area and also the corresponding p'_c/p'_o were less than one, which means that shale compacted by low energy present failure at the mean effective stresses lower than the consolidation pressures. This implies that the compacted shale behaved as NC or slightly OC soils due to the conditions that the shear produces positive increment in the pore pressure while making the mean effective stress decrease. Consequently, the effective critical state friction angle and q_{\max}/p'_o at low compaction energy can be used to describe the shear behavior of compacted shale.

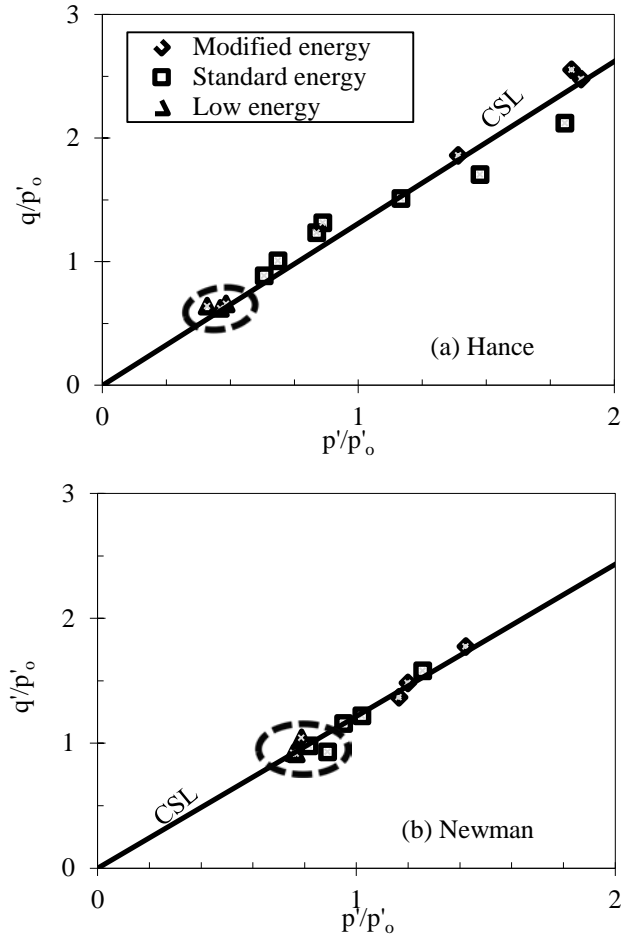


Figure 4-5 Critical states at maximum stress difference for (a) Hance and (b) Newman shale

The critical state friction angles can be calculated from the slopes of CSL presented in Figure 4-5. Due to the independence of ϕ'_c to the stress history, ϕ'_c is suitable to be a material property. The values of ϕ'_c for all tested shale are shown in Table 4-3. The values of ϕ'_c ranged from 29.4 degrees to 42.4 degrees. The lowest value 29.4 degrees was corresponding to Kope shale, and the highest value 42.4 degrees was corresponding to New Albany shale. Referring to Table 4-1, it can be seen that the higher values of ϕ'_c about correspond to the harder shale.

As was discussed earlier in this paper, undrained shear strength is a specific condition of critical state behavior [see equation (4.2)]. By definition, s_u is the half of q_{max} . Regarding to

Figure 4-5, the clusters of q_{max}/p'_o present the normalized undrained shear strength, s_u/p'_o for low energy compacted shale. Since the shale compacted by low energy behaved as NC soil. This normalized undrained shear strength is noted as $(s_u/p'_o)_{NC}$. The values of $(s_u/p'_o)_{NC}$ given in Table 4-3 was calculated from the average of $q_{max}/2p'_o$ for those low energy compacted shale.

Table 4-3 Critical state shear strength parameters for compacted shale

Geologic Name	Critical Friction Angle ϕ'_c (°)	Normalized Undrained Shear Strength $(s_u/p'_o)_{NC}$
New Albany	42.4	0.36
Hance	32.6	0.32
Upper Drakes	33.9	0.57
Nancy	31.2	0.51
Osgood	31.8	0.68
Crab Orchard	30.5	0.45
Kope	29.4	0.51
Newman	30.4	0.48
New Providence	30.6	0.46

4.4.1 Effective Critical State Friction Angle

Several researchers (Skepmpton 1964; Lupini et al. 1981; Mesri and Cepeda-Diaz 1986; Mesri and Abdel-Ghaffar 1993; Stark and Eid 1994; Terzaghi et al. 1996; Stark and Eid 1997; Wesley 2003) have described the relations between residual friction angles or soft friction angles with index properties, such as LL, PI and CF. They have shown a general relation indicating that high LL, high PI and high CF usually imply low values of friction angles. It is important to note that both residual friction angle and soft friction angle were described as effective friction angle when the ultimate state is reached. Therefore, they are corresponding with the effective critical state friction angle of this study. In order to avoid confusion, only effective critical state friction angle will be referred in the following analysis.

Figure 4-6 and Figure 4-7 shows the variation of ϕ'_c with LL and CF of this study, together with the data reported by Mesri and Cepeda-Diaz (1986) and Stark and Eid (1997). These two figures show that there are general trends indicating LL and CF are associated with ϕ'_c . Also, it is observed that the compacted shale of this study were inside the general trends given in the literature. Unlike the variation of ϕ'_c and LL, which is likely to be grouped by different CF values, CF is more appropriate to be used to estimate ϕ'_c . Analyzing all the data shown in Figure 4-7, the following relationship is established.

$$\phi'_c = 34.98 - 0.16 \cdot CF \quad (4.4)$$

Equation (4.4) shows that when CF is zero, the value of ϕ'_c was approximately 35 degrees, and when the CF was 100 percent, the value of was 19 degrees. It is necessary to remark that unlike what was reported by Stark and Eid (1997), the materials exhibited ϕ'_c values were independent of the consolidation pressures as observed in Figure 4-5.

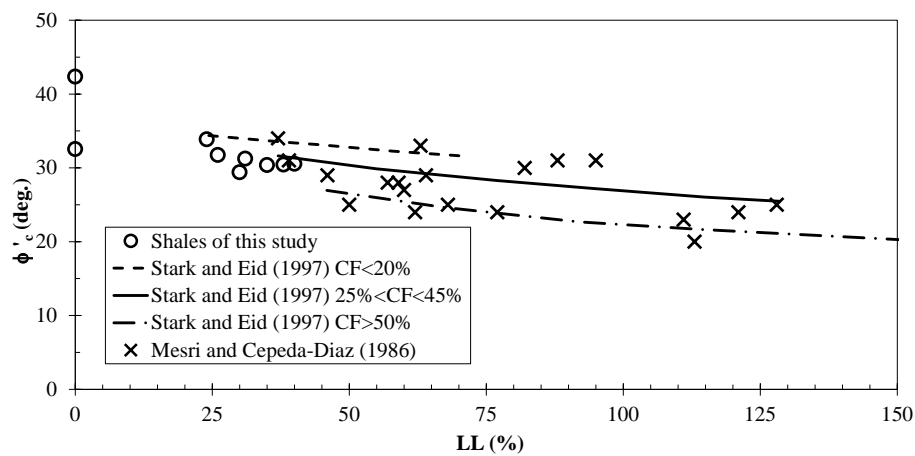


Figure 4-6 Variation of critical state friction angle with liquid limit

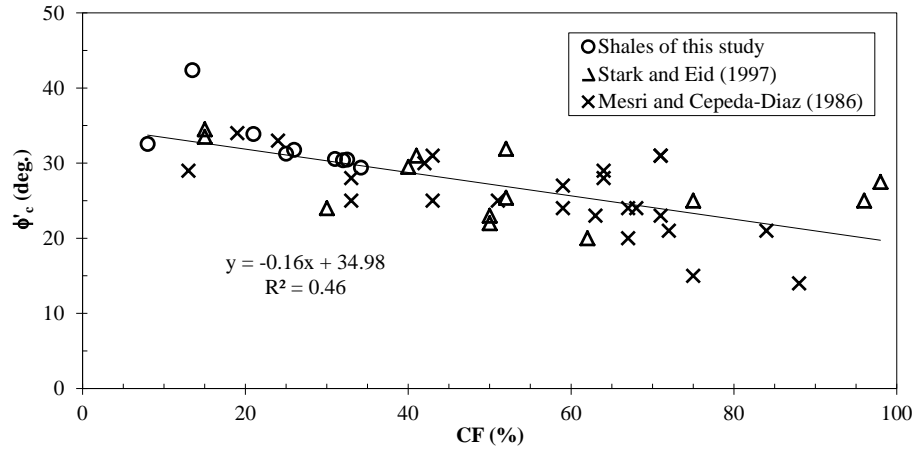


Figure 4-7 Variation of critical state friction angle with clay friction

Regarding PI, Figure 4-8 shows the variation of ϕ'_c with PI. The results of this study are presented together with the results of Mesri and Cepeda-Diaz (1986), Mesri and Abdel-Ghaffar (1993) and Stark and Eid (1997). The ϕ'_c of compacted shale were inside the range of variability given by these authors. As it has been noted, ϕ'_c is related with PI, where high PI implies low values of ϕ'_c .

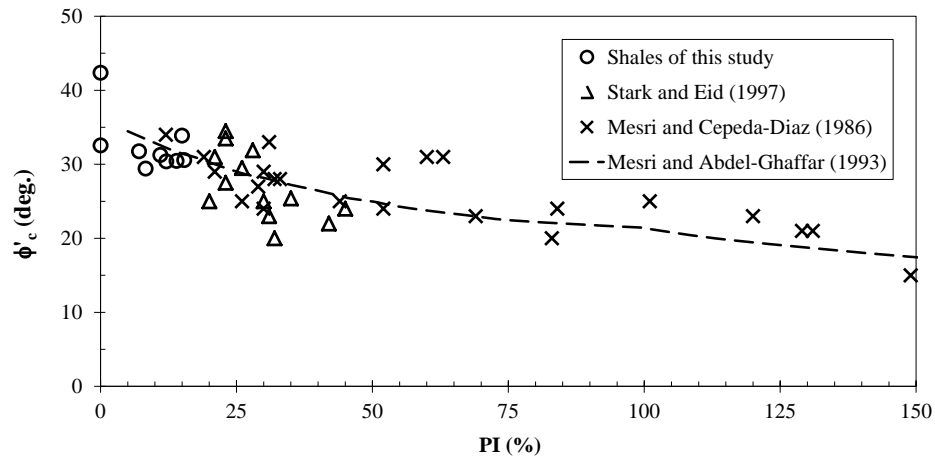


Figure 4-8 Variation of critical state friction angle with plasticity index

4.4.2 Normalized Undrained Shear Strength for Shale Compacted by Low Energy

Similar to critical state friction angle, the previous researchers (Skepmton and Delory 1957; Osterman 1960; Bjerrum 1972; Wroth and Houlsby 1985) have been investigated the relationship relationships between the normalized undrained shear strength and the index properties. However, the results in the literature are highly dispersed, which was shown in Figure 4-9. In spite of the high dispersion of the data of this study, they are still inside the general trend presented in the literature. Unlike the critical state friction angle, the undrained shear strength varied by different compaction energy and consolidation pressures, which may be the reason of the dispersion of the correlations. Even though, the values of $(s_u/p'_o)_{NC}$ for each shale is relatively constant, the direct relations between the undrained shear strength and index properties are not found.

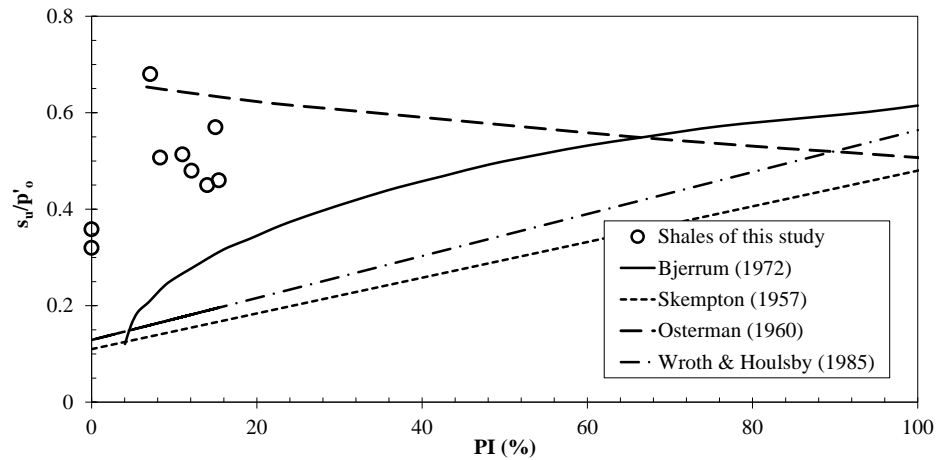


Figure 4-9 Variation of normalized undrained shear strength with plasticity index

However, a fair correlation between $(s_u/p'_o)_{NC}$ and the maximum dry unit weight under low compaction energy was found. The values of the $\gamma_{d(max)}$ under low compaction energy were normalized by the unit weight of water. This normalization scheme was used in order to create a dimensionless relation for both sides the equations, which will be provided later. Figure 4-10

shows the variation of $(s_u/p'_o)_{NC}$ with $\gamma_{d(max)}$, which shows that shale with high values of $\gamma_{d(max)}$ will have high values of $(s_u/p'_o)_{NC}$. A reasonable estimation of $(s_u/p'_o)_{NC}$ can be obtained by Equation (4.5).

$$\left(\frac{s_u}{p'_o} \right)_{NC} = 0.142 \cdot \left(\frac{\gamma_{d(max)}}{\gamma_{water}} \right)^{2.26} \quad (4.5)$$

Hance shale was the exception of the general relation. As was mentioned, Hance was NP with the lowest CF, and was classified as ML. it is possible that this different behavior was due to its low CF comparing to New Albany shale.

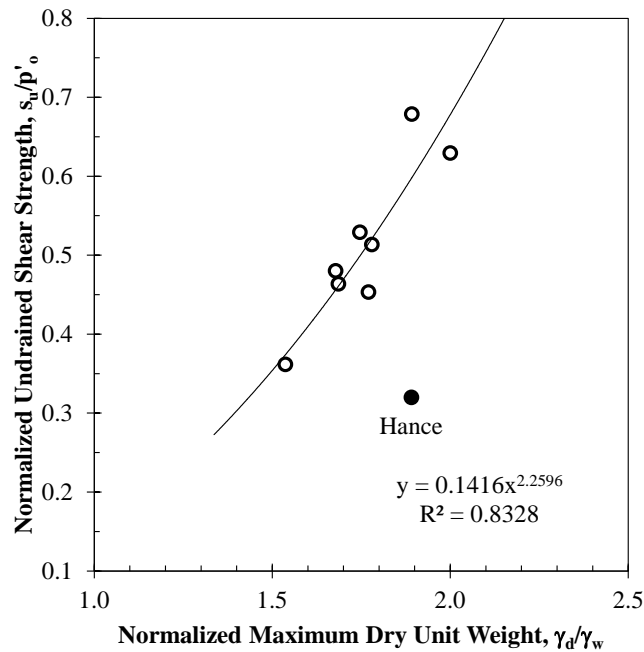


Figure 4-10 Variation of normalized undrained shear strength with maximum dry unit weight

5 Conclusions

5.1 Conclusion for Electrical Jar Test and SWEC Curve

This paper presents the attempt and process to develop a new electrical method to quantitatively measure the long-term durability of shale. The Electrical Jar Test is easy-performed and low-cost, which was developed based on the principle of the shale-water reaction. The suggested two-week monitoring period covers the primary weathering of clay minerals. In the future, it is possible to design certain electrical jar test equipment that integrates the functions of agitation, measurement and protection from evaporation and contamination. It is observed that the distilled water data is regularly related to the tap water data. It is also possible to develop “correction factors” with sufficient numbers of electrical jar tests, so that the tests performed in any slaking fluid conditions can be converted to standard condition. The SWEC curve is an intuitional presentation of shale-water interaction. The slopes and curve parameters can be used to estimate durability and deformation behavior of shale. The study of the SWEC curve is just a beginning. From the observed correlations, it is reasonable to suppose that more shale properties can be interpreted from the SWEC curve. The two-point method supported by a simplified electrical jar test is a quick and effective way to access the properties of shale. The curve parameter method which recommends a complete 20,000-minute electrical jar test is a more reliable way to access the durability and deformation behavior for all types of shale. However, both the 2-point index (i.e., R_p) and curve parameter B can be determined by simple index property of shale. The repeatability of electrical jar test is proved to some extent by comparing the results of this study and the analysis performed by Kirkendoll (2012). However, it is acknowledged that the weathering rates and curve parameters are developed from a limited number of experiments and a limited number of shale samples. Additional testing must be

performed on different shale types with different durability nature from diverse geological ages and formations.

5.2 Conclusion for Access Mechanical Behaviors of Compacted Shale by Electrical Parameters

Testing methods for measurement of 1-D collapse potential and 1-D free swell on compacted shale are introduced. Comparing to intact or core specimen, the testing specimen made of crushed-remolded shale can better simulate the condition where shale is used as a construction material. However, it is possible to involve uncertainties produced by crushing and compaction methods. The proposed new testing methods were conducted on limited numbers of shale samples collected from Kentucky. It is necessary to perform more testing to verify the repeatability and the accuracy of the interstation of material properties.

The flooding method adopted in UU tests were shown to be very sensitive to the fine contents of the specimen. It is necessary to adjust the grain size distribution used to form the specimen, in order to achieve consistent flooding periods for all samples. The goal of developing a time curve of shear strength versus weathering duration is not achieved in this study. However, the changes of shear strength over weathering time were still observed. Water and fine contents can create certain bond to increase the shear strength of compacted shale initially, but the decrease of shear strength due to the weathering mechanism will take control over time.

The relationships between deformation behaviors (i.e., collapse and swelling) and material properties of compacted shale discovered by previous researchers were verified in this study. Some new empirical equations to estimate the deformation behaviors of compacted shale from given index properties are proposed. Based on the observed testing data, the correlations between collapse/swelling and electrical parameters obtained from electrical jar test and SWEC curve are discussed. Equations to predict deformation behavior from electrical parameters are presented.

5.3 Conclusion for Shear Behavior of Weathered Compacted Shale

This paper presents the study on the shear strength behavior of compacted shale through representing and further analysis on the test results by Hopkins and Deen (1984) and Hopkins (1988).

The Index properties provided information that help to infer the composition (i.e. clay mineralogy) and the behavior of the weathered compacted shale. New Albany and Hance were non-plastic; they were classified as low plasticity silt and they had the lowest clay size fraction. Due to these facts, it can be inferred that these shale do not have expansive clays and probably have important quartz content. Upper Drakes, Nancy, Osgood, Crab Orchard, Kope, Newman and New Providence shale were classified as low plasticity clays; they had clay size fraction between 21 to 34 percent. It can be inferred that these shale had no expansive clay minerals and possibly they had low quartz content.

The shear behavior of compacted shale was resulted from different the compaction energy (i.e. optimum water content and maximum dry unit weight) and consolidation pressure. When the samples were compacted to low energy and consolidated to high stresses in comparison with the magnitude of the as-compacted pressure, they behaved as NC or slightly OC soils. When they were compacted at standard or modified energy and the consolidation pressure was low in comparison with the magnitude of the as-compacted pressure, they behaved as heavily OC soils.

It was observed that the maximum stress difference corresponds to the critical state. The maximum stress difference normalized to consolidation pressure values were aligned in a line that was the critical state line with slope function of the critical state friction angle and intercept in the origin.

The critical state friction angle showed to be unique for each shale sample, independent of the compaction energy and consolidation pressure. It was observed that the value of this angle

was controlled by index properties, especially the clay friction. This confirms the well-known fact that the critical state friction angle is by definition, a material property.

For low energy compacted shales, the undrained shear strength normalized to consolidation pressure was roughly constant, that is an indication of NC behavior. It was concluded that the average of these values was the undrained shear strength for NC condition. The normalized undrained shear strength of standard and modified energy compacted shale were spread apart along the critical state line; that indicated that they were OC.

The normalized undrained shear strength of NC compacted shale showed to be a direct result of the maximum dry unit weight. This relation was given by an equation, where the shale with high maximum dry unit weight showed high values of normalized undrained shear strength for NC condition. The variation of these values with plasticity index showed to be inside the variability of the data presented in the literature.

APPENDIX A

ELECTRICAL JAR TEST DATA

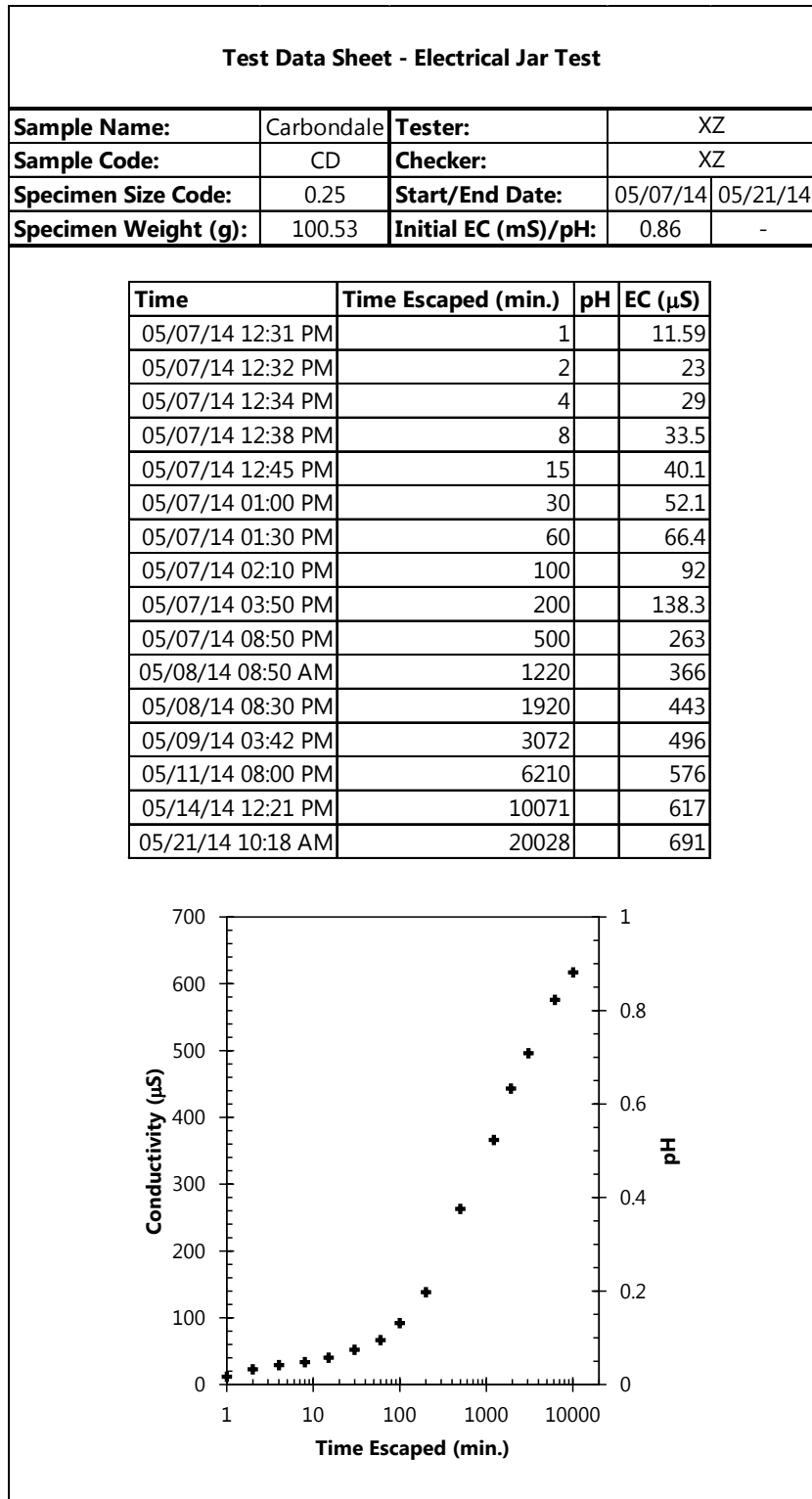


Figure A-1 Electrical Jar Test Data Sheet – CD – 0.25 – Distilled Water

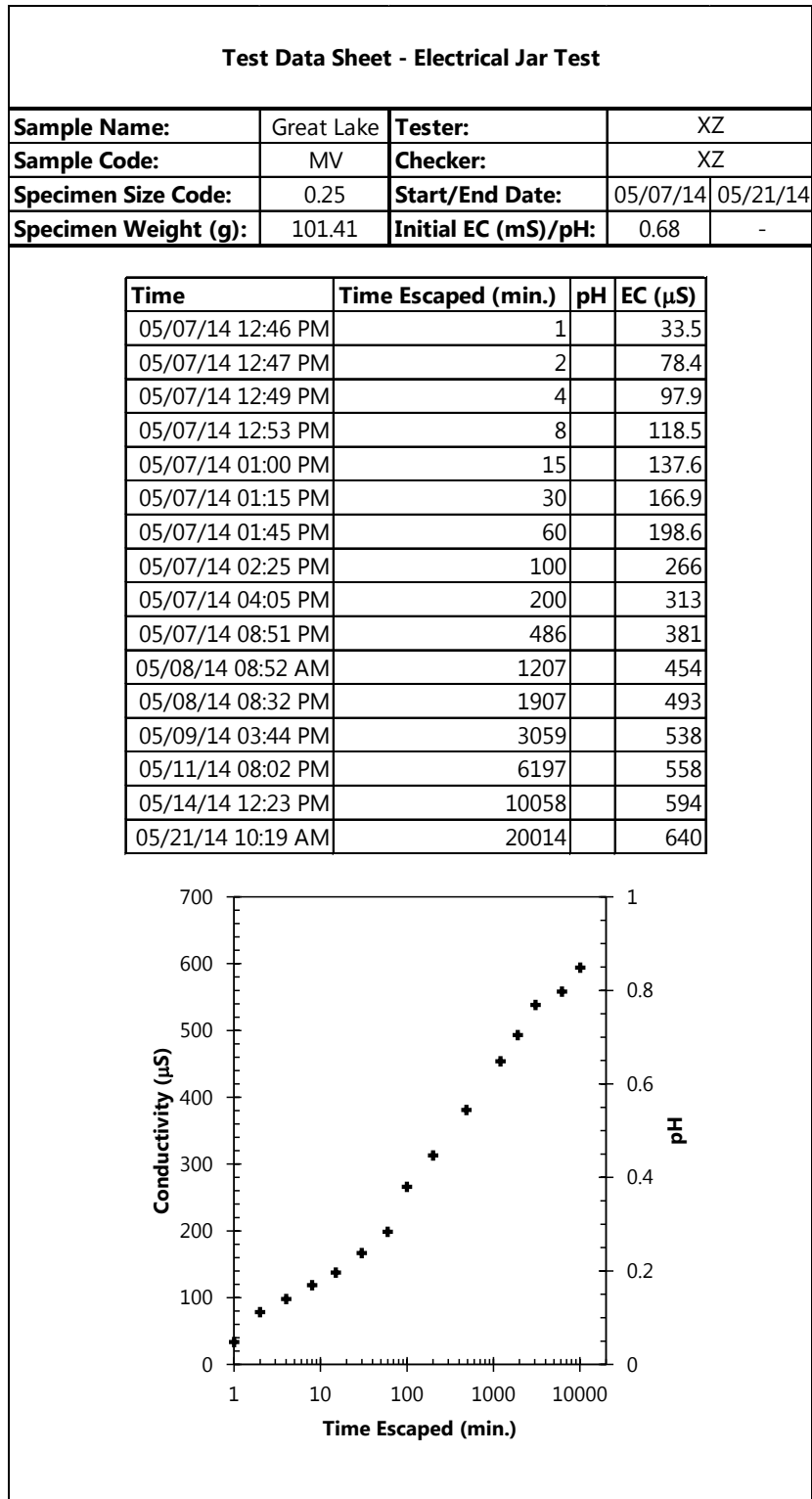


Figure A-2 Electrical Jar Test Data Sheet – MV – 0.25 – Distilled Water

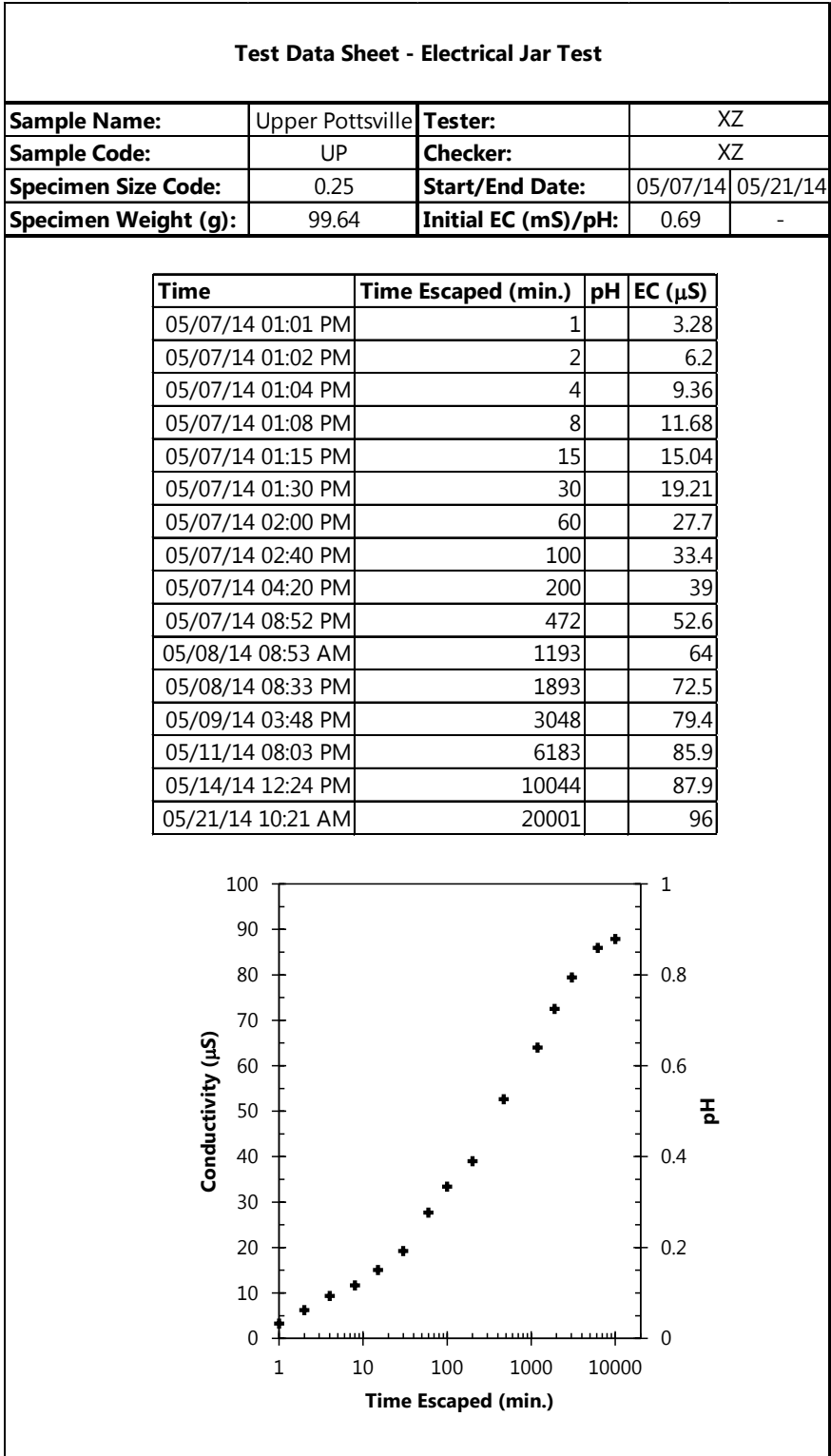


Figure A-3 Electrical Jar Test Data Sheet – UP – 0.25 – Distilled Water

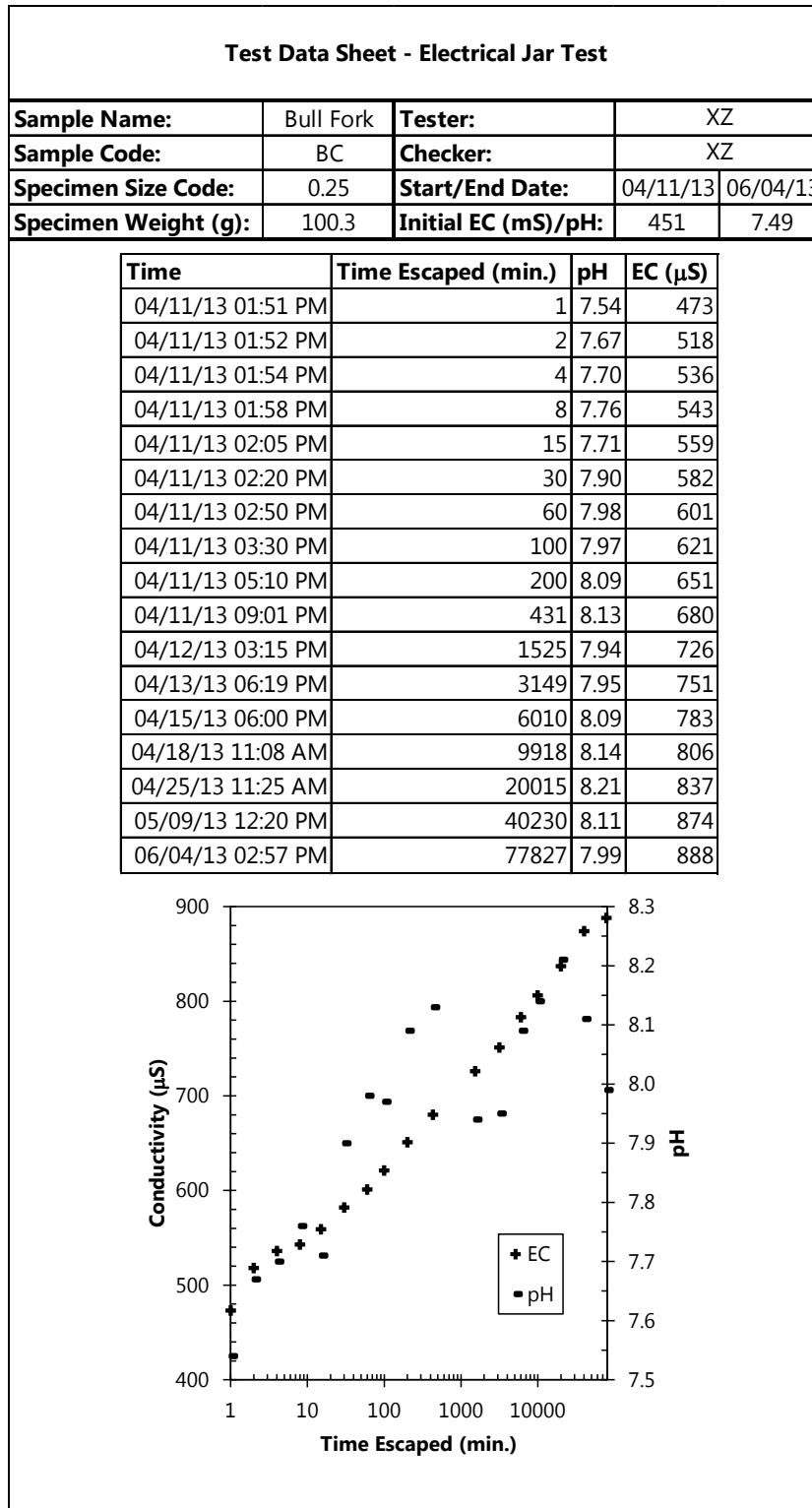


Figure A-4 Electrical Jar Test Data Sheet – BC – 0.25 – Tap Water

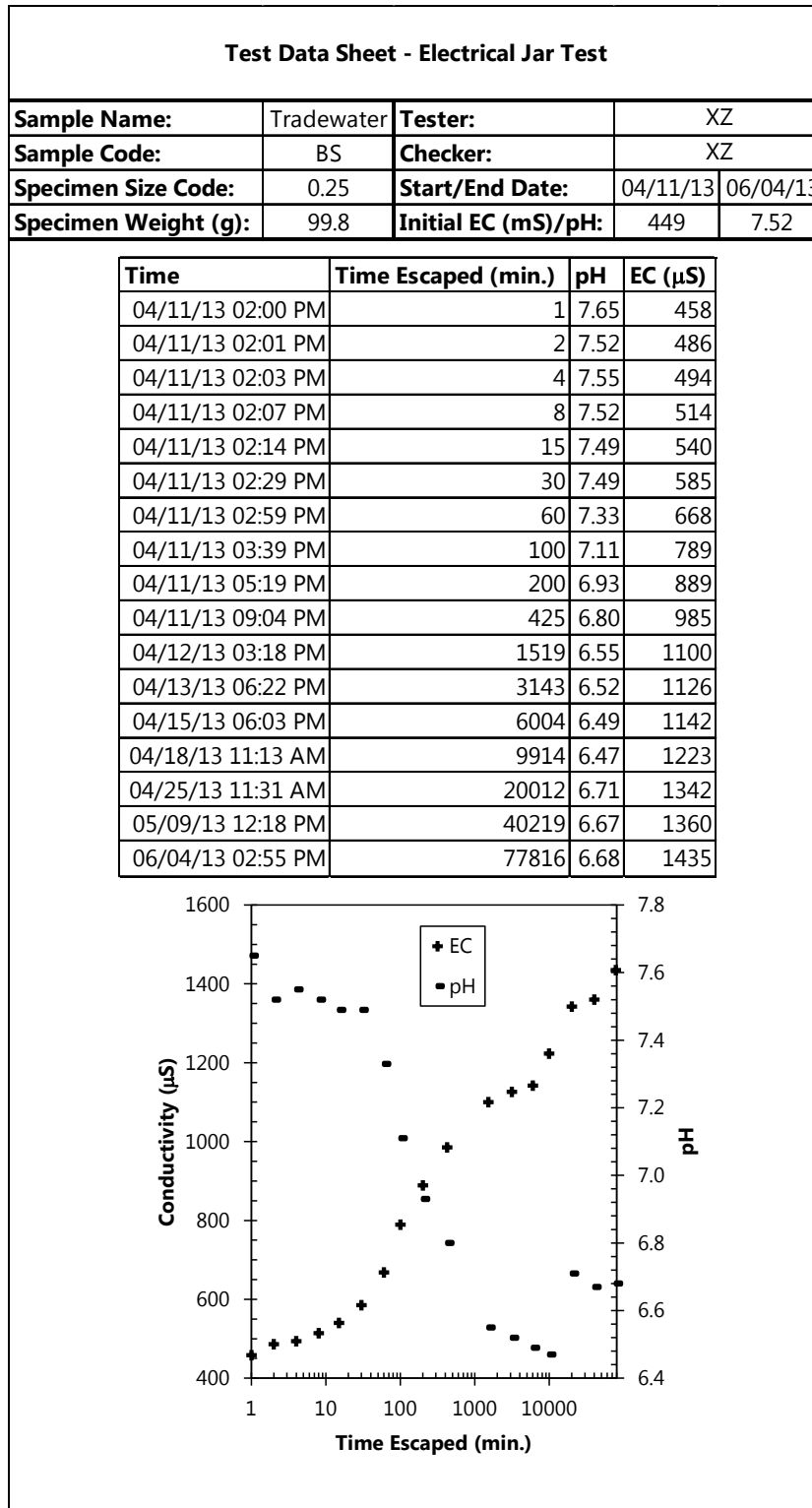


Figure A-4 Electrical Jar Test Data Sheet – BS – 0.25 – Tap Water

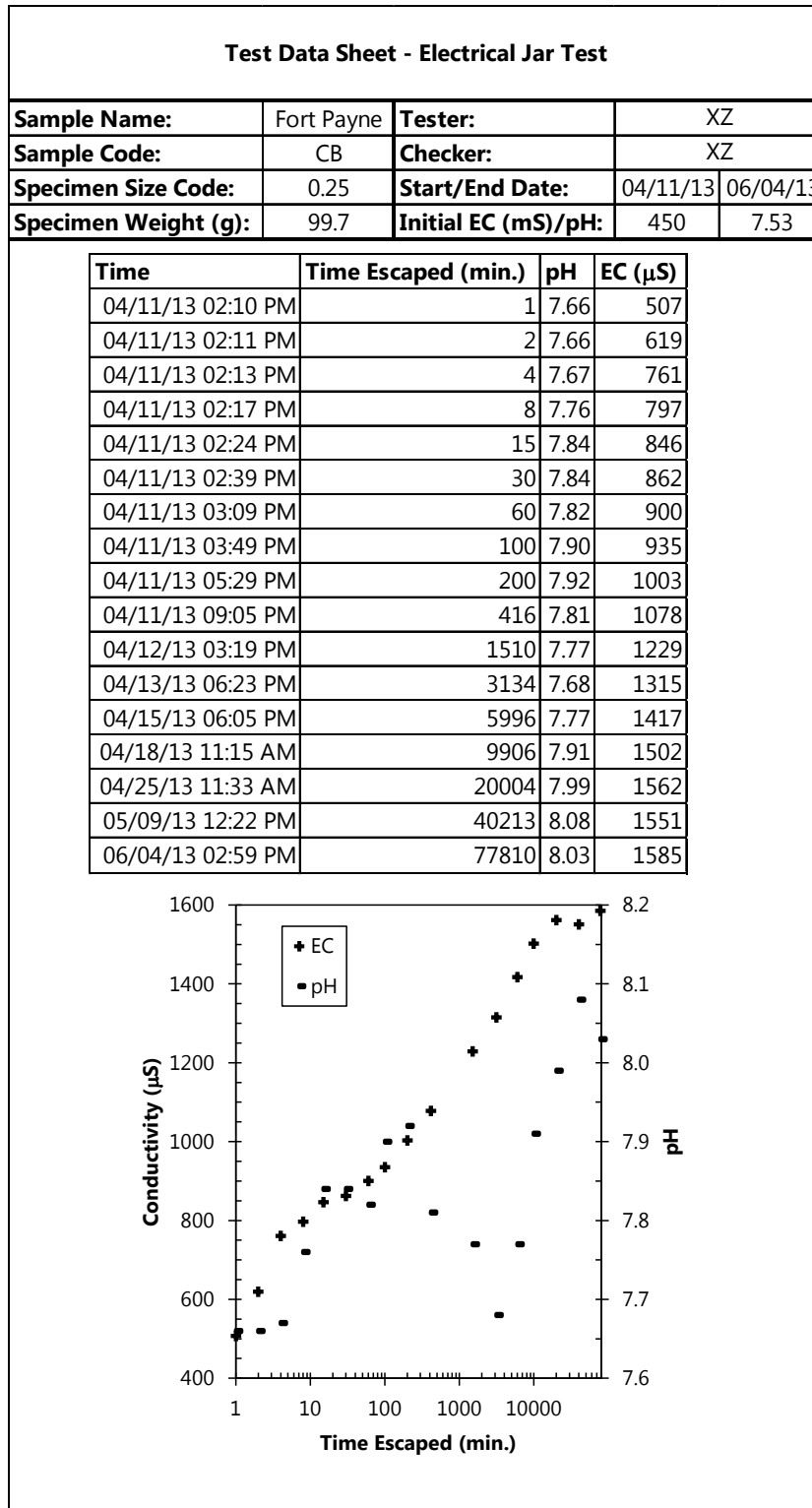


Figure A-5 Electrical Jar Test Data Sheet – CB – 0.25 – Tap Water

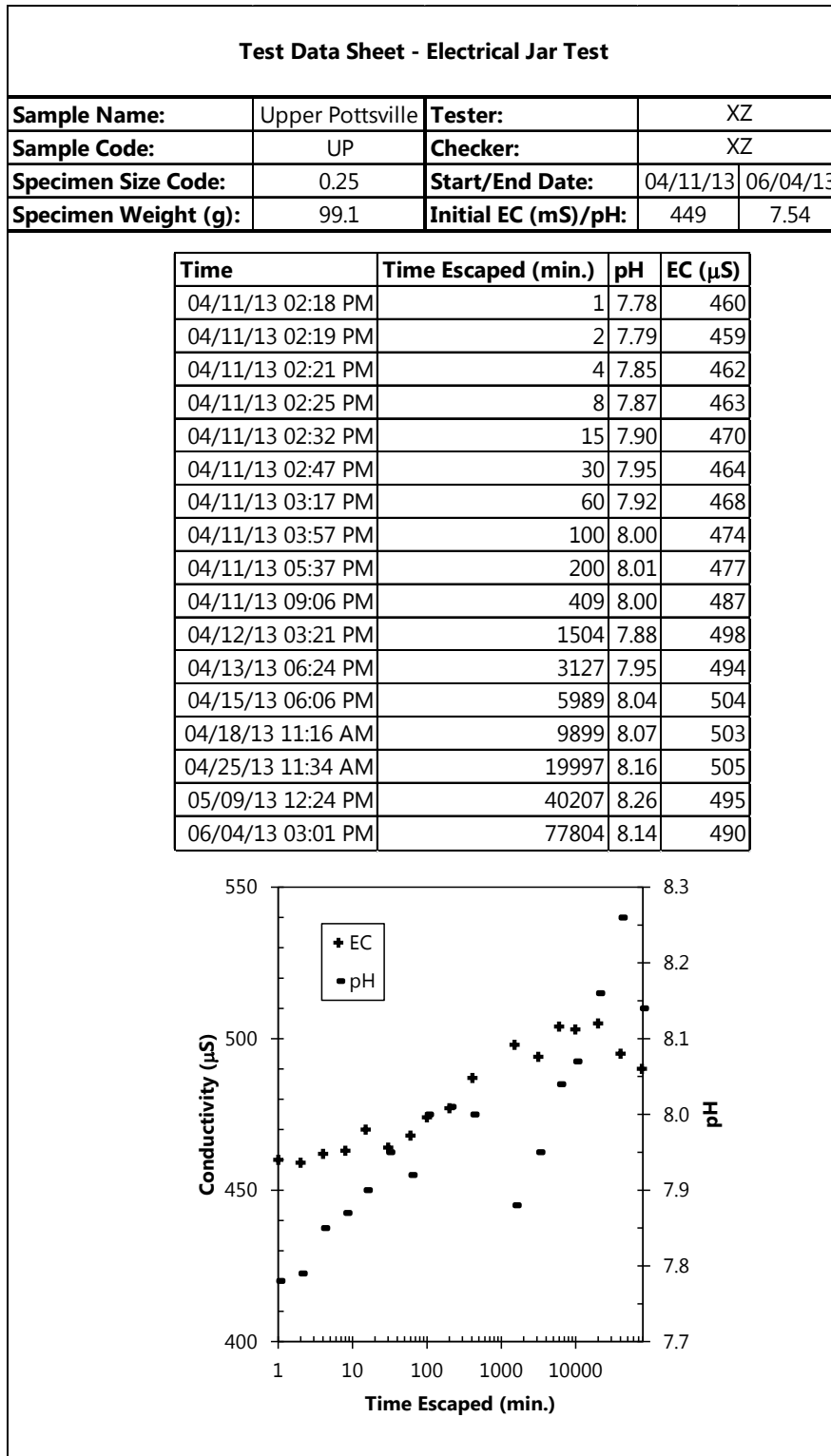


Figure A-6 Electrical Jar Test Data Sheet – UP – 0.25 – Tap Water

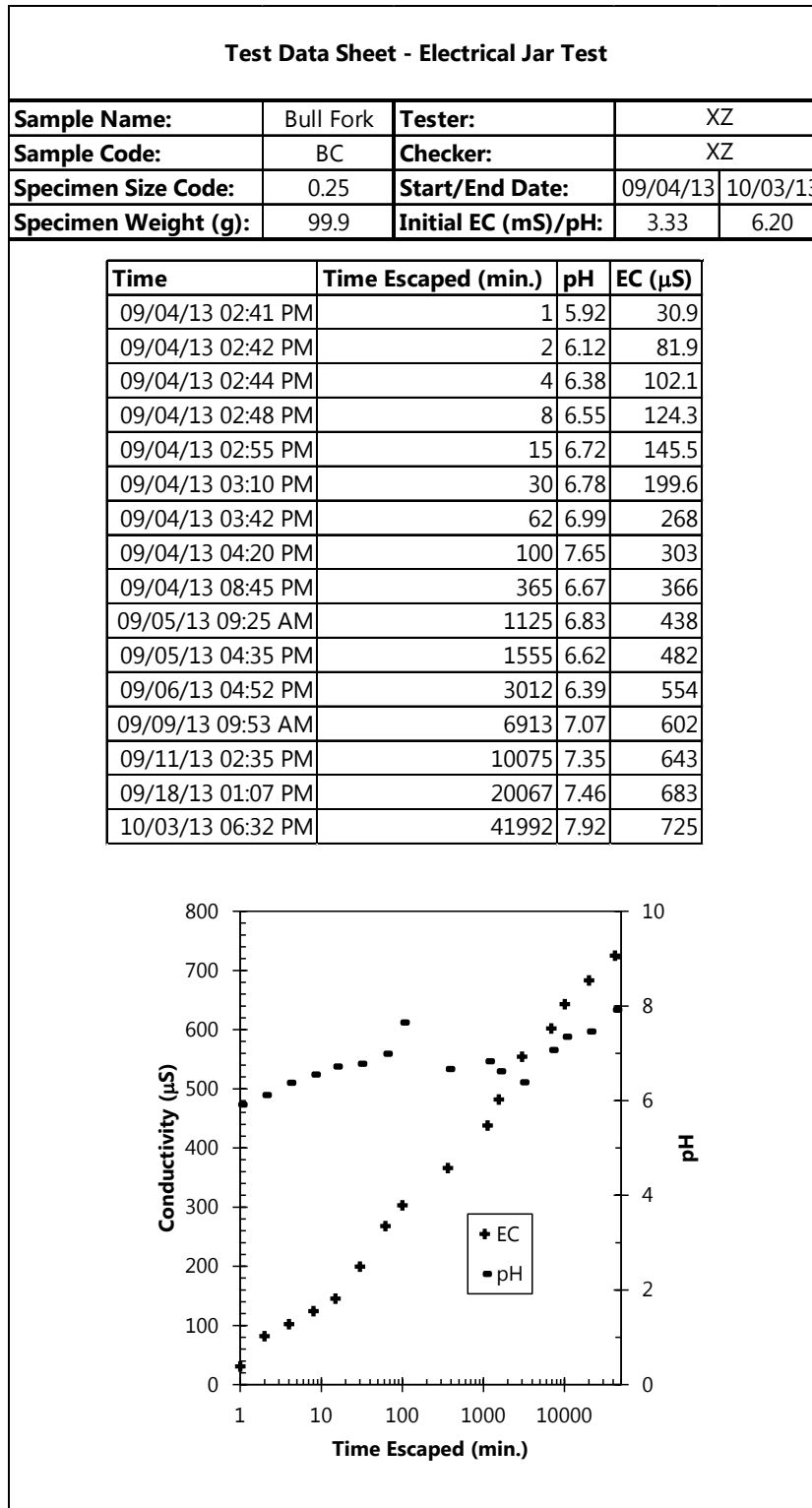


Figure A-7 Electrical Jar Test Data Sheet – BC – 0.25 – Distilled Water

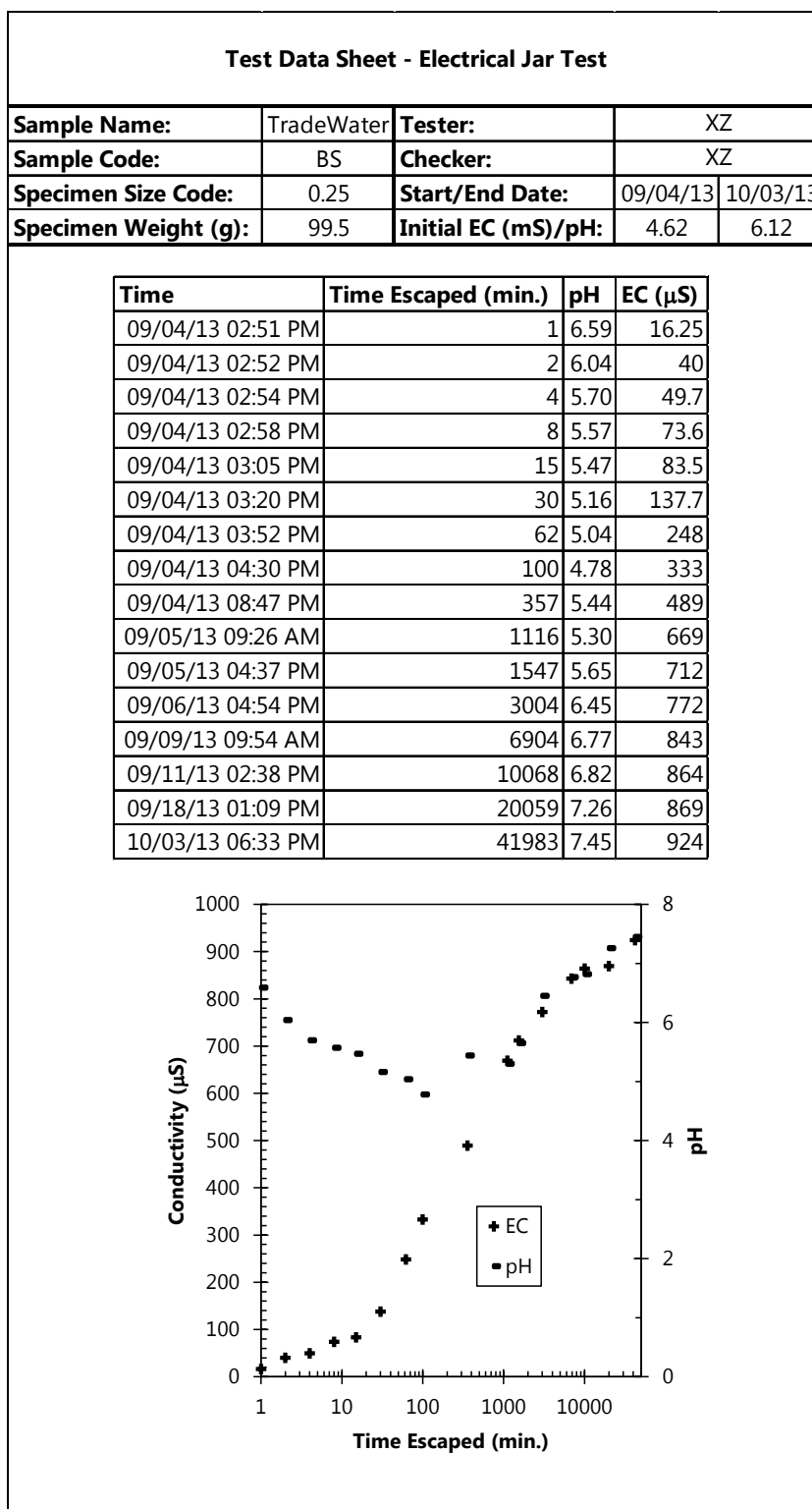


Figure A-8 Electrical Jar Test Data Sheet – BS – 0.25 – Distilled Water

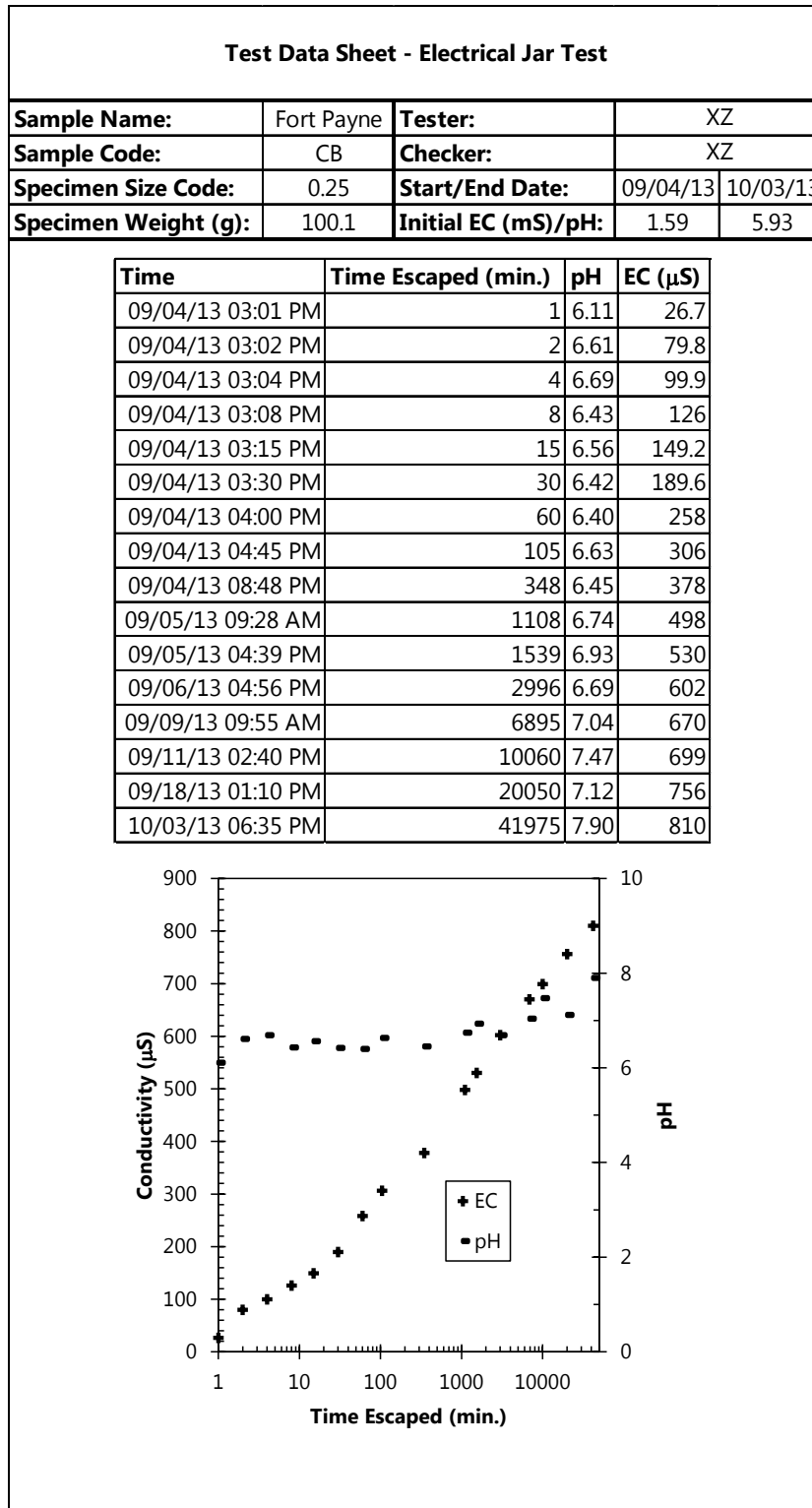


Figure A-9 Electrical Jar Test Data Sheet – CB – 0.25 – Distilled Water

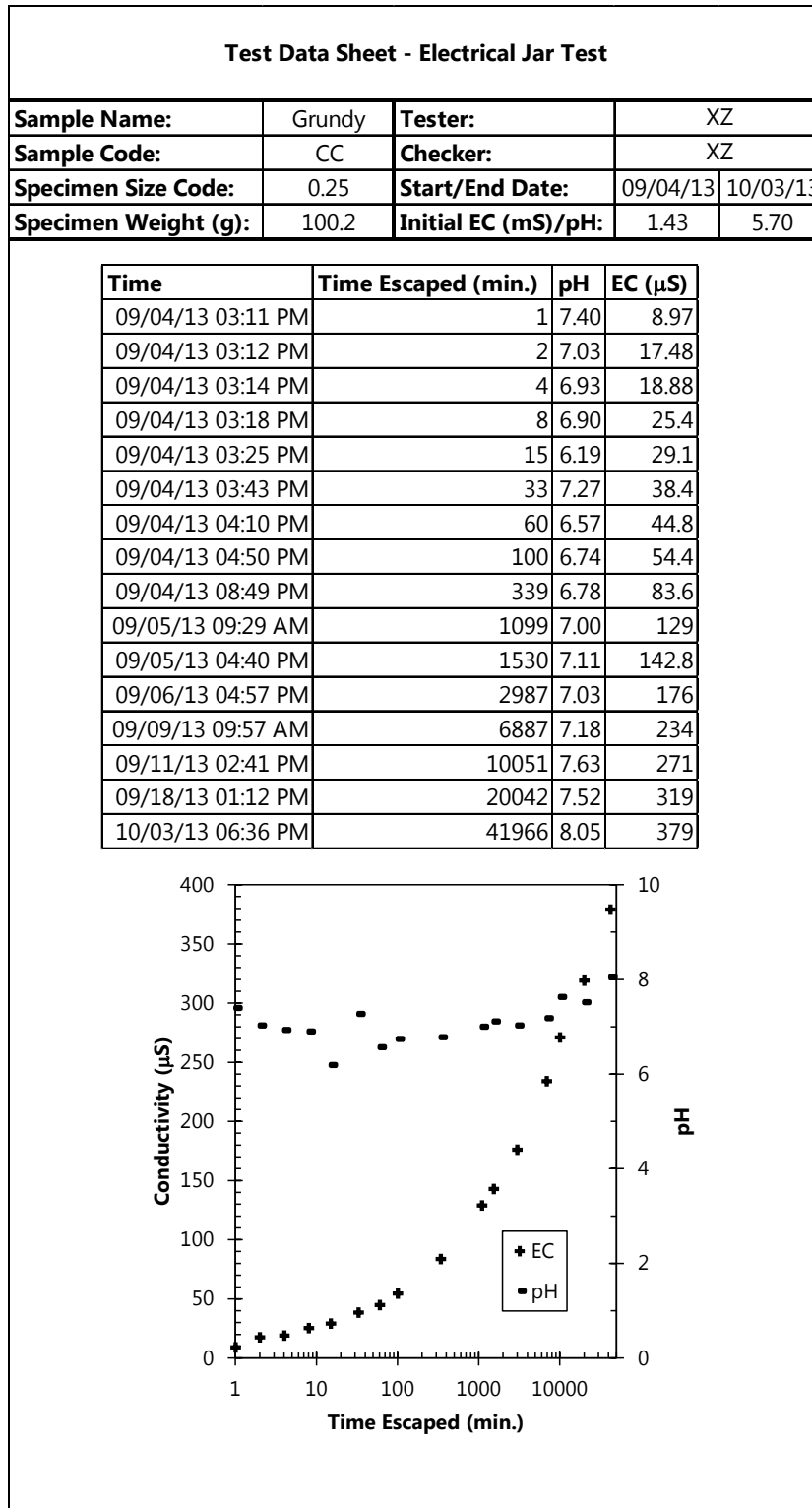


Figure A-10 Electrical Jar Test Data Sheet – CC – 0.25 – Distilled Water

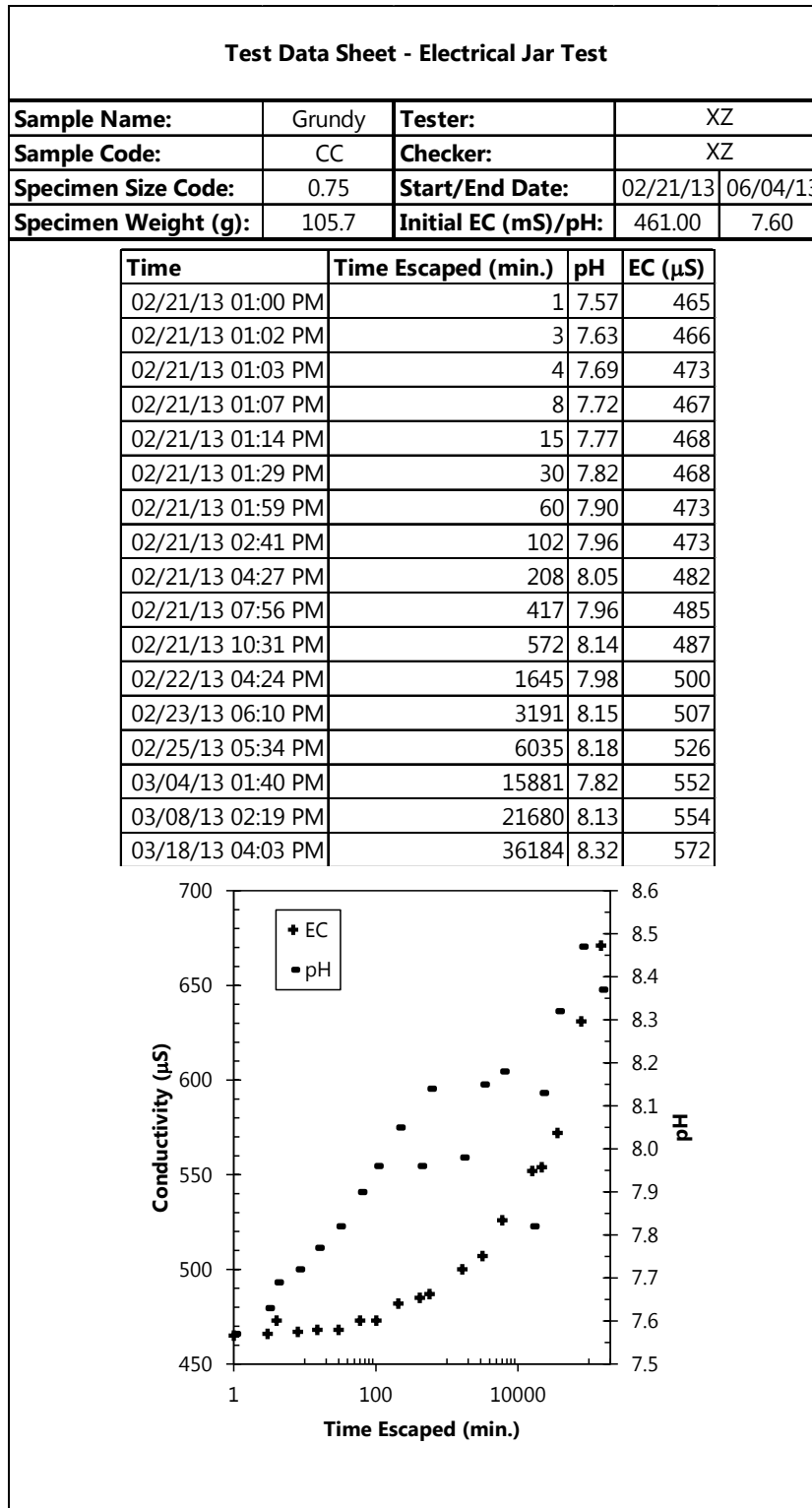


Figure A-11 Electrical Jar Test Data Sheet – CC – 0.75 – Tap Water

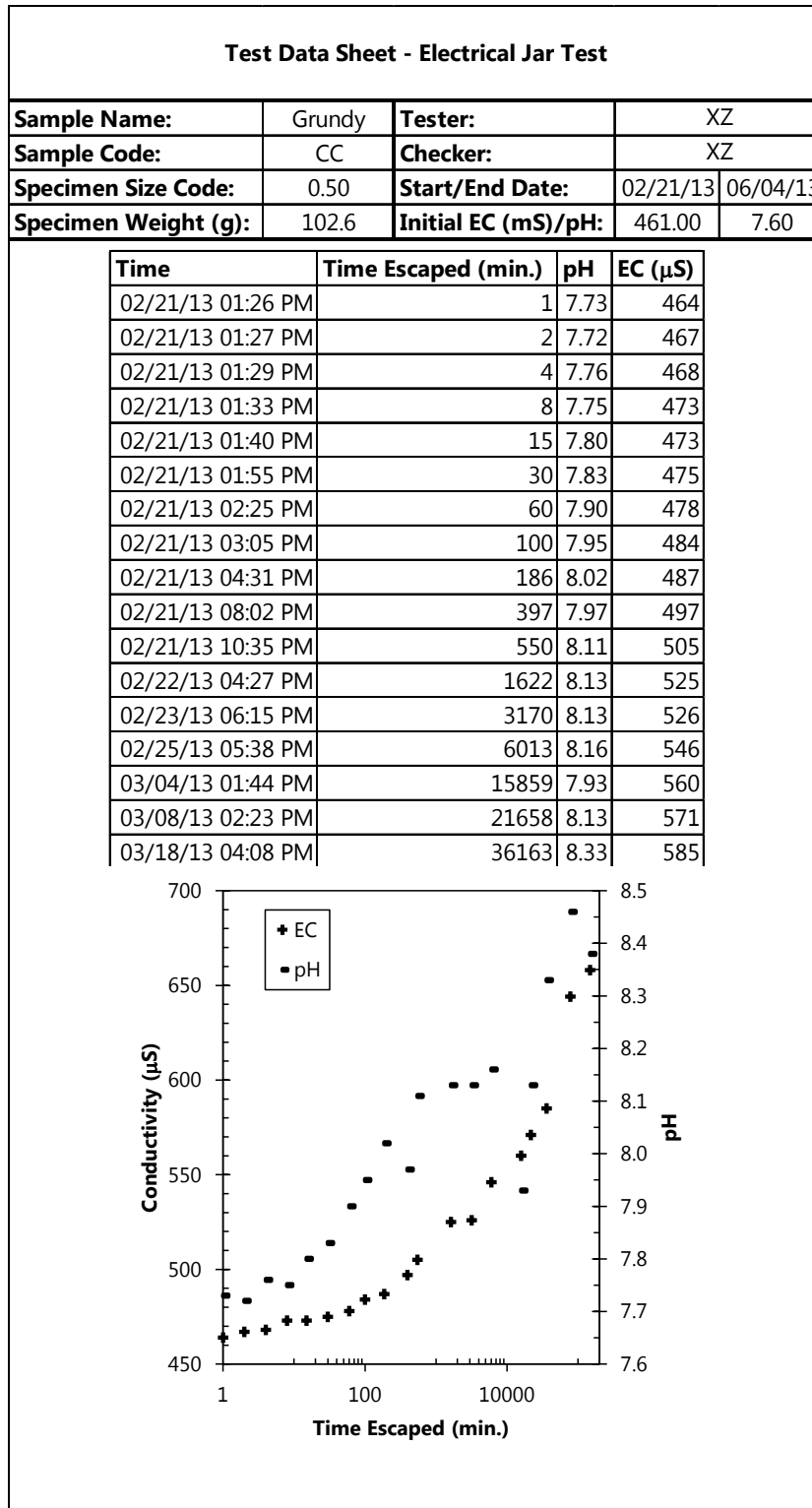


Figure A-12 Electrical Jar Test Data Sheet – CC – 0.50 – Tap Water

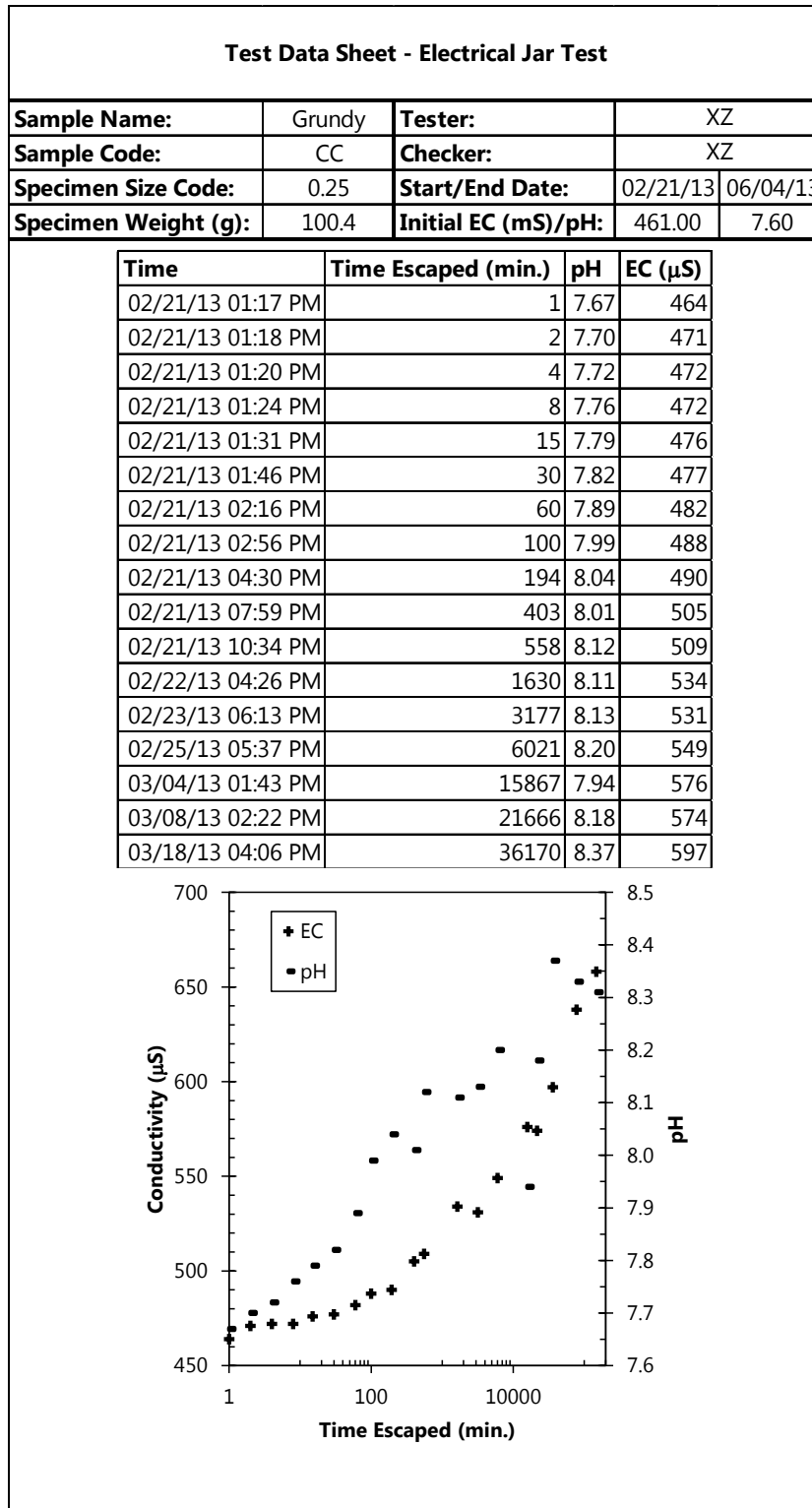


Figure A-13 Electrical Jar Test Data Sheet – CC – 0.25 – Tap Water

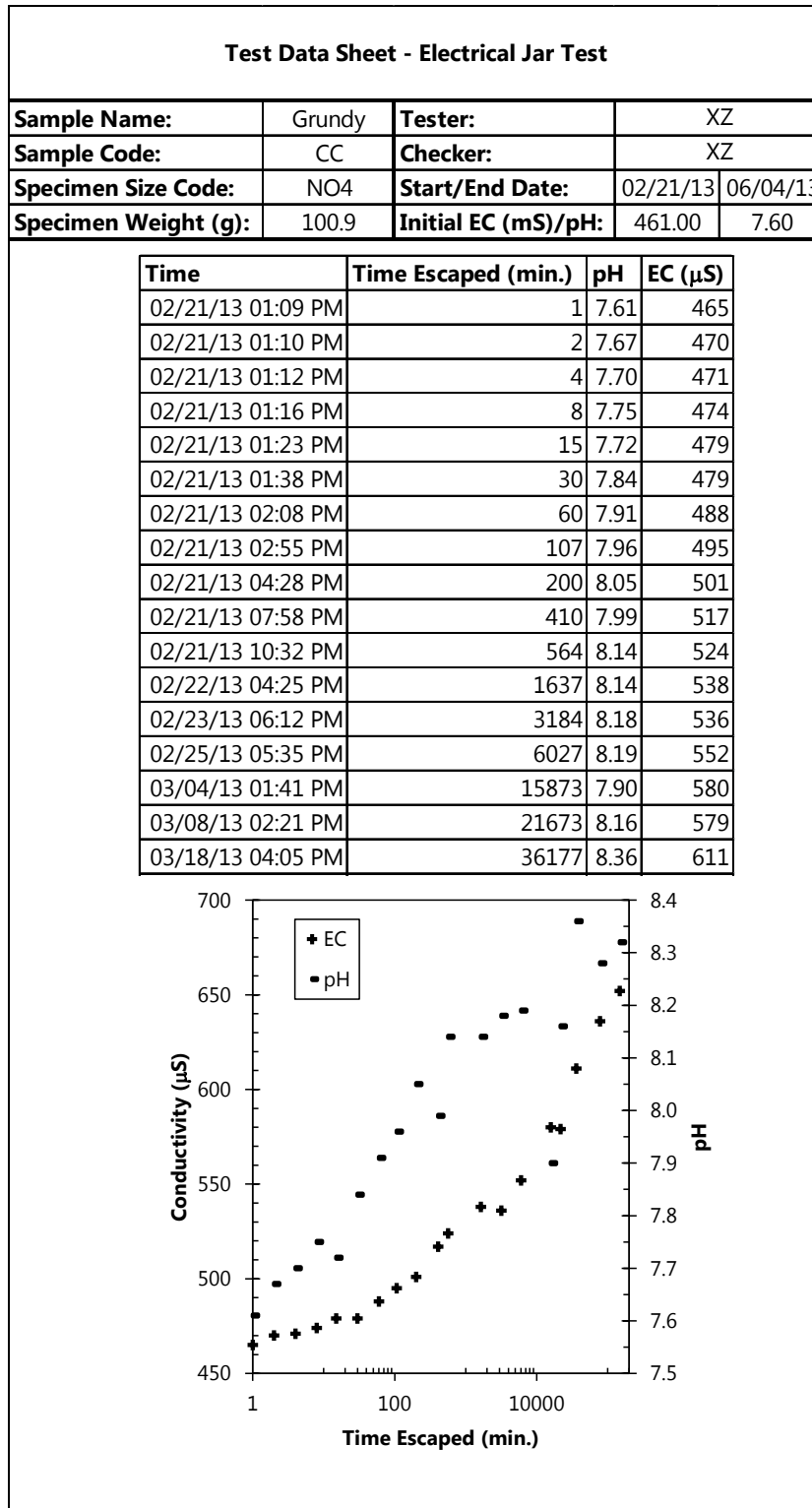


Figure A-14 Electrical Jar Test Data Sheet – CC – NO4 – Tap Water

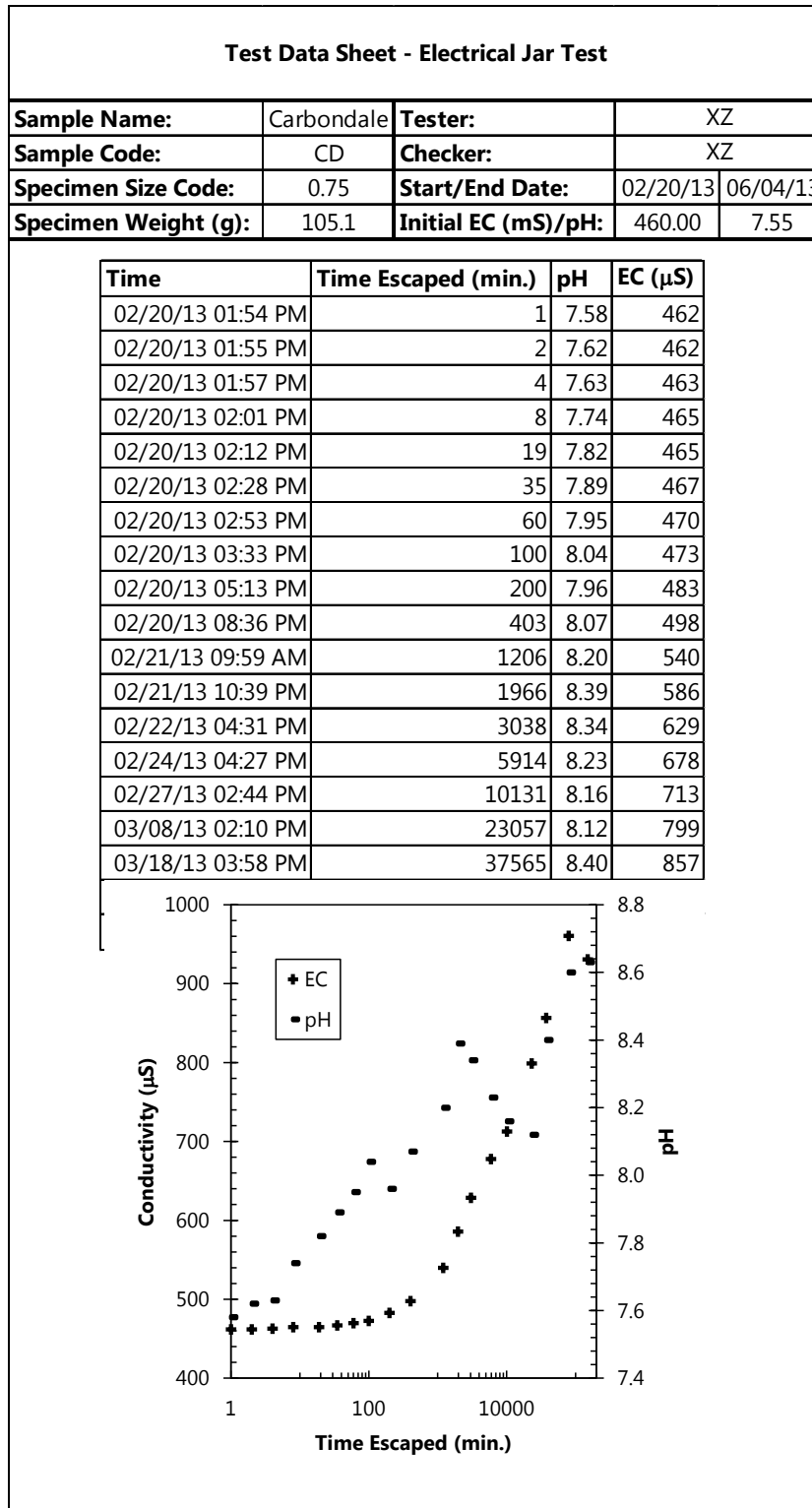


Figure A-15 Electrical Jar Test Data Sheet – CD – 0.75 – Tap Water

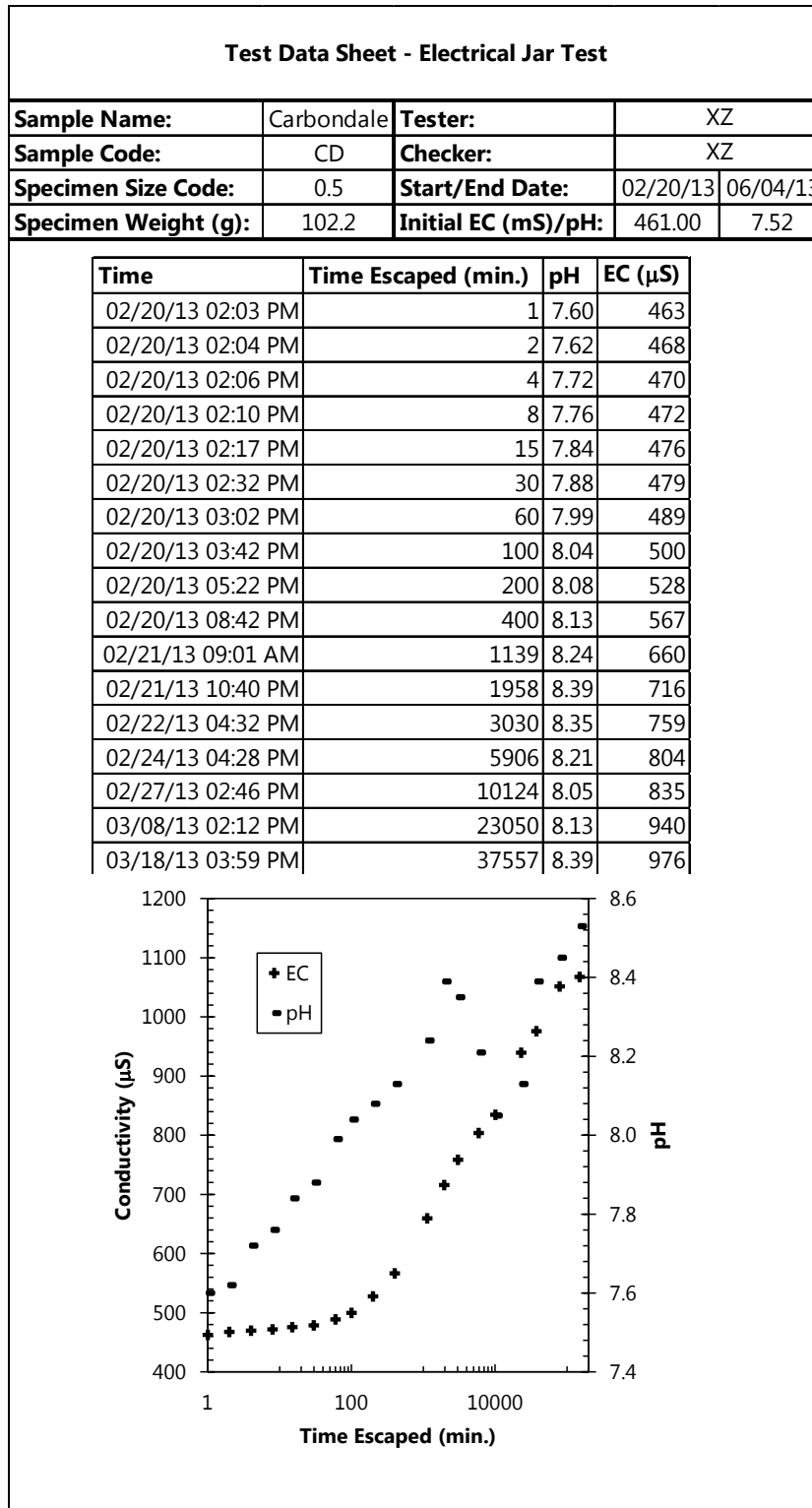


Figure A-16 Electrical Jar Test Data Sheet – CD – 0.5 – Tap Water

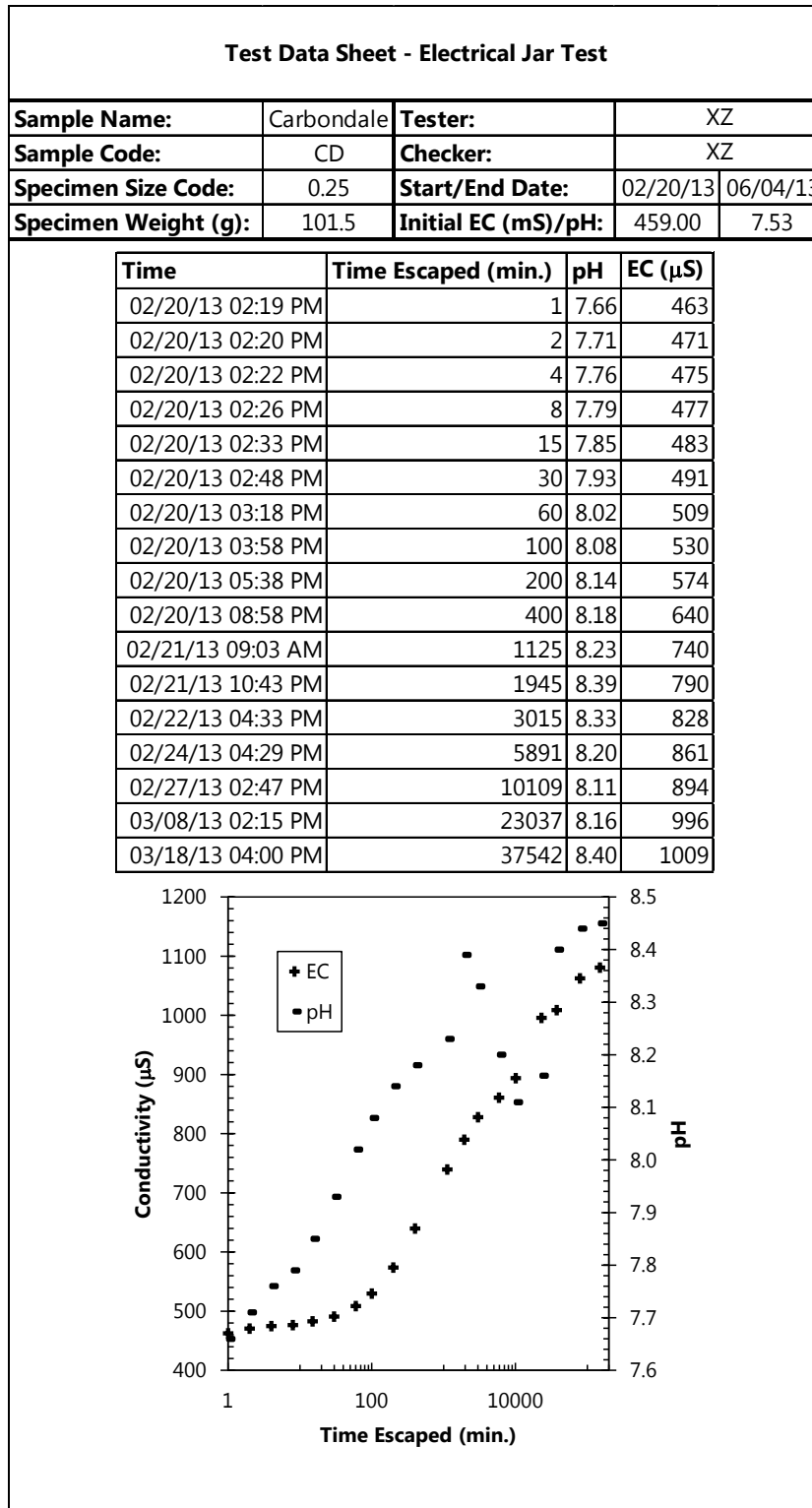


Figure A-17 Electrical Jar Test Data Sheet – CD – 0.25 – Tap Water

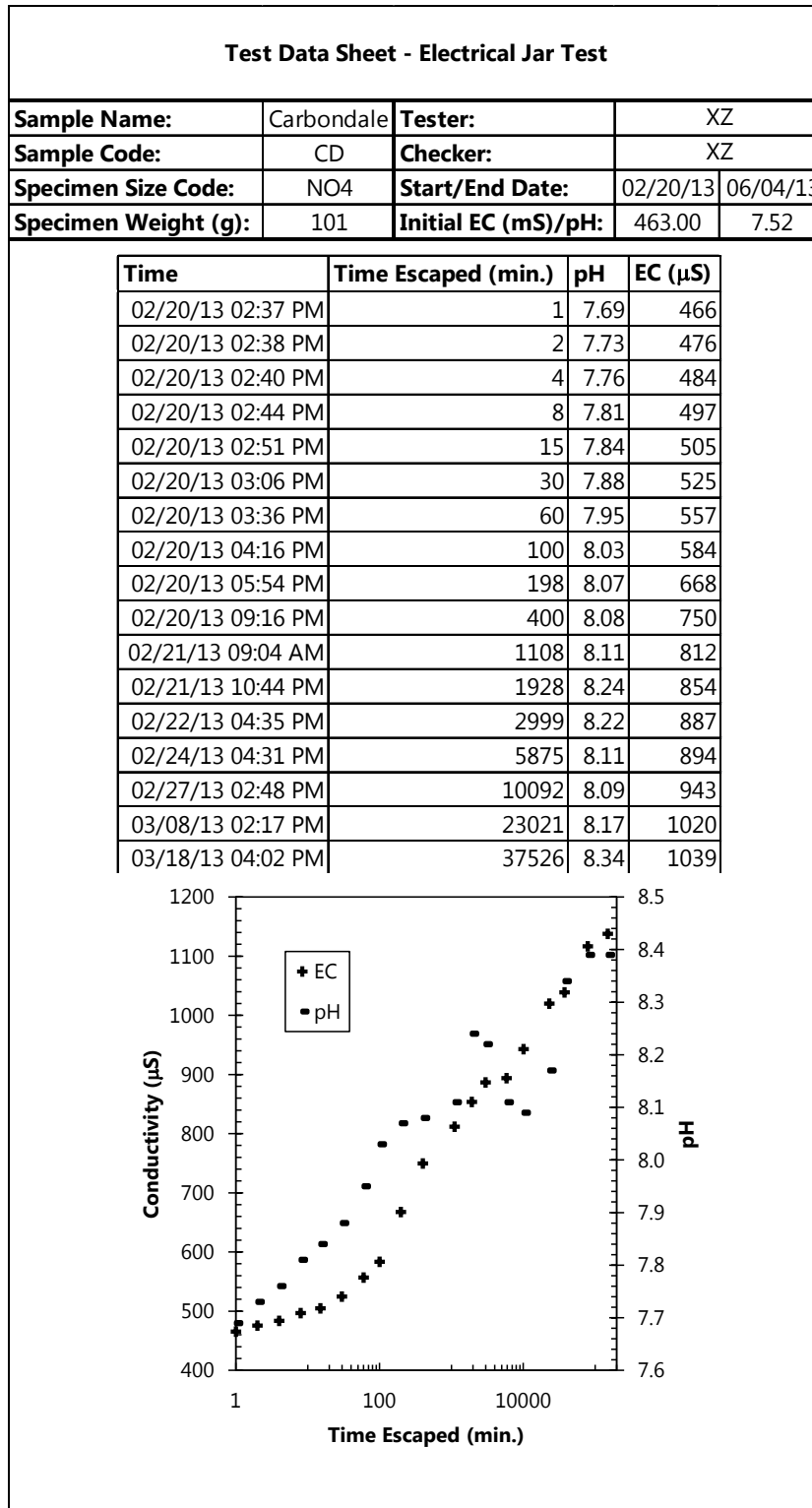


Figure A-18 Electrical Jar Test Data Sheet – CD – NO4 – Tap Water

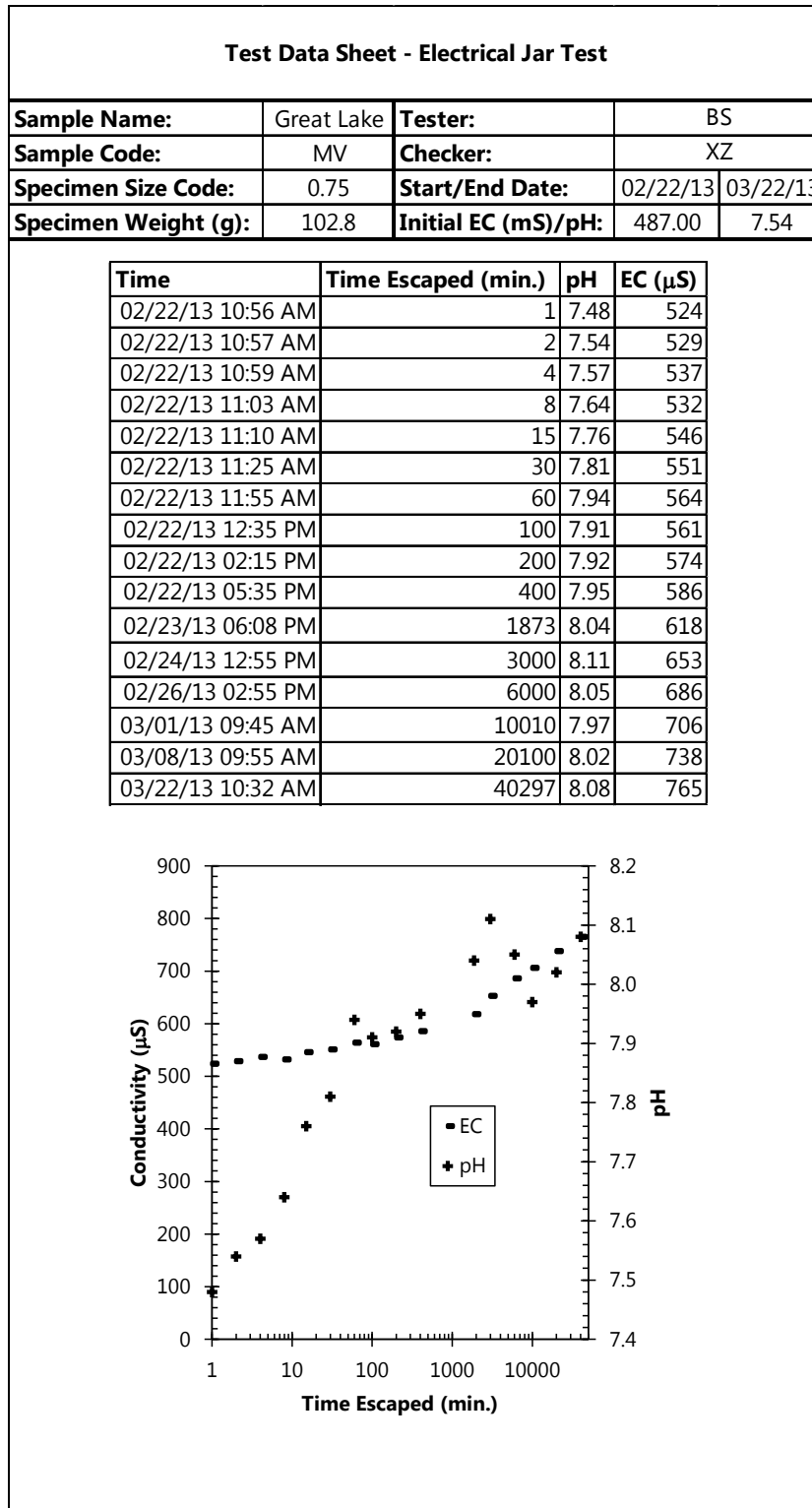


Figure A-19 Electrical Jar Test Data Sheet – MV – 0.75 – Tap Water

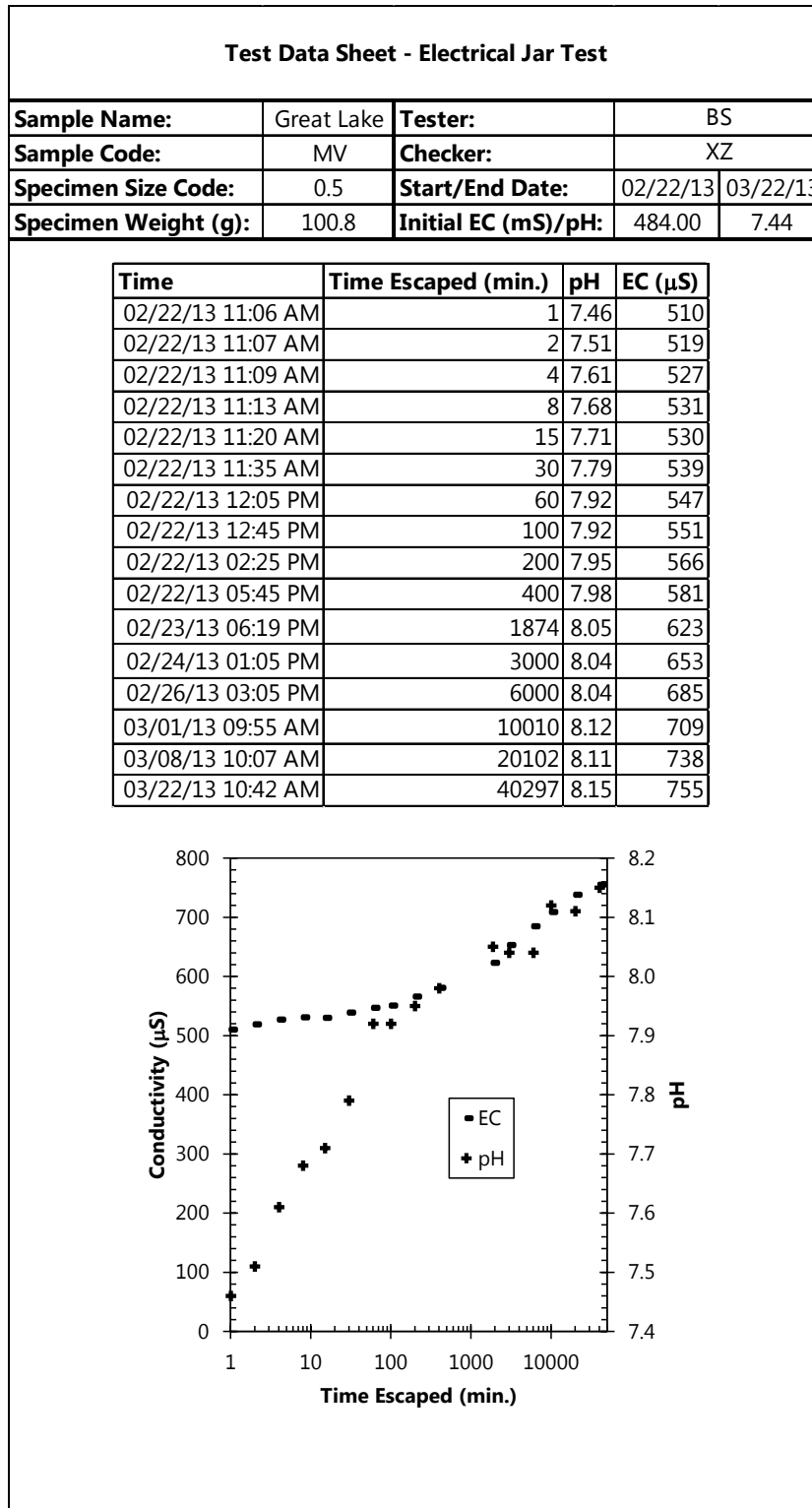


Figure A-20 Electrical Jar Test Data Sheet – MV – 0.5 – Tap Water

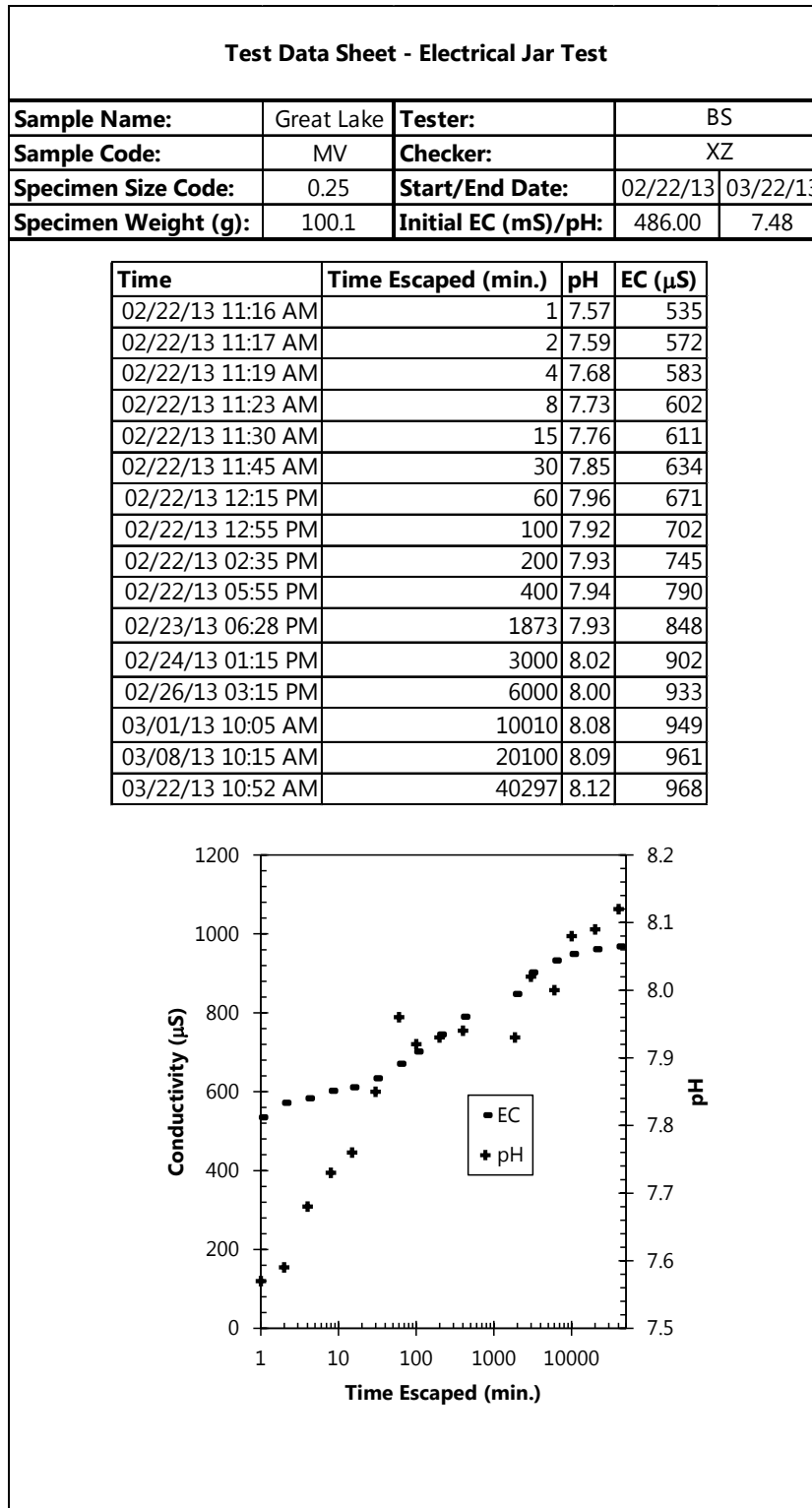


Figure A-21 Electrical Jar Test Data Sheet – MV – 0.25 – Tap Water

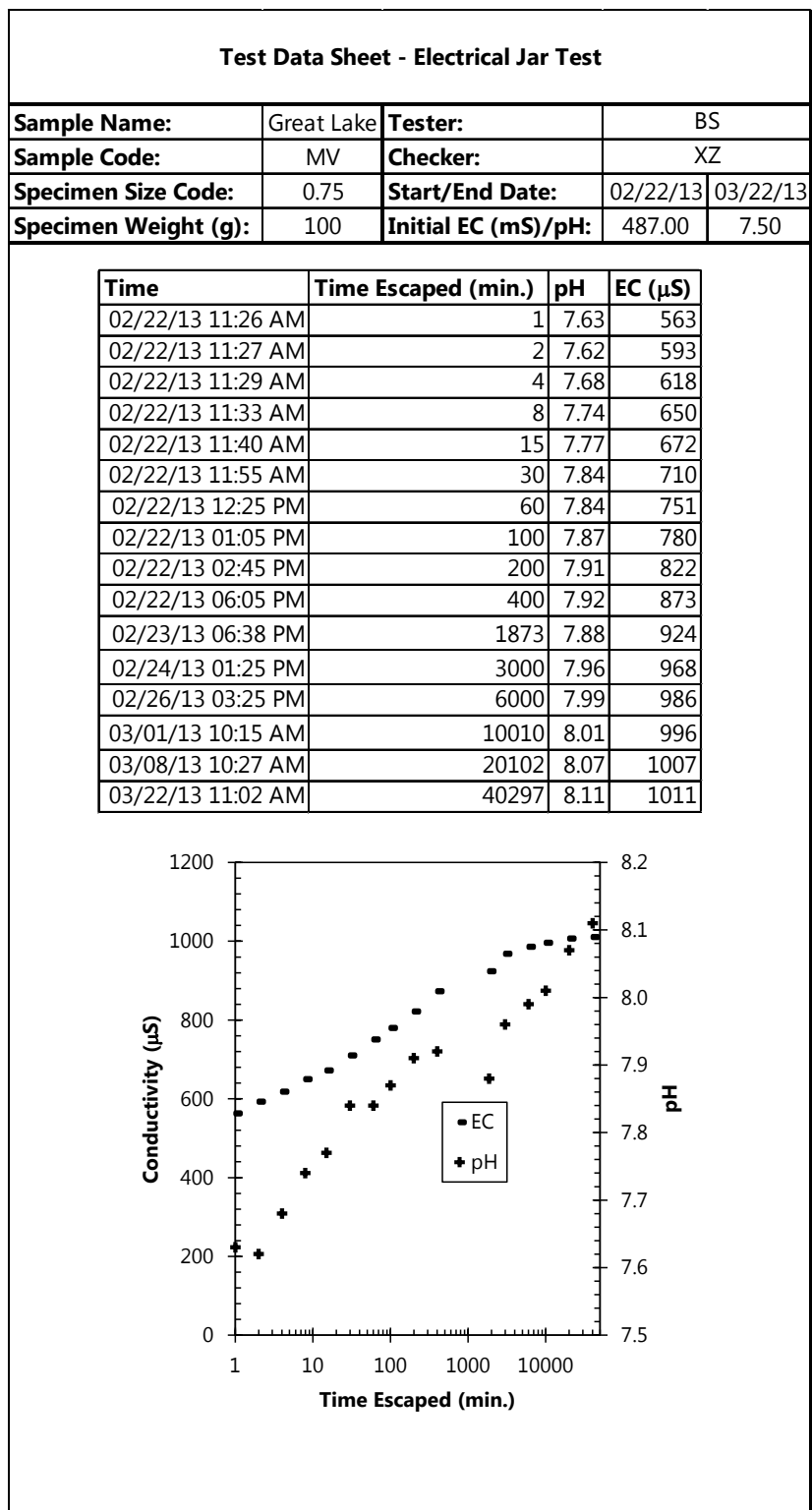


Figure A-22 Electrical Jar Test Data Sheet – MV – NO4 – Tap Water



Figure A-23 Demonstration of Specimen Size of Electrical Jar Test

Additional considerations were given on the correlations between SSA and the curve parameters. Figure A-24 shows Carbondale shale as an example, and the other two shales have similar results. Both A and B parameters show very strong power correlations with SSA. The higher the SSA values (i.e., smaller particle size), the lower values of A and B parameters.

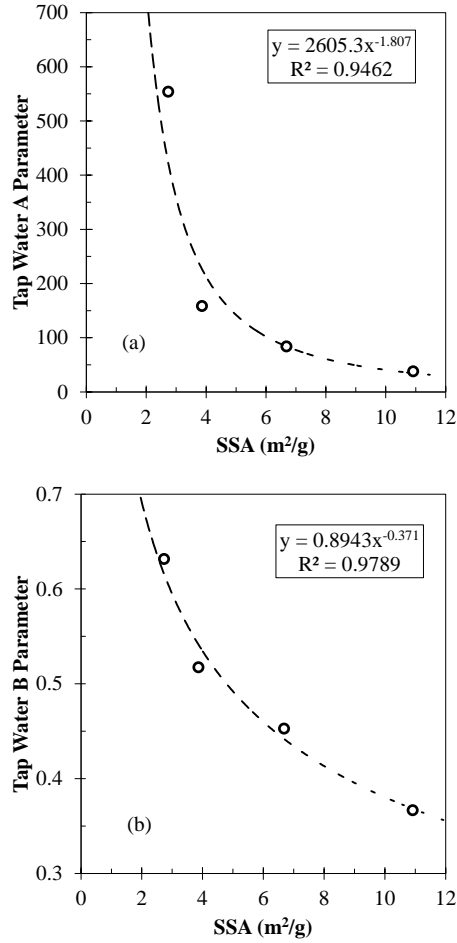


Figure A-24 Carbondale shale: correlations between SSA and (a) A & (b) B parameters

Additional analysis was conducted to see how the curve parameters and slopes obtained from tap and distilled water related to each other. The results are shown in Figure A-25. It was found that the distilled water A and B parameters were power-correlated with those A and B parameters obtained from tap water tests, which are shown in Figure A-25 (a) and (b). Figure A-25 (c) and (d) also shows power relations between dissolution and primary weathering rates of tap and distilled water. Due to the variety of tap water conditions, these correlations shown in Figure A-25 will only be valid for this study or experiments performed using the same tap and distilled water as this study.

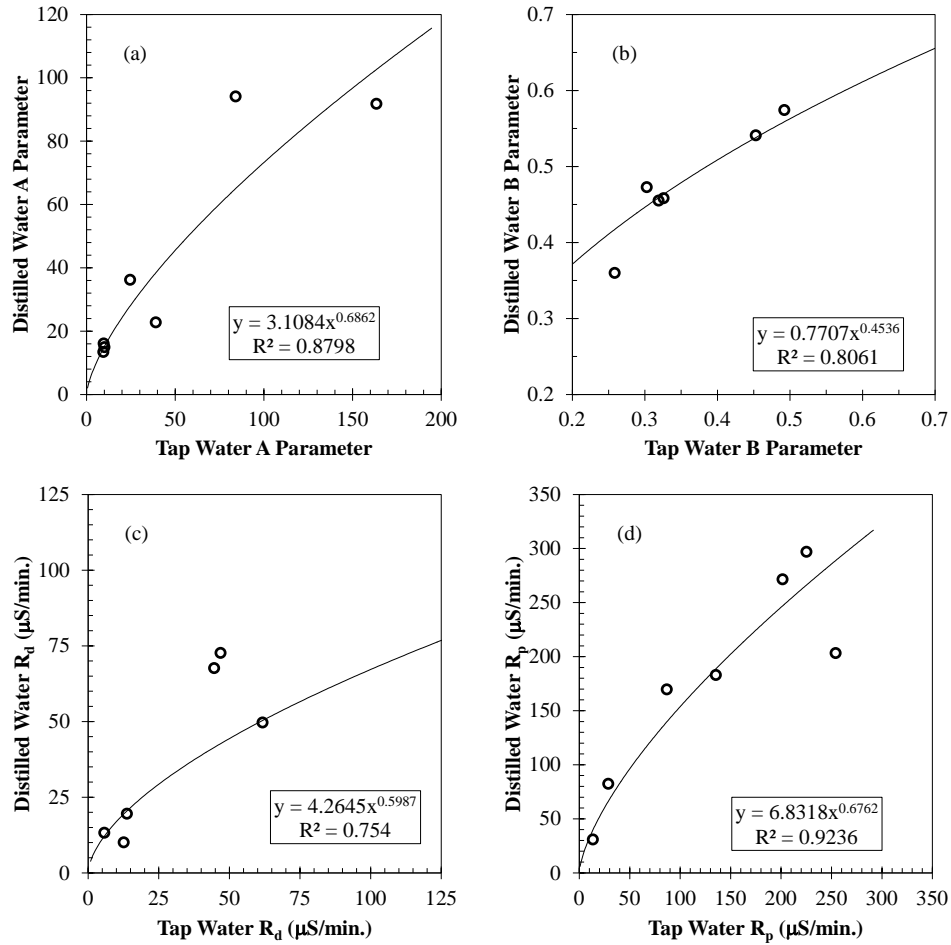


Figure A-25 Correlations between tap and distilled water data: (a) A parameter, (b) B parameter, (c) dissolution rate, and (d) primary weathering rate

It is also found that even when very limited data are available for a particular shale sample; it is still possible to make estimation on its EC_r . With the EC_r values calculated from the modified hyperbolic criterion, a correlation between the EC_r and natural moisture content (ω_n) is found and shown in Figure A-26. Then, EC_r can be calculated using Equation (A-1), when ω_n is known.

$$EC_r = 536 \cdot \ln(\omega_n) + 304 \quad (A-1)$$

It is very important to realize that the EC_r calculated by the modified hyperbolic criterion or by Equation (A-1) are not the true residual value of the EC that can be finally reached in the shale-water solution. The only purpose for the estimation of EC_r in this study is to best curve-fit out a complete view of the dissolution and primary weathering phases. Due to the limitation of current monitoring length (limited by evaporation and contamination over time), a complete view of the residual phase is still unknown.

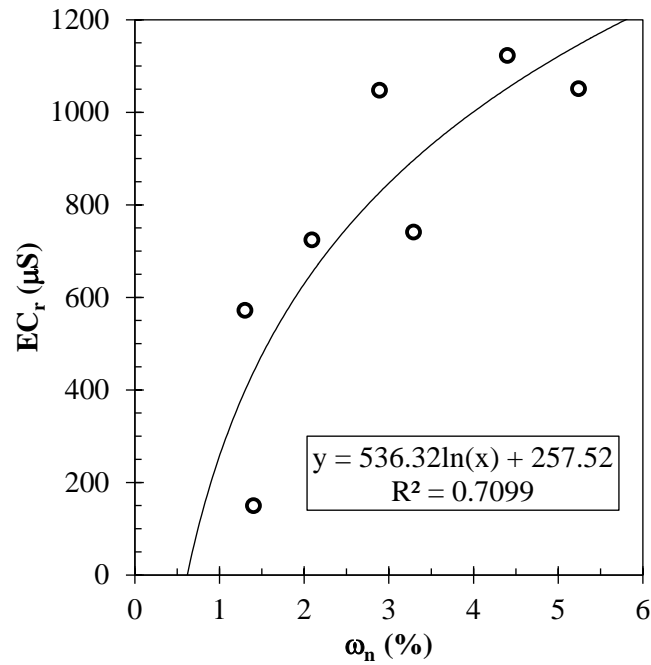


Figure A-26 Correlation between residual EC and natural moisture content

The B parameter can be obtained through curve-fit when electrical jar test data is available. Alternatively it can be estimated by Equation (A-2) using mineralogy data. Similar to R_p , determining the B parameter from basic shale index properties are found to be possible. The plots of the distilled water B parameter versus PI are shown in Figure A-27. Shale with high plasticity index trends to have higher value of B. This correlation is shown in the following equation.

$$B = 0.323 \cdot PI^{0.242} \quad (A-2)$$

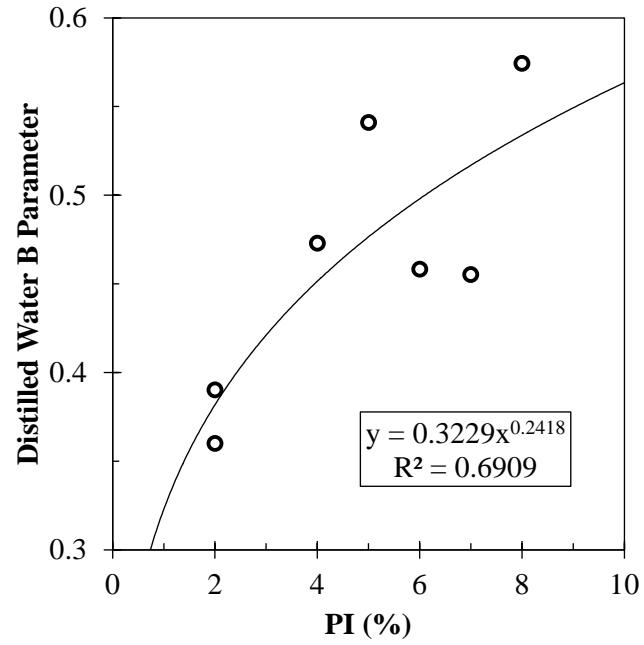


Figure A-27 Correlation between distilled water B parameter and plasticity index

APPENDIX B
COLLAPSE TEST DATA

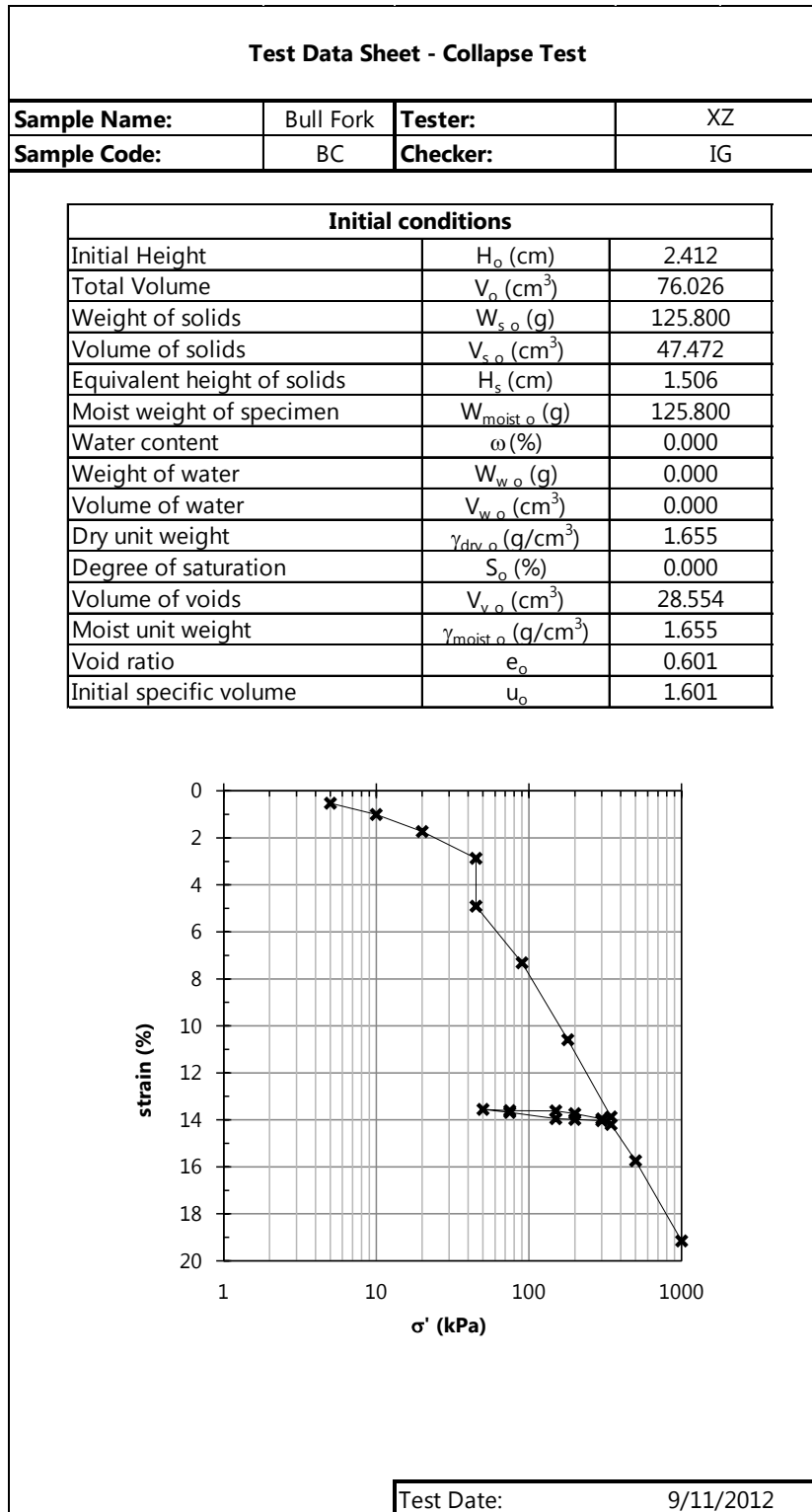


Figure B-1 Collapse Test Data Sheet – Bull Fork

Test Data Sheet - Collapse Test			
Sample Name:	Grundy	Tester:	XZ
Sample Code:	CC	Checker:	IG
Initial conditions			
Initial Height	H_o (cm)		2.41
Total Volume	V_o (cm ³)		76.03
Weight of solids	$W_{s,o}$ (g)		126.10
Volume of solids	$V_{s,o}$ (cm ³)		46.02
Equivalent height of solids	H_s (cm)		1.460
Moist weight of specimen	$W_{moist,o}$ (g)		126.10
Water content	ω (%)		0.00
Weight of water	$W_{w,o}$ (g)		0.00
Volume of water	$V_{w,o}$ (cm ³)		0.00
Dry unit weight	$\gamma_{dry,o}$ (g/cm ³)		1.659
Degree of saturation	S_o (%)		0.00
Volume of voids	$V_{v,o}$ (cm ³)		30.00
Moist unit weight	$\gamma_{moist,o}$ (g/cm ³)		1.66
Void ratio	e_o		0.6519
Initial specific volume	u_o		1.6519

Effective Stress (σ' in kPa)	Strain (%)
5	0
10	0
20	0.5
30	1.5
40	2.5
60	4
100	6
150	6
200	6
300	6
400	6
500	7.5
1000	11

Test Date:	9/14/2012
------------	-----------

Figure B-2 Collapse Test Data Sheet – Grundy

Test Data Sheet - Collapse Test			
Sample Name:	Carbondale	Tester:	XZ
Sample Code:	CD	Checker:	IG
Initial conditions			
Initial Height	H_o (cm)		2.412
Total Volume	V_o (cm ³)		76.026
Weight of solids	$W_{s o}$ (g)		126.400
Volume of solids	$V_{s o}$ (cm ³)		45.632
Equivalent height of solids	H_s (cm)		1.448
Moist weight of specimen	$W_{moist o}$ (g)		126.400
Water content	ω (%)		0.000
Weight of water	$W_{w o}$ (g)		0.000
Volume of water	$V_{w o}$ (cm ³)		0.000
Dry unit weight	$\gamma_{dry o}$ (g/cm ³)		1.663
Degree of saturation	S_o (%)		0.000
Volume of voids	$V_{v o}$ (cm ³)		30.394
Moist unit weight	$\gamma_{moist o}$ (g/cm ³)		1.663
Void ratio	e_o		0.666
Initial specific volume	u_o		1.666

Test Date:	9/18/2012
------------	-----------

Figure B-3 Collapse Test Data Sheet – Carbondale

Test Data Sheet - Collapse Test			
Sample Name:	Tradewater	Tester:	XZ
Sample Code:	BS	Checker:	IG

Initial conditions		
Initial Height	H_o (cm)	2.41
Total Volume	V_o (cm ³)	76.03
Weight of solids	W_{s_o} (g)	126.00
Volume of solids	V_{s_o} (cm ³)	47.01
Equivalent height of solids	H_s (cm)	1.492
Moist weight of specimen	W_{moist_o} (g)	126.00
Water content	ω (%)	0.00
Weight of water	W_{w_o} (g)	0.00
Volume of water	V_{w_o} (cm ³)	0.00
Dry unit weight	γ_{dry_o} (g/cm ³)	1.657
Degree of saturation	S_o (%)	0.00
Volume of voids	V_{v_o} (cm ³)	29.01
Moist unit weight	γ_{moist_o} (g/cm ³)	1.66
Void ratio	e_o	0.6171
Initial specific volume	u_o	1.6171

Test Date:	9/20/2012
-------------------	-----------

Figure B-4 Collapse Test Data Sheet – Tradewater

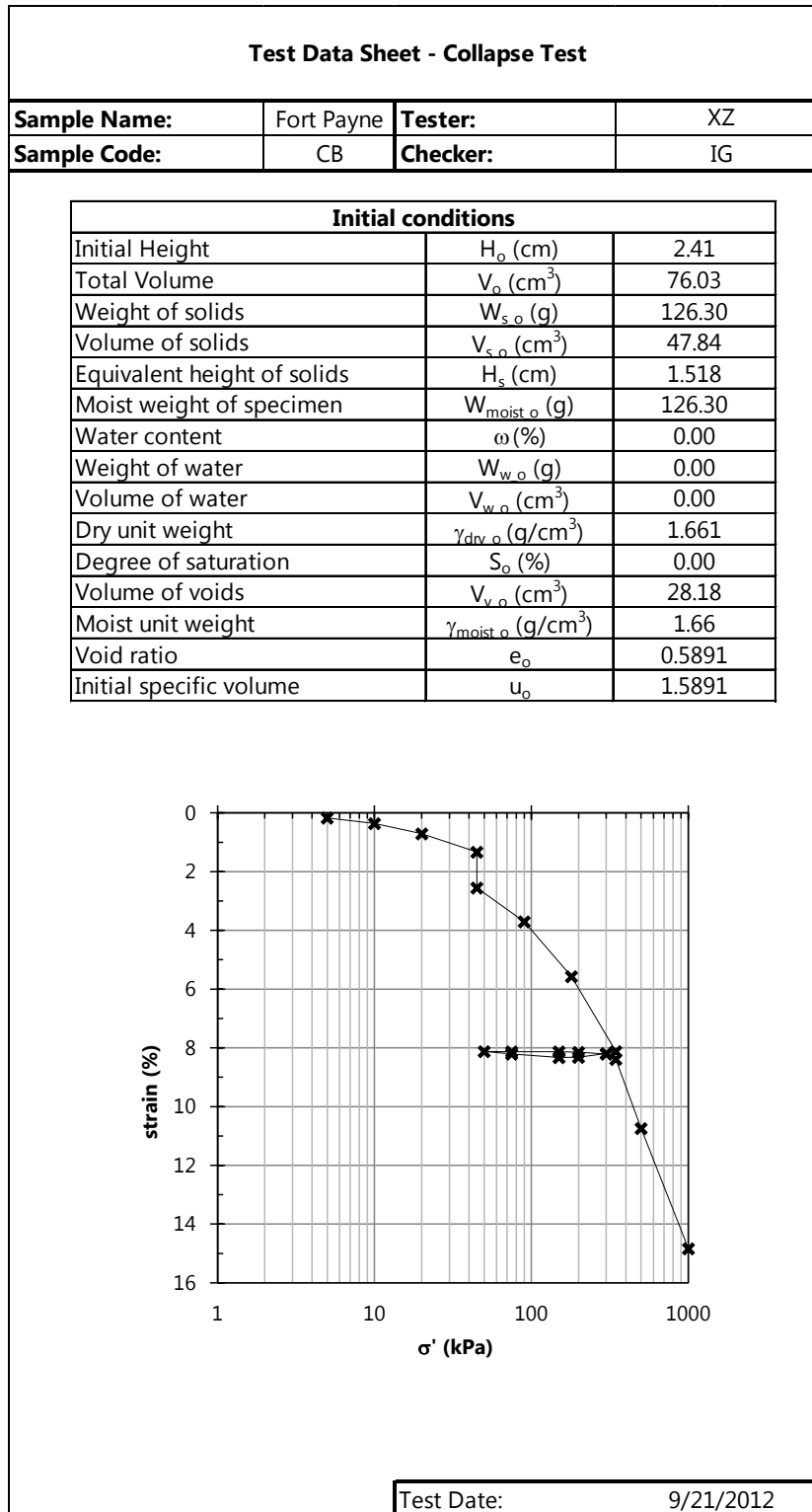


Figure B-5 Collapse Test Data Sheet – Fort Payne

APPENDIX C

SWELL TEST DATA

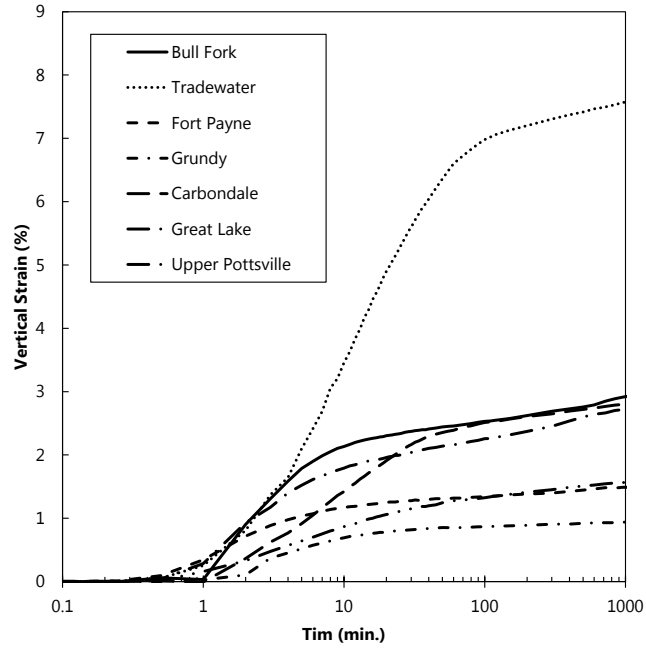


Figure C-1 Swell Test Data Sheet – Strain-time Curve – All Samples

Additional considerations on the rate of the primary swell were studied. The rate of primary swell is found to be correlated very well with the R_p of SWEC curve (Figure C-2), which indicates that if a shale deteriorate faster during weathering, it will also expand faster under wet condition.

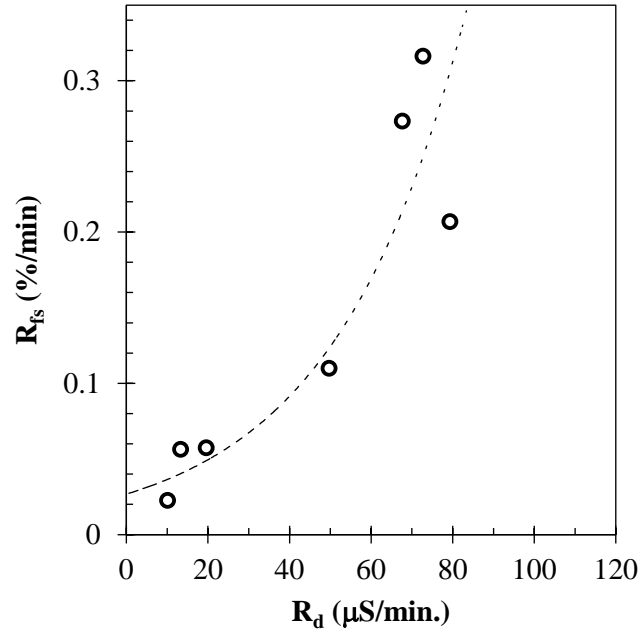


Figure C-2 Variation of Primary Swell Rate with Dissolution Rate

APPENDIX D

UNDRAINED-UNCONSOLIDATED TRIAXIAL (UU) TEST DATA

Table D-1 UU Test Data Sheet – Bull Fork

Date	10/19/2013	10/21/2013	11/5/2013	11/6/2013
Time Flood Finish	10/18/13 03:35 PM	10/21/13 01:14 PM	11/06/13 03:28 PM	11/07/13 04:00 PM
Time Shear Finish	10/18/13 05:34 PM	10/21/13 04:53 PM	11/26/13 12:55 PM	11/10/13 03:16 PM
Duration Shear Phase (h:m)	1:43	1:43	1:43	1:43
Time Shear Start	10/18/13 03:51 PM	10/21/13 03:10 PM	11/26/13 11:12 AM	11/10/13 01:33 PM
Duration Soak Phase (min)	16	116	28544	4173
Specimen #	9	10	13	14
Shale Name	Bull Fork	Bull Fork	Bull Fork	Bull Fork
Shale Code	BC	BC	BC	BC
Cell Code	T	T	T	D
Diameter (mm)	70.26667	69.68	69.85666667	70.17666666
Height (mm)	137	143.833333	137.5	140.5
Area (m²)	0.003877829	0.003813346	0.003832707	0.003867901
Volume (m³)	0.000531263	0.000548486	0.000526997	0.00054344
Weight Soil (g)	985.6	985.9	985.5	986
Unit Weight (pcf)	115.7646841	112.1635501	116.689807	113.2165268
Water Flood Thru (mL)	450	428.5	425	425
Weight Pan (g)	105.4	105.4	105.4	105.4
Weight Pan+WetSoil (g)	1202.3	1158	1226.5	1230.4
Weight Pan+DrySoil (g)	1061.2	1010.4	1075.6	1078.8
Water Content (%)	14.76250262	16.30939227	15.55349412	15.57427573

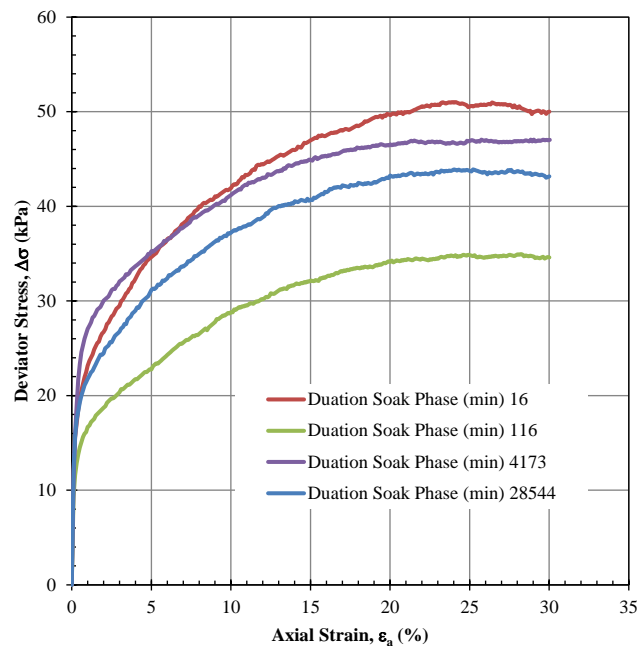


Figure D-1 UU Test – Stress-strain Curve – Bull Fork

Table D-2 UU Test Data Sheet – Tradewater

Date	11/5/2013	11/11/2013	11/13/2013	11/20/2013
Time Flood Finish	11/05/13 02:56 PM	11/11/13 02:59 PM	11/14/13 03:31 PM	11/21/13 02:05 PM
Time Shear Finish	11/05/13 04:52 PM	11/13/13 12:14 PM	11/19/13 01:15 PM	12/12/13 01:02 PM
Duration Shear Phase (h:m)	1:43	1:43	1:43	1:43
Time Shear Start	11/05/13 03:09 PM	11/13/13 10:31 AM	11/19/13 11:32 AM	12/12/13 11:19 AM
Duration Soak Phase (min)	13	2612	6961	30074
Specimen #	12	15	16	17
Shale Name	Tradewater	Tradewater	Tradewater	Tradewater
Shale Code	BS	BS	BS	BS
Cell Code	D	D	D	D
Diameter (mm)	70.03333333	70.47333333	70.13666667	70.73
Height (mm)	148.5	144	143	143
Area (m²)	0.003852117	0.003900673	0.003863493	0.003929137
Volume (m³)	0.000572039	0.000561697	0.000552479	0.000561867
Weight Soil (g)	986.1	985.8	985.9	985.7
Unit Weight (pcf)	107.5671391	109.514444	111.352839	109.4702503
Water Flood Thru (mL)	425	450	450	450
Weight Pan (g)	105.4	105.4	105.4	105.4
Weight Pan+WetSoil (g)	1230.4	1230.4	1236	1233.4
Weight Pan+DrySoil (g)	1053.3	1078.8	1070.6	1069.2
Water Content (%)	18.68340542	15.57427573	17.1363448	17.03672961

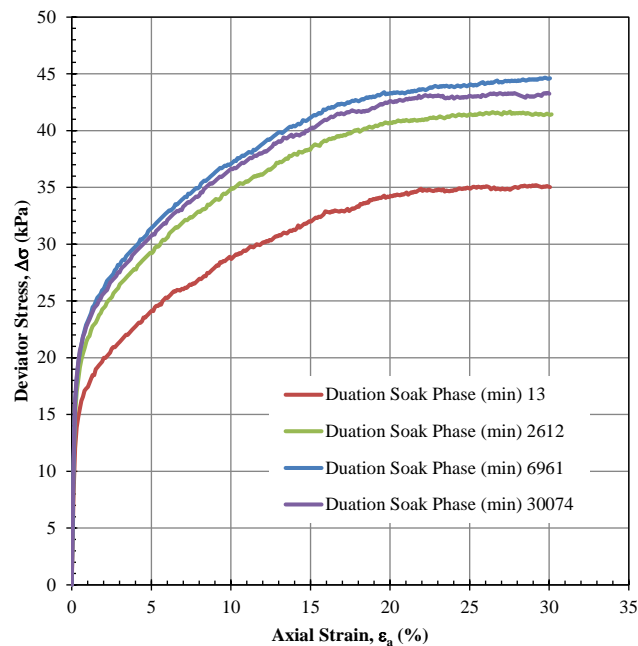


Figure D-2 UU Test – Stress-strain Curve – Tradewater

Table D-3 UU Test Data Sheet – Grundy

Date	9/16/2013	10/14/2013	10/14/2013	1/21/2014
Time Flood Finish	09/18/13 10:55 AM	10/14/13 02:57 PM	10/15/13 03:07 PM	01/21/14 03:29 PM
Time Shear Finish	09/19/13 01:09 PM	10/14/13 04:40 PM	10/15/13 05:50 PM	02/03/14 12:00 PM
Duration Shear Phase (h:m)	1:43	1:43	1:43	1:43
Time Shear Start	09/19/13 11:26 AM	10/14/13 02:57 PM	10/15/13 04:07 PM	02/03/14 10:17 AM
Duration Soak Phase (min)	1471	0	60	18408
Specimen #	2	6	7	18
Shale Name	Grundy	Grundy	Grundy	Grundy
Shale Code	CC	CC	CC	CC
Cell Code	T	D	T	D
Diameter (mm)	70.21	70.27	70.38	70.269
Height (mm)	142	140	143	142.1667
Area (m²)	0.003871576	0.003878196	0.003890348	0.003878086
Volume (m³)	0.000549764	0.000542947	0.00055632	0.000551335
Weight Soil (g)	985.84	985.7	985.7	985.7
Unit Weight (pcf)	111.8960751	113.2847687	110.5617495	111.5614206
Water Flood Thru (mL)	434.1	428	444	450
Weight Pan (g)	164.5	105.4	105.4	105.4
Weight Pan+WetSoil (g)	1283.4	1212.8	1209.8	1220.1
Weight Pan+DrySoil (g)	1132.1	1077.6	1073.4	1079.4
Water Content (%)	15.63662671	13.90660358	14.09090909	14.44558522

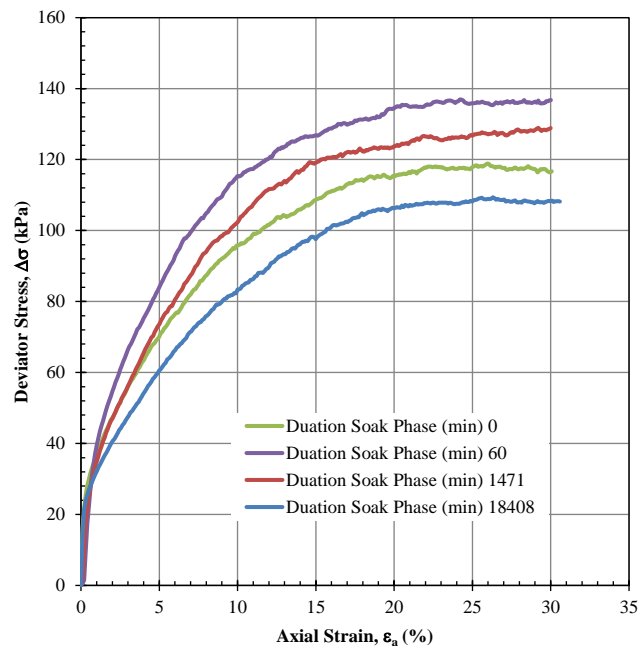


Figure D-3 UU Test – Stress-strain Curve – Grundy

Table D-4 UU Test Data Sheet – Carbondale

Date	9/16/2013	9/20/2013	9/23/2013	10/16/2013
Time Flood Finish	09/18/13 04:05 PM	09/23/13 11:14 AM	09/23/13 04:22 PM	10/16/13 03:14 PM
Time Shear Finish	09/18/13 05:48 PM	09/23/13 01:57 PM	09/24/13 05:49 PM	11/01/13 12:05 PM
Duration Shear Phase (h:m)	1:43	1:43	1:43	1:43
Time Shear Start	09/18/13 04:05 PM	09/23/13 12:14 PM	09/24/13 04:06 PM	11/01/13 10:22 AM
Duration Soak Phase (min)	0	60	1424	22748
Specimen #	3	4	5	5
Shale Name	Carbondale	Carbondale	Carbondale	Carbondale
Shale Code	CD	CD	CD	CD
Cell Code	D	D	T	D
Diameter (mm)	70.54	70.53	70.58	70.083333
Height (mm)	144.7	141	140.3	143
Area (m²)	0.003908056	0.003906948	0.00391249	0.003857619
Volume (m³)	0.000565496	0.00055088	0.000548922	0.00055164
Weight Soil (g)	985.8	984.3	985.8	986.1
Unit Weight (pcf)	108.7787541	111.4949798	112.063077	111.5450068
Water Flood Thru (mL)	427.1	425.5	431.5	446
Weight Pan (g)	106	164.8	106	105.4
Weight Pan+WetSoil (g)	1222.5	1271.6	1219.6	1222.7
Weight Pan+DrySoil (g)	1065.6	1120.1	1065.4	
Water Content (%)	16.35056273	15.85889249	16.07254534	

Figure D-4 UU Test – Stress-strain Curve – Carbondale (see Figure 3-9)

REFERENCES

- Abdullah, W. S., Al-Zou'bi, M. S., and Alshibli, K. A. (1997). "On the physicochemical aspects of compacted clay compressibility." *Canadian Geotechnical Journal*, 34(4), 551-559.
- Abeyesekera, R., Lovell, C., and Wood, L. (1979). "Strength testing of compacted shale." *Geotechnical Testing Journal*, 2(1), 11-19.
- Abeyesekera, R., Lovell, C., and Wood, L. "Stress-deformation and strength characteristics of a compacted shale." *Proc., Proceedings from the Clay Fills Conference, held at the Institution of Civil Engineers, November 14-15, 1978.*
- Al-Shayea, N., Abduljawwad, S., Bashir, R., Al-Ghamedy, H., and Asi, I. (2003). "Determination of parameters for a hyperbolic model of soils." *Proceedings of the ICE - Geotechnical Engineering*, 156(2), 105-117.
- Alonso, E., and Cardoso, R. (2010). "Behavior of materials for earth and rockfill dams: Perspective from unsaturated soil mechanics." *Front. Archit. Civ. Eng. China*, 4(1), 1-39.
- Alonso, E. E., Gens, A., and Josa, A. (1990). "A constitutive model for partially saturated soils." *Géotechnique*, 40(3), 405-430.
- Aziz, M., Towhata, I., Yamada, S., Qureshi, M. U., and Kawano, K. (2010). "Water-induced granular decomposition and its effects on geotechnical properties of crushed soft rocks." *Nat. Hazards Earth Syst. Sci.*, 10(6), 1229-1238.
- Bjerrum, L. "Embankments on soft ground." *Proc., Performance of earth and earth-supported structures*, ASCE, 1-54.
- Blatt, H., Tracy, R. J., and Owens, B. (2006). *Petrology: Igneous, Sedimentary, and Metamorphic*, W. H. Freeman, New York, NY.
- Brown, E. T. (1981). *Rock characterization, testing & monitoring: ISRM suggested methods* Pergamon Press, Oxford, UK.
- Bryson, L. S., Gomez-Gutierrez, I. C., and Hopkins, T. C. (2011). "Correlations between Durability and Geotechnical Properties of Compacted Shales." *Proc., Geo-Frontiers Congress 2011*, ASCE, 4109-4118.
- Bryson, L. S., Gomez-Gutierrez, I. C., and Hopkins, T. C. (2012). "Development of a new durability index for compacted shale." *Engineering Geology*, 139, 66-75.
- Budhu, M. (2011). *Soil Mechanics and Foundations, 3e*, John Wiley & Sons, Inc., Danvers, MA.
- Carrier, W. (2003). "Goodbye, Hazen; Hello, Kozeny-Carman." *Journal of Geotechnical and Geoenvironmental Engineering*, 129(11), 1054-1056.
- Czerewko, M. A., and Cripps, J. C. (2001). "Assessing the durability of mudrocks using the modified jar slake index test." *Quarterly Journal of Engineering Geology and Hydrogeology*, 34(2), 153-163.
- Erguler, Z. A., and Ulusay, R. (2009). "Assessment of physical disintegration characteristics of clay-bearing rocks: Disintegration index test and a new durability classification chart." *Engineering Geology*, 105(1-2), 11-19.
- Fair, G. M., Hatch, L. P., and Hudson, H. E. (1933). "Fundamental factors governing the streamline flow of water through sand." *Journal American Water Works Association*, 25(11), 1551-1565.
- Franklin, J. A., and Chandra, R. (1972). "The slake-durability test." *International Journal of Rock Mechanics and Mining Sciences & Geomechanics Abstracts*, 9(3), 325-328.
- Fuenkajorn, K. (2011). "Experimental assessment of long-term durability of some weak rocks." *Bull Eng Geol Environ*, 70(2), 203-211.
- Gemici, U. (2001). "Durability of shales in Narlidere, Izmir, Turkey, with an emphasis on the impact of water on slaking behavior." *Env Geol*, 41(3-4), 430-439.

- Gokceoglu, C., Ulusay, R., and Sonmez, H. (2000). "Factors affecting the durability of selected weak and clay-bearing rocks from Turkey, with particular emphasis on the influence of the number of drying and wetting cycles." *Engineering Geology*, 57(3-4), 215-237.
- Gomez-Gutierrez, I., Bryson, L., and Hopkins, T. (2011). "Correlations between Geotechnical Properties and the Swell Behavior of Compacted Shales." *Geo-Frontiers 2011*, 4119-4128.
- Gomez-Gutierrez, I. C. (2013). "Development of a constitutive model of compacted shales and determination of the effect of weathering on its parameters." doctoral dissertation, University of Kentucky, Lexington, KY.
- Grace, H., Henry, J., Skempton, A., Jones, R. L., Jones, R., Golder, H., Millard, R., Tomlinson, M., Broadbent, R., Rangeley, W., Hoare, C., and Alston, J. (1957). "Discussion on airport paper No. 35: The planning and design of the new hong kong airport." *ICE Proceedings*, 7(2), 305-325.
- Hopkins, T. C. (1988). "Shear Strength of Compacted Shales." *Kentucky Transportation Center Research Reports*, Kentucky Transportation Center, Lexington, KY.
- Hopkins, T. C., and Deen, R. C. (1984). "Identification of Shales." *Geotechnical Testing Journal*, 7(1), 10-18.
- Hopkins, T. C., and Gilpin, B. C. (1981). "Identification of Kentucky shales." *Kentucky Transportation Center Research Reports*, Kentucky Transportation Center, Lexington, KY.
- Jamiolkowski, M. "New developments in field and laboratory testing of soils," State of the Art Report." *Proc., 11th Int. Conf. on SMFE.*, 57-153.
- Johnson, L. t., and Snethen, D. (1978). "Prediction of potential heave of swelling soil." *ASTM Geotechnical Testing Journal*, 1(Tech Note).
- Kirkendoll, J. S. (2012). "Development of a new testing procedure for durability of compacted shale." M.S. thesis, University of Kentucky, Lexington, KY.
- Klein, K. A. (1999). "Electromagnetic properties of high specific surface minerals." doctoral dissertation, Georgia Institute of Technology, Atlanta, Georgia.
- Klein, K. A., and Santamarina, J. C. (2003). "Electrical conductivity in soils: Underlying phenomena." *Journal of Environmental & Engineering Geophysics*, 8(4), 263-273.
- Koncagul, E. C., and Santi, P. M. (1999). "Predicting the unconfined compressive strength of the Breathitt shale using slake durability, Shore hardness and rock structural properties." *International Journal of Rock Mechanics and Mining Sciences*, 36(2), 139-153.
- Kondner, R. L. (1963). "Hyperbolic stress-strain response: cohesive soils." *Journal of the soil mechanics and foundations division, ASCE*, 89(1), 115-143.
- Ladd, C. (1991). "Stability Evaluation during Staged Construction." *Journal of Geotechnical Engineering*, 117(4), 540-615.
- Ladd, C. C., and Foott, R. (1974). "New design procedure for stability of soft clays." *Journal of Geotechnical and Geoenvironmental Engineering*, 100(7), 763-786.
- Lashkaripour, G. R., and Ghafouri, M. (2003). "Mineralogical controls of mudrock durability." *Proc., 9th Congress of the International Association for Engineering Geology Engineering geology for developing countries.*
- Lawton, E., Fragaszy, R., and Hardcastle, J. (1989). "Collapse of Compacted Clayey Sand." *Journal of Geotechnical Engineering*, 115(9), 1252-1267.
- Lawton, E., Fragaszy, R., and Hardcastle, J. (1991). "Stress Ratio Effects on Collapse of Compacted Clayey Sand." *Journal of Geotechnical Engineering*, 117(5), 714-730.
- Lawton, E., Fragaszy, R., and Hetherington, M. (1992). "Review of Wetting-Induced Collapse in Compacted Soil." *Journal of Geotechnical Engineering*, 118(9), 1376-1394.
- Liang, Y., and Lovell, C. W. (1983). "Strength of field compacted clays." *Canadian Geotechnical Journal*, 20(1), 36-46.

- Lim, Y., and Miller, G. (2004). "Wetting-Induced Compression of Compacted Oklahoma Soils." *Journal of Geotechnical and Geoenvironmental Engineering*, 130(10), 1014-1023.
- Lovell, C. W., and Johnson, J. M. (1981). "Shearing behavior of compacted clay after saturation." *Proc., Laboratory Shear Strength of Soil: A Symposium*, ASTM, Baltimore, MD, 277-293.
- Low, P. F. (1961). "Physical chemistry of clay-water interaction." *Advances in agronomy*, 13, 269-327.
- Lupini, J. F., Skinner, A. E., and Vaughan, P. R. (1981). "The drained residual strength of cohesive soils." *Géotechnique*, 31(2), 181-213.
- Manasseh, J., and Olufemi, A. I. (2008). "Effect of lime on some geotechnical properties of Igumale shale." *Electronic Journal of Geotechnical Engineering*, 13(6), 1-12.
- Mesri, G. (1989). "A reevaluation of $S_{u(mob)} = 0.22 \sigma'_p$ using laboratory shear tests." *Canadian Geotechnical Journal*, 26(1), 162-164.
- Mesri, G., and Abdel-Ghaffar, M. (1993). "Cohesion Intercept in Effective Stress-Stability Analysis." *Journal of Geotechnical Engineering*, 119(8), 1229-1249.
- Mesri, G., and Cepeda-Diaz, A. F. (1986). "Residual Shear strength of clays and shales." *Geotechnique*, 36, 269-274.
- Miller, G. A., Azad, S., and Dhar, B. (1997). "The effect of cement kiln dust on the collapse potential of compacted shale." *ASTM SPECIAL TECHNICAL PUBLICATION*, 1275, 232-245.
- Miller, G. A., Muraleetharan, K. K., and Lim, Y. Y. (2001). "Wetting-induced settlement of compacted-fill embankments." *Transportation Research Record: Journal of the Transportation Research Board*, 1755(1), 111-118.
- Nandi, A., and Whitelaw, M. (2009). "Effect of Physico-Chemical Factors on the Disintegration Behavior of Calcareous Shale." *Environmental & Engineering Geoscience*, 15(4), 273-285.
- Noble, D. F. (1977). "Accelerated weathering of tough shales." Virginia Highway and Transportation Research Council & Federal Highway Administration, Charlottesville, VA
- Nwabuokei, S. O., and Lovell, C. W. (1986). "Compressibility and Settlement of compacted fills." *Proc., Consolidation of Soils: Testing and Evaluation : a Symposium*, ASTM, Baltimore, MD, 184-202.
- O'Neill, M. W., and Poormoayed, M. (1980). "Methodology for foundations on expansive clays." *Journal of Geotechnical and Geoenvironmental Engineering*, 106(ASCE 15949).
- Oakland, M. W., and Lovell, C. W. (1982). "Classification and Other Standard Tests for Shale Embankments." Purdue University/Indiana Department of Transportation JHRP, West Lafayette, IN.
- Orhan Erol, A., and Dhowian, A. (1990). "Swell behaviour of arid climate shales from Saudi Arabia." *Quarterly Journal of Engineering Geology and Hydrogeology*, 23(3), 243-254.
- Osterman, J. (1960). "Views on the Stability of Clay Slopes." *Geologiska Föreningen i Stockholm Förhandlingar*, 82(3), 346-366.
- Pansu, M., and Gautheyrou, J. (2007). *Handbook of Soil Analysis: Mineralogical, Organic and Inorganic Methods*, Springer.
- Pappas, D. M., and Vallejo, L. E. (1997). "The settlement and degradation of nondurable shales associated with coal mine waste embankments." *International Journal of Rock Mechanics and Mining Sciences*, 34(3-4), 241.e241-241.e213.
- Pinyol, N., Vaunat, J., and Alonso, E. E. (2007). "A constitutive model for soft clayey rocks that includes weathering effects." *Géotechnique*, 57(2), 137-151.
- Pye, K., and Miller, J. A. (1990). "Chemical and biochemical weathering of pyritic mudrocks in a shale embankment." *Quarterly Journal of Engineering Geology and Hydrogeology*, 23(4), 365-382.

- Rao, S., and Revanasiddappa, K. (2000). "Role of Matric Suction in Collapse of Compacted Clay Soil." *Journal of Geotechnical and Geoenvironmental Engineering*, 126(1), 85-90.
- Richardson, D., and Wiles, T. (1990). "Shale Durability Rating System Based on Loss of Shear Strength." *Journal of Geotechnical Engineering*, 116(12), 1864-1880.
- Satttil, P. M., and Higgins, J. D. (1998). "Methods for predicting shale durability in the field." *Geotechnical Testing Journal*, 21(3), 195-202.
- Skepmpton, A. W. (1964). "Long-term stability of clay slopes." *Geotechnique*, 14(2), 75-101.
- Skepmpton, A. W., and Delory, F. A. "Stability of natural slopes in London clay." *Proc., 4th Int. Conf. Soil Mech.*, 378-381.
- Spears, D. A., and Taylor, R. K. (1972). "The influence of weathering on the composition and engineering properties of in situ coal measures rocks." *International Journal of Rock Mechanics and Mining Sciences & Geomechanics Abstracts*, 9(6), 729-730.
- Stark, T., and Eid, H. (1994). "Drained Residual Strength of Cohesive Soils." *Journal of Geotechnical Engineering*, 120(5), 856-871.
- Stark, T., and Eid, H. (1997). "Slope Stability Analyses in Stiff Fissured Clays." *Journal of Geotechnical and Geoenvironmental Engineering*, 123(4), 335-343.
- Stroh Jr, W., Bragg Jr, G., and Ziegler, T. (1978). "Design and construction of compacted shale embankments; Volume 5, Technical guidelines." Federal Highway Administration, Washington, DC.
- Taylor, R. K. (1988). "Coal Measures mudrocks: composition, classification and weathering processes." *Quarterly Journal of Engineering Geology and Hydrogeology*, 21(1), 85-99.
- Taylor, R. K., and Spears, D. A. (1981). "Laboratory investigation of mudrocks." *Quarterly Journal of Engineering Geology and Hydrogeology*, 14(4), 291-309.
- Terzaghi, K., Peck, R. B., and Mesri, G. (1996). *Soil Mechanics in Engineering Practice*, John Wiley & Sons, Inc., New York, NY.
- Tucholke, B. E., C, S. J., and Klaus, A. (2004). "Initial Reports Volume 210." *Proc., Ocean Drilling Program*, Texas A&M University, College Station, TX.
- Van Eeckhout, E. M. (1976). "The mechanisms of strength reduction due to moisture in coal mine shales." *International Journal of Rock Mechanics and Mining Sciences & Geomechanics Abstracts*, 13(2), 61-67.
- Velde, B. (1992). *Introduction to clay minerals: chemistry, origins, uses, and environmental significance*, Chapman & Hall.
- Weaver, C. E. (1989). *Clays, Muds, and Shales*, Elsevier Science.
- Wesley, L. D. (2003). "Residual strength of clays and correlations using Atterberg limits." *Geotechnique*, 53(7), 669-672.
- Witsman, G. R., and Lovell, C. W. (1979). "The effect of compacted prestress on compacted shale compressibility." Purdue University/Indiana Department of Transportation JHRP, Alexandria, VA.
- Wong, R. C. K. (1998). "Swelling and softening behaviour of La Biche shale." *Canadian Geotechnical Journal*, 35(2), 206-221.
- Wroth, C. P., and Houlsby, G. T. "Soil mechanics - property characterization and analysis procedures." *Proc., 11th Int. Conf. on SMFE*, 1-54.
- Wu, T., Randolph, B., and Huang, C. (1993). "Stability of Shale Embankments." *Journal of Geotechnical Engineering*, 119(1), 127-146.
- Yagiz, S. (2011). "Correlation between slake durability and rock properties for some carbonate rocks." *Bull Eng Geol Environ*, 70(3), 377-383.
- Yoshida, N., and Hosokawa, K. (2004). "Compression and Shear Behavior of Mudstone Aggregates." *Journal of Geotechnical and Geoenvironmental Engineering*, 130(5), 519-525.

VITA

Author's Name – Xu Zhang

Place of Birth – Xu Zhou, Jiangsu, China

Education

Bachelor of Science in Civil Engineering

University of Kentucky, 2010 – 2012

Bachelor of Engineering in Civil Engineering

China University of Mining and Technology, 2008 – 2010

Professional Experience

Staff Professional

Building & Earth Sciences, Inc., 2014 – Present

Research and Teaching Assistant

University of Kentucky, 2012 – 2014

Professional Certificate

Engineer in Training

Kentucky State Board of Licensure for Professional Engineers and Land Surveyors, 2013

Graduate Certificate in Power and Energy

Power and Energy Institute of Kentucky & College of Engineering University of Kentucky, 2012